

Annual Report 2016

Laboratory of Radiochemistry

Cover

Hot cell containing the chemical separation system for Sc-44.

PAUL SCHERRER INSTITUT



u^b

b
UNIVERSITÄT
BERN

LABOR FÜR RADIO- UND UMWELTCHEMIE
DER UNIVERSITÄT BERN UND
DES PAUL SCHERRER INSTITUTS

Annual Report 2016

Laboratory of Radiochemistry

Editors

A. Türlér, R. Eichler, A. Blattmann

Paul Scherrer Institut

Labor für Radiochemie

5232 Villigen PSI

Switzerland

Durchwahl +41 56 310 24 04

Sekretariat +41 56 310 24 01

Fax +41 56 310 44 35

Universität Bern

Departement für Chemie und Biochemie

Labor für Radio- und Umweltchemie

Freiestrasse 3, 3012 Bern, Switzerland

Durchwahl +41 31 631 42 64

Sekretariat +41 31 631 42 42

Fax +41 31 631 42 20

Reports are available from

Angela Blattmann

angela.blattmann@psi.ch

Paul Scherrer Institut

5232 Villigen PSI

Switzerland



See also our web-page
<https://www.psi.ch/lrc/>

TABLE OF CONTENTS

Editorial.....	1
Heavy Elements	
ATTEMPT TO INVESTIGATE THE ADSORPTION OF Cn AND Fl ON Se SURFACES	3
N. M. Chiera, R. Eichler, B. Kraus, S. Martz, A. Türler, Y. Wittwer, R. Dressler, D. Piguet, A. Vögele, N. V. Aksenov, G. A. Bozhikov, V. I. Chepigina, S. N. Dmitriev, S. Madumarov, O. N. Malyshev, Y. A. Popov, A. V. Sabel'nikov, P. Steinegger, A. I. Svirikhin, G. K. Vostokin, A. V. Yeremin	
STABILITY OF GROUP 6 HEXACARBONYL COMPOUNDS $M(CO)_6$	4
R. Eichler	
IMPROVED SET UP FOR THE EVALUATION OF CARBONYL COMPLEX FORMATION OF FISSION PRODUCTS AS MODELS FOR SHE.....	5
Y. Wittwer, R. Eichler, D. P. Herrmann, A. Türler	
ISOTHERMAL VACUUM CHROMATOGRAPHY OF ^{211}Pb ON SiO_2	7
B. Kraus, R. Eichler, A. Türler, P. Steinegger	
CHARACTERISATION OF SAMPLE AND TARGET THICKNESSES USING ADVANCED ALPHA-SPECTROSCOPY SIMULATION.....	8
R. Dressler	
Radwaste Analytics	
ANITA (ADVANCED NETWORK FOR ISOTOPE AND TARGET LABORATORIES) - THE URGENT NEED FOR AN EUROPEAN TARGET PREPARATION NETWORK	10
D. Schumann	
EVAPORATION AND ADSORPTION BEHAVIOUR OF RADIOTRACERS RELEASED FROM IRRADIATED TELLURIUM DOPED LBE	11
E. Karlsson, J. Neuhausen, A. Vögele, R. Eichler, A. Türler	
ADSORPTION BEHAVIOUR OF CAESIUM ON FUSED SILICA AND STAINLESS STEEL SURFACES.....	13
E. Karlsson, A. Colldeweih, J. Neuhausen, R. Eichler, A. Türler	
PREPARATION OF LBE SAMPLES CONTAINING Cs FOR VOLATILIZATION STUDIES	15
I. I. Danilov, J. Neuhausen, A. Vögele, E. Müller	
MEASUREMENT OF THE $^7Be(n,\alpha)^4He$ REACTION CROSS-SECTION FOR THE COSMOLOGICAL LITHIUM PROBLEM AT THE n_TOF FACILITY AT CERN.....	17
M. Barbagallo, A. Musumara, S. Heinitz, E. A. Maugeri, N. Kivel, R. Dressler, D. Schumann	
PREPARATION AND CHARACTERIZATION OF A 7Be IMPLANTED TARGET FOR NUCLEAR ASTROPHYSICS RESEARCH.....	18
E. A. Maugeri, S. Heinitz, R. Dressler, N. Kivel, D. Schumann, T. Stora, R. Reckermann, A. Hagel, H. Orlick, V. Neims, O. Morath, N. Frey, T. Schneider, K. Geissmann	
PREPARATION OF ^{148}Gd AND ^{154}Dy SAMPLES FROM p-IRRADIATED Pb TARGETS	20
Z. Talip, R. Dressler, A. Vögele, D. Schumann, R. Michel	
SEPARATION OF LONG-LIVED RADIONUCLIDES FROM PROTON-IRRADIATED Ta TARGETS.....	22
Z. Talip, A. Vögele, D. Schumann, E. Strub, C. Vockenhuber	

ON THE PRODUCTION AND SEPARATION OF ^{163}Ho FOR PHYSICS RESEARCH EXPERIMENTS	24
S. Heinitz, N. Kivel, D. Schumann, U. Köster, A. Nucciotti	
PREPARATION OF ^{10}Be SAMPLES FOR NUCLEAR STRUCTURE RESEARCH AT RADIOACTIVE ION BEAM FACILITIES	26
S. Heinitz, T. Stowasser, D. Schumann, A. DiPietro	
TOWARDS NEUTRON CAPTURE CROSS-SECTION MEASUREMENTS WITH ULTRACOLD NEUTRONS	27
J. Ulrich, R. Dressler, B. Lauss	
PREPARATION OF A ^{60}Fe STANDARD FOR ACCELERATOR MASS SPECTROMETRY	29
D. Schumann, N. Kivel	
WASTE TREATMENT AND ISOTOPE RECLAMATION.....	31
M. Lin, I. Kajan, H. D. Potthast, A. Türler, D. Schumann	

Radionuclide Development

NEW 6 mm PELLETT TARGETS FOR ^{44}Sc PRODUCTION.....	32
C. Vermeulen, N.P. van der Meulen	
^{43}Sc PRODUCTION DEVELOPMENT BY CYCLOTRON IRRADIATION OF ^{43}Ca & ^{46}Ti	33
K. Domnanich, C. Umbricht, M. Benešová, C. Müller, A. Blanc, M. Behe, R. Schibli, A. Türler, N.P. van der Meulen	
PRODUCTION AND SEPARATION OF ^{47}Sc FOR RADIOPHARMACEUTICAL APPLICATIONS.....	34
K. Domnanich, U. Köster, B. Ponsard, M. Benešová, K. Siwowska, C. Müller, R. Schibli, A. Türler, N.P. van der Meulen	

Radiopharmaceutical R&D Universität Bern

THE DCB-UNIBE RADIOPHARMACEUTICAL LABORATORY AT SWAN HOUSE.....	35
J. Moreno, O. Leib, M. Bunka, T. Basaco, N. Meneses, A. Türler	
CHARACTERIZATION OF GIRENTUXIMAB CONJUGATES FOR RADIOIMMUNOTHERAPY	36
T. Basaco, S. Pektor, J. Moreno, M. Miederer, A. Türler	
EVALUATION OF CAIX EXPRESSION IN NUDE MOUSE XENOGRAFT MODEL.....	38
T. Basaco, J.A. Galván, S. Pektor, J. Moreno, M. Miederer, A. Türler	

Environmental Radionuclides Universität Bern

SOURCE APPORTIONMENT OF CARBONACEOUS AEROSOLS BY CONTINUOUS-FLOW ^{14}C MEASUREMENTS: STATISTICAL ANALYSIS.....	40
G. Salazar, K. Agrios, S. Szidat	
RADIOCARBON DATING OF BONES AT THE LARA LABORATORY IN BERN	41
S. Szidat, E. Vogel, R. Gubler, S. Lösch	
ISOLATION OF BLACK CARBON AND ELEMENTAL CARBON FOR SOURCE APPORTIONMENT IN SEDIMENTS BASED ON ^{14}C ANALYSIS	42
M. Vonwiller, C. Steiner, S. Szidat	
RADIOCARBON ANALYSIS OF METHANE 1: OPTIMIZATION OF THE CHROMATOGRAPHIC SEPARATION OF PRECONCENTRATED AIR SAMPLES.....	43
C. Espic, M. Liechti, M. Battaglia, S. Szidat	

RADIOCARBON ANALYSIS OF METHANE 2: DEVELOPING A PREPARATIVE GAS CHROMATOGRAPHY TECHNIQUE FOR METHANE PURIFICATION.....	44
M. Liechti, C. Espic, M. Battaglia, S. Szidat	
List of publications	45
Bookchapters, Reports and technical notes, Internal reports.....	52
Contributions to conferences, workshops and seminars.....	53
Public relations and outreach activities.....	60
Lectures and courses	61
Members of scientific committees, external activities	62
Master thesis	63
Doctoral thesis.....	64
Awards.....	65
Summer Students, Semesterwork, Visiting guests.....	66
Organigram.....	67
Author index	68
Affiliation index.....	69

EDITORIAL

While it was not clear last year whether the new Laboratory of Radiochemistry (LRC) will continue the tradition of the old Laboratory of Radio- and Environmental Chemistry (LCH) of publishing an overview of ongoing research in the form of an annual report, a decision was taken to present PhD students and staff scientists alike with an opportunity to report on their progress made during the past year.

Looking back at the first year of operation of LRC in the Nuclear Energy and Safety (NES) division, I can draw a very positive conclusion. The NES division is very well structured and organized. At a workshop for all NES group leaders in Filzbach (SG), it became evident that the know-how and competences of LRC ideally complement the NES division. In turn, LRC was welcomed without any reservations and, thus, LRC found a division within PSI where its research topics and language are understood. An extremely positive sign was that Dorothea Schumann's group, in collaboration with the Hot Laboratory, was able to acquire a research project funded by Swissnuclear. In 2016, two students successfully defended their PhD theses, namely, Patrick Steinegger who graduated with "summa cum laude" and Nadine Chiera - both from the Heavy Element group. I am very happy to communicate that in 2016 seven (!) new PhD students and two PostDocs have joined LRC.

Scientifically, LRC continues to make a significant impact. In 2016, a total of 44 papers were published by members of LRC as main authors or co-authors. Noteworthy is an article by former PhD student Bernadette Hammer-Rotzler in the European Physical Journal Plus that featured on the cover of the July issue. In this article, the distribution and surface enrichment of radionuclides in lead-bismuth eutectic from spallation targets was investigated. The radiopharmaceutical laboratory in Bern prepared two quality dossiers for Swissmedic and received a limi-

ted distribution license for the diagnostic radiopharmaceutical ^{68}Ga -PSMA-11 and the therapeutic radiopharmaceutical ^{177}Lu -DOTATOC in early January 2017. Furthermore, congratulations go to two of our graduate students which were awarded prizes; Nadine Chiera won a prize in the category 3rd/4th year PhD student at the 8th NES PhD Day, while Katharina Domnanich was the winner of the oral presentation award at the NRC9 conference in Helsinki.

Our social outing in mid-2016 took us to the Spiez Laboratory, where we were introduced to its facilities and instrumentation. The Spiez Laboratory belongs to the Federal Office for Civil Protection (FOCP) from nuclear, biological, and chemical warfare and is among the leading institutions of its kind worldwide. Due to inclement weather, we then visited the Tropenhaus in Frutigen, which offers a unique indoor tropical garden featuring an interactive exhibition and an integrated fish farm. The year-end function was organized by the LRC-PhD-Party-Organizing-Committee (LP²OC) and led us to Baden for a visit of its brewery, where we were able to sample their latest creations, followed by an apero in a local restaurant.

From the laboratory overview above, it is apparent that the new LRC - following its separation from LUC - is going strong and continues to generate high-quality research.



Andreas Türler

ATTEMPT TO INVESTIGATE THE ADSORPTION OF Cn AND Fl ON Se SURFACES

N. M. Chiera, R. Eichler, B. Kraus, S. Martz, A. Türler, Y. Wittwer (Uni. Bern & PSI), R. Dressler, D. Piguet, A. Vögele (PSI), N. V. Aksenov, G. A. Bozhikov, V. I. Chepigin, S. N. Dmitriev, S. Madumarov, O. N. Malyshev, Y. A. Popov, A. V. Sabel'nikov, P. Steinegger, A. I. Svirikhin, G. K. Vostokin, A. V. Yeregin (FNL, JINR)

In order to confirm the Cn / t-Se chemical interaction observed in [1], and to shed some light on the chemical behavior of Flerovium, additional on-line studies with Hg, Cn, and Fl on both trigonal and amorphous selenium surfaces were performed in Fall 2016 in Dubna, Russia. During the entire experimental campaign, four ^{242}Pu oxide targets (1.3 mg/cm^2 ^{242}Pu , $50 \text{ }\mu\text{g/cm}^2$ $^{\text{nat}}\text{Nd}$ admixture) were used. A $^{48}\text{Ca}^{18+}$ beam with a primary energy of 276 MeV was delivered from the U-400 cyclotron, in order to produce ^{185}Hg and ^{287}Fl in the nuclear fusion reactions $^{142}\text{Nd}(^{48}\text{Ca},5n)$ and $^{242}\text{Pu}(^{48}\text{Ca},5n)$, respectively. The evaporation residues were thermalized in a recoil chamber internally covered with quartz, and transported with a mixed gas flow (Ar/ He - 30:70, 2 L/min gas flow rate) through a 4 m long PFA[®] Teflon capillary to the thermochromatographic detection system COLD [2]. A vacuum evaporation and deposition technique for a homogeneous coating of the silicon detector surfaces with Se was applied. The detectors freshly covered by red amorphous Se were stored in darkness, at a pressure of 10^{-4} mbar to prevent recrystallization. They were mounted under red light into COLD as Det#2-7 and #9-16. Det#1, 8 and 7 were uncovered detectors with SiO_2 surfaces and Det#18-32 were covered with Au. Despite a total target beam dose of 2.6×10^{18} $^{48}\text{Ca}^{18+}$ particles and an estimated transport efficiency of 63% for ^{283}Cn and 2% for ^{287}Fl , no decay events associated to the two SHEs were observed during the entire experimental campaign. Unfortunately, after the change to the second ^{242}Pu target, a massive contamination of the recoil chamber and the detection system by unknown volatile organic compounds occurred. Despite thorough cleaning efforts, the results from the remaining experiment are ambiguous. During the first part of the experiment (i.e., while using the first ^{242}Pu target), the ^{185}Hg ($t_{1/2} = 45.2$ s; $E_{\alpha} = 5.65$ MeV) deposition pattern revealed immediately an advanced crystallization (>95%) of the thin layers of red amorphous Se, as well as a slight contamination of the first Au detectors Det#18 (70%) and Det#19 (40%). Moreover, an efficient transport of ^{211}At ($t_{1/2} = 7.2$ h; $E_{\alpha} = 5.87$ MeV) to the COLD setup, produced in nuclear transfer reactions, was observed (Fig. 2). The deposition pattern of this At species, here referred to as AtO_xH_y , was reproduced in Monte Carlo simulations, revealing its higher volatility in comparison to elemental At [3]. In [4], an At species with similar volatility was already observed and ascribed to AtHO . However, the different experimental conditions and gas carrier composition from the ones reported in [3] does not allow for an unambiguous identification of the At species observed here. In fact, the on-line gas composition analysis by MKS CIR-RUS 2 mass spectrometer showed a H_2O and O_2 content below the ppm level, and a dew point of

-99.8 °C was measured with a Michell Easydew[®] sensor. Furthermore, due to the high efficiency of the Ta getter included in the gas loop, a ratio of $\text{H}_2:\text{H}_2\text{O}:\text{O}_2$ of 10:1:1 was obtained in the gas carrier. The harsh conditions in the recoil chamber may allow for the atomization of the hydrogen traces in the gas carrier, yielding to a considerable amount of atomic H able to react with At. Hence, it cannot be excluded that the observed transport of ^{211}At is related to the formation of a hydride species, e.g. HAT , similar to the already observed *in situ* formation of BiH_3 and PoH_2 [4]. This interesting observation needs to be confirmed in further data analysis and future experiments.

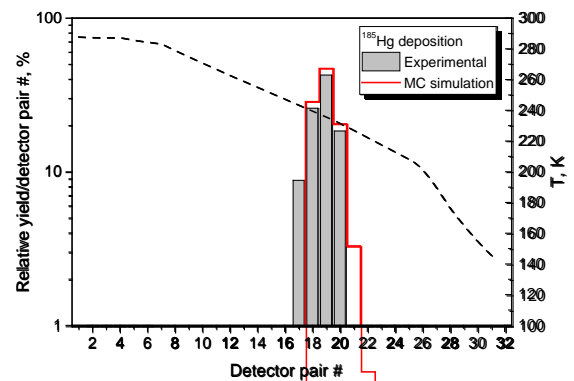


Fig. 1: Experimental ^{185}Hg deposition pattern (grey bars) and its related Monte Carlo simulation (red line), indicating a contamination of the first Au covered detectors.

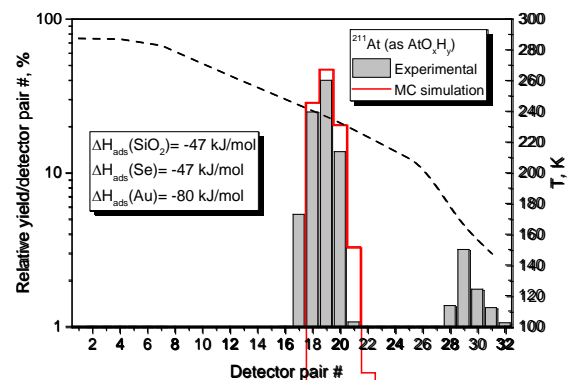


Fig. 2: Experimental ^{211}At deposition pattern (grey bars). The contamination of the Au detectors and the crystallization of the Se detectors are included in the Monte Carlo simulation (red line).

- [1] N. Chiera et al., Ann Rep. Lab. of Radio- & Environ Chem., Univ. Bern & PSI, 7 (2015).
- [2] R. Eichler et al., Radiochim. Acta **98**, 133 (2010).
- [3] A. Serov et al., Radiochim. Acta **99**, 593 (2010).
- [4] R. Eichler, J. Phys. Conf. Ser. **420**, 012003 (2013).

STABILITY OF GROUP 6 HEXACARBONYL COMPOUNDS $M(\text{CO})_6$

R. Eichler (PSI & Univ. Bern) for the “Carbonyl” collaboration*

Second generation experiments are under way to investigate the thermodynamic stability of the intramolecular bond between the central metal atom of complexes and the ligands addressing the influence of relativistic effects in the heaviest compounds. The relevant thermodynamic measure for this property is typically represented as the first carbonyl bond dissociation enthalpy (FBDE). Relativistic density functional theory indicates the hexacarbonyl species of Mo, W, and Sg as the most stable ones and suggests a stability (FBDE) increase towards the heavier elements [1]. Model experiments with isotopes of Mo and W revealed [2,3] that thermal decomposition studies on a silver surface assess the FBDE on a molecular level. A typical decomposition setup used for this purpose comprised a tubular flow reactor of 1 m length and 4 mm inner diameter entirely covered inside with thin silver foils. The reactor could be heated to defined temperatures between room temperature and 600 °C. The amount of hexacarbonyl species able to pass this reactor in dependence of the selected isothermal temperature is measured in comparison to the total amount produced. In a three weeks campaign, first decomposition experiments with $^{265}\text{Sg}(\text{CO})_6$ have been performed successfully. The preliminary results are shown in Figure 1 ($\text{Sg}(\text{CO})_6$ red symbols). The results obtained previously [2,3] for $\text{Mo}(\text{CO})_6$ (blue symbols) and $\text{W}(\text{CO})_6$ (green symbols) are shown. A kinetic decomposition model was developed superimposing gas chromatographic transport of species through the open tubular reactor with heterogeneous decomposition of the species upon adsorption on the inner surfaces of the reactor [3]. This model is applied to relate the decomposition observations to the FBDE given for the hexacarbonyl complexes and was used in [3] to formulate an expectation for the behaviour of $\text{Sg}(\text{CO})_6$ based on the predicted stability from [1] (see Fig. 1, red shaded area). The final data analysis of the experiment is ongoing and certainly one obvious outcome is, that more data is required to improve the statistical significance of the interesting observation. Therefore, the finalization of the experimental work is highly desirable in the near future. Even more exciting are the results of recent predictions from relativistic density functional theory [4] revealing a lower stability of $\text{Sg}(\text{CO})_6$ compared to $\text{W}(\text{CO})_6$ (see Fig. 1, grey shaded area).

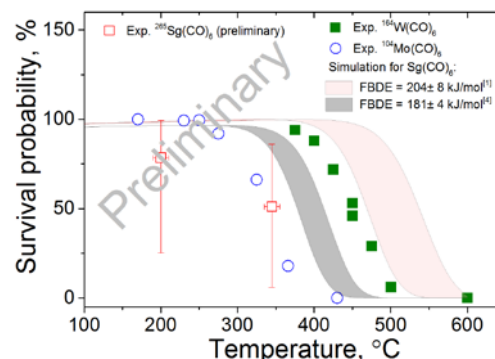


Fig. 1: Experimental decomposition curves of $\text{Mo}(\text{CO})_6$ (blue symbols), $\text{W}(\text{CO})_6$ (green symbols), and preliminary for $\text{Sg}(\text{CO})_6$ (red symbols). The prediction intervals for $\text{Sg}(\text{CO})_6$ as given in [1,4] are shown (shaded areas).

- [1] C. S. Nash, B. E. Bursten, *J. Am. Chem. Soc.* **121**, 10830 (1999).
- [2] I. Usoltsev et al. *Radiochim. Acta* **104**, 141 (2016).
- [3] I. Usoltsev, R. Eichler, A. Türlér, *Radiochim. Acta* DOI: 10.1515/ract-2015-2447 (2016).
- [4] M. Iliaš, V. Pershina, *Inorg. Chem.* DOI: 10.1021/acs.inorgchem.6b02759.

The Carbonyl Collaboration:

M. Asai³, H. Brand⁴, N.M. Chiera^{1,2}, A. Di Nitto^{4,5}, R. Dressler¹, Ch.E. Düllmann^{4,5,6}, J. Even^{4,6}, R. Eichler^{1,2}, F. Fangli⁷, M. Goetz^{4,5,6}, H. Haba⁸, W. Hartmann⁴, E. Jäger⁴, D. Kaji⁸, J. Kanaya⁸, Y. Kaneya³, J. Khuyagbaatar^{4,6}, B. Kindler⁴, Y. Komori⁸, B. Kraus^{1,2}, J.V. Kratz⁵, J.Krier⁴, Y. Kudou⁸, N. Kurz⁴, S. Miyashita^{3,9}, K. Morimoto⁸, K. Morita^{8,10}, M. Murakami^{8,11}, Y. Nagame³, K. Ooe¹¹, D. Piguet¹, N. Sato⁸, T.K. Sato³, J. Steiner⁴, P. Steinegger^{1,2}, T. Sumita⁸, M. Takeyama⁸, K. Tanaka⁸, T. Tomitsuka¹, A. Toyoshima³, K. Tsukada³, A. Türlér^{1,2}, I. Usoltsev^{1,2}, Y. Wakabayashi⁸, Y. Wang⁷, N. Wiehl^{5,6}, A. Yakushev^{4,6}, S. Yamaki⁸, S. Yano⁸, S. Yamaki⁸, Z. Qin⁷

¹Paul Scherrer Institute, 5232 Villigen, Switzerland.

²University of Bern, 3012 Bern, Switzerland.

³Advanced Science Research Center, Japan Atomic Energy Agency, Tokai, Ibaraki 319-1195, Japan.

⁴GSI Helmholtzzentrum für Schwerionenforschung GmbH, 64291 Darmstadt, Germany.

⁵Johannes Gutenberg-Universität Mainz, 55099 Mainz, Germany.

⁶Helmholtz-Institut Mainz, 55099 Mainz, Germany.

⁷Institute of Modern Physics Lanzhou; Chinese Academy of Sciences, 730000 Lanzhou, China.

⁸Nishina Center for Accelerator-Based Science, RIKEN, Wako, Saitama 351-0198, Japan.

⁹Hiroshima University, Kagamiyama, Higashi-Hiroshima 739-8526, Japan.

¹⁰Kyushu University, Higashi-Ku, Fukuoka, 812-8581, Japan.

¹¹Niigata University, Niigata, Niigata 950-2181, Japan.

IMPROVED SET UP FOR THE EVALUATION OF CARBONYL COMPLEX FORMATION OF FISSION PRODUCTS AS MODELS FOR SHE

Y. Wittwer (Univ. Bern & PSI), R. Eichler, D. P. Herrmann (PSI), A. Türler (Univ. Bern & PSI)

Since the first synthesis and detection of a Sg carbonyl complex was reported by Even et al. [1] in 2014, a number of experiments were initiated in order to further investigate the molecular properties of this new compound. Along this direction model experiments were performed to investigate the thermal stability of group 6 hexacarbonyls under various conditions [2] and a model was developed to quantify thermodynamic dissociation enthalpies from these experimental results [3]. First research campaigns investigating seaborgium carbonyls were performed at GSI and RIKEN [4]. Despite all of this experiments resulting in very promising results, it appears that especially the experiments with the transactinide element are suffering from low statistics, which can be partially assigned to very low chemical yields of the desired carbonyl complexes and the formation of yet unidentified side products. In order to understand and tackle these problems, we decided to construct a new experimental apparatus that allows us to perform a number of model experiments targeted at identifying factors influencing the formation of various carbonyl complexes synthesized at a single atom scale. From the re-evaluation of older datasets, we are especially expecting impurities in the synthesis gas and the kinetic energy of the carbonyl forming nuclei at entering the reaction chamber to be crucial factors for the formation of carbonyl complexes. Both factors will be controlled by the new setup.

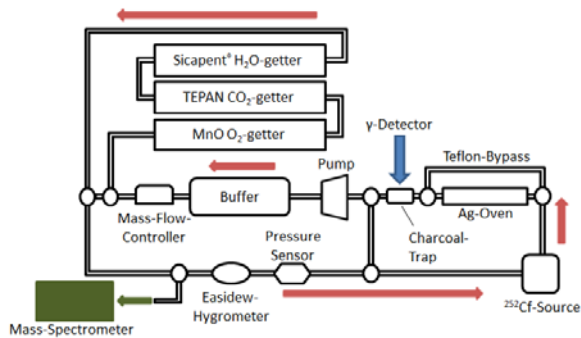


Fig. 1: Principle of the new apparatus. The red arrows show the gas flow direction, the round circles represent valves that are used to separate different parts of the apparatus.

The apparatus is based on the working principle of Miss Piggy [5] that was already successfully used by Usoltsev et al. [2] for their model experiments. A ^{252}Cf source mounted in a Teflon housing produces a constant amount of fission products recoiling out of the source. The source is flushed with a gas stream, allowing volatile products to leave the housing and being trapped in a charcoal trap, where they can be detected by a HPGe γ -detector. By adding carbon monoxide to

the gas stream, the formation of volatile carbonyl compounds is initiated.

Basically, the new setup can be divided into three parts as shown in Fig. 1: A gas purification loop, a simple oven with bypass suitable for decomposition studies and the source itself. The gas purification loop consists of three purification steps, thereby following a well-established cleaning arrangement that was already used successfully in experiments at RIKEN. Briefly, a first column filled with MnO is used for catalysing the transformation of trace oxygen with the surplus carbon monoxide to carbon dioxide followed by a TEPAN-on-PMMA filled column for removing the produced CO_2 and a last one filled with Sicapent[®] for the removal of water. The purity of the used gas is constantly monitored using a MKS CIRRUS 2[®] mass spectrometer and a MICHELL-Easidew[®] hygrometer. The use of an internal loop purification unit allows us to work under much cleaner conditions than it was possible using the initial setup with Miss Piggy [2-3]. Additionally, the purification is constructed to allow an easy exchange or regeneration of each cleaning column.



Fig. 2: Representation of the new ^{252}Cf fission source. Most prominent is the wheel containing 8 holes for different stopping foils and a blind position for closing the source. Above the wheel, the reaction chamber with gas in- and outlets is visible. The holder containing the ^{252}Cf sample is placed directly below the recoil volume. The entire setup is surrounded by a vacuum tight chamber.

While in the old Miss Piggy setup it was not possible to adjust or vary the energies at which the recoiling fission products enter the gas, the new source design provides an easy way to achieve this. As pictured in Fig. 2, a wheel is placed directly above the ^{252}Cf -

source holder containing a number of holes, spanned with aluminium foils of different thicknesses. Thus, simply by turning the wheel the energy of the fission products entering the gas flushed reaction chamber can be selectively degraded. Fig. 3 shows a series of simulations using the TRIM software by J.F. Ziegler [6] and an empirical correction factor to account for the overestimation of gas stopping powers commonly done by TRIM [7]. The figures illustrate the possibilities to stop fission products emitted by the ^{252}Cf -source in the adjacent reaction chamber. Through variations of the used gas mixture and stopping foils, the stopping position as well as the energy distribution can be easily adjusted.

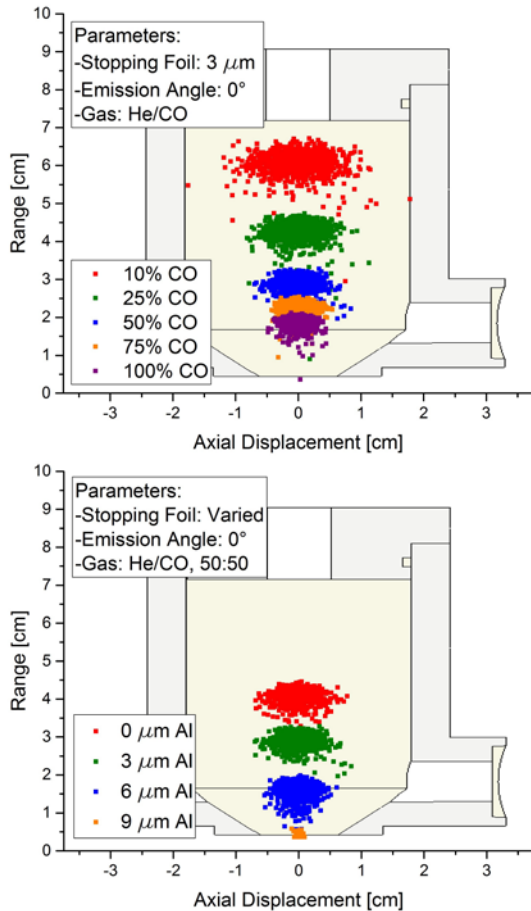


Fig. 3: Example of simulations showing the effect of different gas compositions on the range of ^{105}Mo as it is produced by a ^{252}Cf -source located at the origin. The schematic of the reaction chamber (see also Fig. 2) is shown in the background in order to illustrate the position of ions after complete stopping. The wheel containing the stopping foils is placed directly between the chamber and the x-axis (not shown here). Note that there is an additional 6 μm Al foil permanently placed as a source cover included in the simulation. For each picture, 1000 ion-trajectories were simulated with an emission angle of 0° with respect to the y-axis. All simulations were done using the TRIM software[6]. **Top:** Emission through a 3 μm Al-foil into a reaction chamber filled with He/CO-mixtures of different compositions. **Bottom:** Emission into a 50:50 He/CO-gas mixture with varied Al-stopping-foil-thicknesses.

The source is designed to easily allow the exchange of the pre-stopping foils in order to insert different foil thicknesses or even different foil geometries. The main parts of the reaction chamber are manufactured from PFA[®]-Teflon in order to minimize adsorption effects of the produced, volatile species. All the non-Teflon parts which might come in contact with the formed carbonyl compounds are made out of Al, which was shown previously not to interact with the fragile species [2].

After a series of simulations using the TRIM software and a number of Monte Carlo Simulations implemented in Matlab[®], we decided to use aluminium foils with thicknesses between 3 and 20 μm together with a simple, flat geometry in our first experiments. If a serious effect of the stopping range on the formation of carbonyls is identified, a dome-like shape of the pre-stopping foils might be considered to account for the various emission angles of the fission products. Even if the experiments done with Sg are the trigger for this project, we are also planning to extend our studies to group 7, group 8, and possibly group 9 elements, which should be easily possible using the same setup. Since most parts of the new apparatus are already build and ready for operation, we expect the apparatus to be fully useable in the first quarter of 2017.

ACKNOWLEDGEMENT

The work is supported by the Swiss National Science Foundation (200021_162769).

- [1] J. Even et al, *Science*, **345**, 1491 (2014).
- [2] Usoltsev et al., *Radiochim. Acta* **104**, 141 (2016).
- [3] Usoltsev et al., *Radiochim. Acta* **104**, 531 (2016).
- [4] TASCAs 16 Workshop GSI, 26.08.2016.
- [5] Ch. E. Düllmann et al., *Nucl. Instr. Meth. Phys. A* **595**, 512 (2003).
- [6] J. F. Ziegler et al., *Nucl. Instr. Meth. Phys. B* **268**, 1818 (2010).
- [7] D. Wittwer et al., *Nucl. Instr. Meth. Phys. B* **268**, 28 (2010).

ISOTHERMAL VACUUM CHROMATOGRAPHY OF ^{211}Pb ON SiO_2

B. Kraus, R. Eichler, A. Türler (Univ. Bern & PSI), P. Steinegger (FLNR)

Gas chromatographic investigations have been and still represent the state-of-the-art chemical investigations of transactinides [1, 2]. The short half-lives of these elements forced scientists to develop very fast and highly efficient systems, which led to highly sophisticated experimental setups [2]. Nevertheless, their advancement still requires further development, especially with regard to speed, which could offer an even broader range of shorter-lived heavy elements to investigate. The speed gain can be achieved by evacuating the gas chromatographic setup and exploiting the molecular flow regime. This regime is governed by the so-called “random walk” as particles move due to adsorption and desorption processes in random directions of straight trajectories without collisional interactions. One of the methods which rely on the molecular flow regime and the random walk is the isothermal vacuum chromatography (IVAC). The continuously running IVAC method is spotlighted in this report, where lead (Pb) was investigated as a lighter homolog of element 114, flerovium (Fl), regarding its adsorption behavior on a quartz surface.

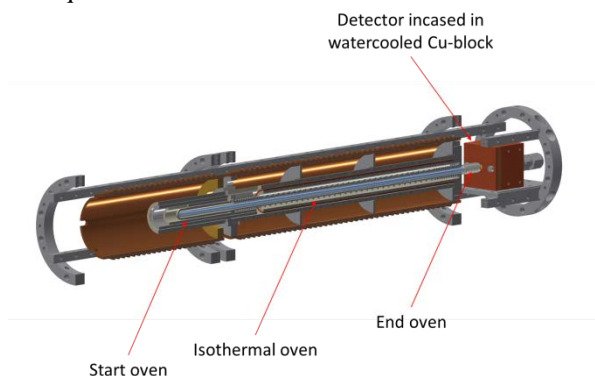


Fig. 1: IVAC setup with three independent ovens and cooled diamond detector.

The desired lead-isotope ^{211}Pb was provided by an intermetallic Pt^{227}Ac source, and was released into the one-side closed quartz column by continuously heating the source in the start oven part to above $1000\text{ }^\circ\text{C}$. The temperature of the quartz column could be varied using the isothermal oven. Freshly prepared diamond detectors were used for the detection of the single atoms of ^{211}Pb or its decay daughter ^{211}Bi by on-line alpha-spectroscopy. A Monte Carlo approach is often chosen to simulate radioactive decay and the random walk, and ultimately to determine the thermodynamic properties from experimental results [3] – in this case an existing Monte Carlo simulation (MCS) written in Pascal/Delphi was adapted to the programming language C# and extended in regard to feature the real temperature profile of the used IVAC setup. As a validation for the code’s correctness, the simulated

data of a previous experiment performed with Tl on SiO_2 [4] achieved results in good accordance to the experimentally determined values.

Surprisingly, the comparison of simulated data (see Fig. 2) with the first experimental results (black symbols) revealed an adsorption enthalpy of about $-\Delta H_{\text{ads}} = 235$ to 240 kJ/mol . Empirical correlations between the microscopic adsorption enthalpy and the macroscopic sublimation enthalpy expect this adsorption interaction for PbO. The anticipated Pb would be expected in the range of ca. $-\Delta H_{\text{ads}} = 160$ to 205 kJ/mol .

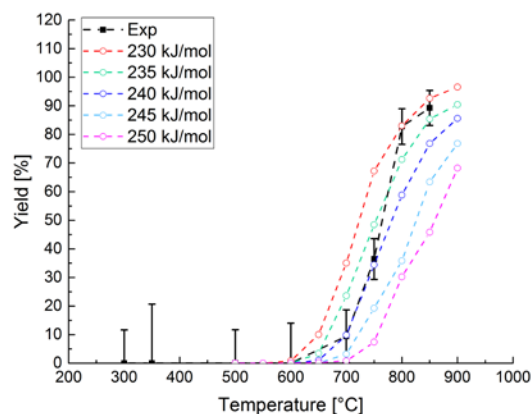


Fig. 2: Comparison of experimental (black) and simulated results (coloured).

In general, the IVAC method was successfully applied, but it needs further chemical R&D to obtain elemental Pb. The future use of Ta metal foil in the hot region inside the starting oven shall secure the elemental state of Pb. The success of this tweak represents an important prerequisite also for the future investigations of transactinides Nh to Lv. Therefore, the model system presented in this report is very valuable and will be further exploited. Furthermore, the advancement of the IVAC method described in [4] to an applicable on-line method for direct investigation of short-lived superheavy nuclei at an accelerator site will be pursued, especially with a focus on speed investigations and efficiency optimizations.

- [1] K.J. Moody, et al., *The Chemistry of Superheavy Elements*. 2nd Ed. (2014).
- [2] A. Türler, V. Pershina. *Chem. Rev.* **113**, 1237 (2013).
- [3] I. Zvara; *The Inorganic Radiochemistry of Heavy Elements*. 1st Ed. (2008).
- [4] P. Steinegger, et al., *J. Phys. Chem. C* **120**, 7122 (2016).

CHARACTERISATION OF SAMPLE AND TARGET THICKNESSES USING ADVANCED ALPHA-SPECTROSCOPY SIMULATION

R. Dressler (PSI)

A major prerequisite to extract cross section data from nuclear reaction studies is the knowledge about the composition, content, and thickness of the target. The technical demands to handle and characterise radioactive targets are more complicated compared with targets using stable isotopes only. The radio protection regulations, but also the mechanical sensibility and the particular uniqueness require special care.

The determination of the absolute thickness of the target assembly plays a special role, if charged particles are involved in the entrance- or exit-channel of the nuclear reaction. Not only the thickness of the deposition layer containing the target isotopes but also the thickness of backing- or cover-foils must be known if the kinetic properties of the charged particles are directly exploited to determine the wanted quantity.

Performing suitable measurements of layer thickness with uncertainties of less than 10% is a challenging task for such samples. On the one hand measurement using a mechanical profilometer cannot be applied to radioactive or very fragile samples without risk to destroy the sample or contaminate the measurement device. On the other hand the use of an optical profilometer is limited to transparent samples. In addition, both types of profilometry are relative measurements related to a well-defined reference height within the sample setup in the device itself.

An alternative approach to determine layer or deposition thicknesses is to exploit the energy loss of α -particles passing the entire sample assembly.

Alpha-rays as a current of massive charged particles lose a considerable amount of their kinetic energy while passing matter. An extensive data collection of stopping force measurements of α -particle in various media exists (see [1] for an overview and [2] and [3] for all available data) and present-day Monte-Carlo simulation codes take advantage of this knowledge.

We present here investigations utilizing the “advanced alpha-spectroscopy simulation” (AASI) program version 1.1 [4-6] to characterise the deposition-layer and backing thicknesses of a (24.47 ± 0.53) GBq ^7Be target produced at PSI [7]. This target was used recently to measure the excitation function of the astrophysical interesting $^7\text{Be}(n, \alpha)^4\text{He}$ reaction at the experimental area II of n_TOF facility at CERN [8].

The AASI program provides the energy response of silicon-based detectors using a Monte-Carlo approach taking into account not only the intrinsic detector parameters as they are the intrinsic full width at half maximum (FWHM) of the electronic signal, the thickness of the silicon substrate but also the thicknesses of the detector dead layer, two independent tailing parameters describing the fast- ($1/\lambda$) and the slow-tailing

($1/\mu$) as well as the area ratio between both tailings (ρ), the material between the detector and the source, and the thickness of the source itself (self-absorption effects). In addition, scattering effects of the α -particles onto the source backing and α - β -coincidence summing effects were taken into account.

Fig. 1 visualizes the change of the energy spectrum if different features related to target or detection were activated in the Monte-Carlo simulation. The α -spectra were simulated using 5×10^7 particles emitted from a 7.8 mm diameter sample placed in 21 mm distance in front of a PIPS silicon detectors (Canberra A-450-21AM, 450 mm² active surface, silicon substrate 150 μm , dead layer 50 nm SiO₂, 21 keV guaranteed resolution). To simplify the discussion of the effects changing the spectra a hypothetical mono-energetic 5500 keV α -emitter was used.

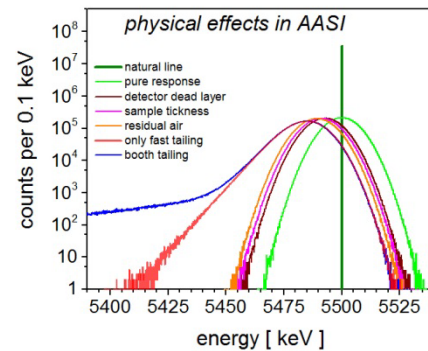


Fig. 1: Physical effects taken into account using AASI visualized for the case of a 5500 keV α -emitter.

The dark green line symbolizes the spectrum of the emitted α -particles. The natural line with of α -rays is connected via the Heisenberg Uncertainty Principle with the live-time of the decaying isotope. For all known α -emitters the natural line width is very small and does not exceed 1 μeV even for the very short lived. The green line shows the signal from the bare Si-crystal connected to the amplification and digitisation stages. The wine, magenta, and orange line shows the additional energy degradation effect of the dead-layer, the self-absorption in the 20 nm thick sample and in the residual gas between the sample and the detector (about 12 mbar), respectively. The red and blue lines show the effect of additional tailing parameters. At least two such tailing parameters are needed for a reasonable model description of experimental spectra [9]. There is a notable energy shift caused by the used convolution formula as a mathematical artefact.

The most important prerequisite to determine layer thicknesses is an as good as possible determination of the four detector immanent peak shape parameters

(FWHM, $1/\lambda$, $1/\mu$ and ρ) and the intrinsic energy shift between recorded and simulated spectra. In addition to fixing these parameters, special care must be taken to a stable operation of the α -spectroscopic setup to prevent unobserved gain- or offset-drifts. The estimation of the shape parameters was performed using a two-step minimum least square estimate, first of the FWHM and the fast-tailing parameter and subsequent of the slow-tailing and the area ratio of the tailings.

In Fig. 2 the spectrum of a ^{241}Am reference source recorded over 16 h (grey line original; dark green shifted by 17.61 keV) is plotted together with AASI results using the best fit shape parameters ($1/\lambda = 5.57$ keV, $1/\mu = 51.08$ keV, $\rho = 47.81$ and FWHM = 16.19 keV).

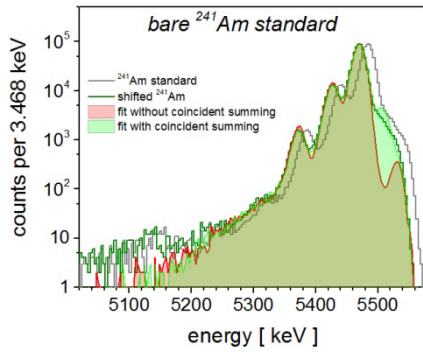


Fig. 2: Comparison of a recorded and shifted spectrum of a ^{241}Am standard with AASI results without and with coincident summing

Although ^{241}Am is one of the common used reference nuclides for α -spectroscopy, it exhibits the special feature that in coincidence with the most abundant α -particles energy Auger electrons with energies between 6.04 keV and 13.52 keV are emitted which may pile-up with the registered α -particles energy. These pile-ups affect most prominently the high energetic part of the spectrum. Fig. 2 shows in addition the AASI results without (red filled area) and with (green filled area) coincident summing. Although the AASI results agree well considering the coincident summing effect, the high energy edge is not sufficient reproduced and is therefore not taking into account further.

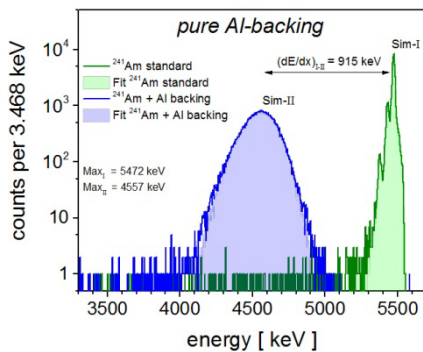


Fig. 3: α -spectra of ^{241}Am standard without and with Al-backing between the source and the detector.

Finally, both effects to the recorded spectrum – the energy shift as well as the change in the shape – where respected to determine the layer thickness of the investigated samples. The fit was realized first varying only the Al-thickness yields and after that tuning the

layer fluctuation. A value of $(5.25 \pm 0.07) \mu\text{m}$ for the thickness and $(0.50 \pm 0.02) \mu\text{m}$ for the fluctuation was obtained. Fig. 3 shows the best result of the Al-backing (blue line recorded data, blue filled area best AASI fit) in comparison to the data of the pure ^{241}Am standard (green line and green filled area).

The same procedures were applied to the final molecular plated ^7Be target after performing the experiments at n_TOF CERN. Herein, it was assumed that beryllium was deposited as $\text{Be}(\text{OH})_2$ and the above obtained parameters for the Al-backing were used. At least, three different layer thicknesses are needed to describe the measured peak shape reasonably. To keep the number of parameters small, no thickness fluctuations were taken into account. Fig. 4 shows the obtained results of the pure ^{241}Am standard (green line and green filled area) and the ^7Be target (blue line) together with deduced energy degradations. The main part of the deposition about 84% of the surface exhibit a thickness of $(1.04 \pm 0.40) \mu\text{m}$ (red filled area), about 1% was covered with a $(3.02 \pm 0.83) \mu\text{m}$ layer (blue filled area), and whereas about 15% of the surface shows a significant depleted deposition simulated as empty part (yellow filled area).

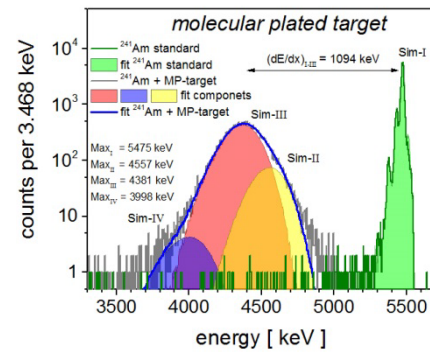


Fig. 4: α -spectra of ^{241}Am standard without and with molecular plated target between the source and the detector.

These investigations established a suitable method to determine layer thicknesses of inactive and also highly radioactive samples using energy loss measurements of α -particles in connection with sophisticated Monte-Carlo simulations.

- [1] H. Paul, D. Semrad, A. Seilinger, Nucl. Instr. Meth. B, **61**, 261(1991).
- [2] www-nds.iaea.org/stopping/stopping_heli.html.
- [3] www-nds.iaea.org/stopping/stopping_upda.html literature cut off 17.1.2017.
- [4] T. Siiskonen, R. Pöllänen, Nucl. Instr. Meth. A **550**, 425 (2005).
- [5] T. Siiskonen, R. Pöllänen, Nucl. Instr. Meth. A **558**, 437 (2006).
- [6] T. Siiskonen, R. Pöllänen, T. Karhunen, ESARDA Bull., **40**, 26 (2008).
- [7] E. A. Maugeri, et al., JINSTaccepted for publication (2016).
- [8] M. Barbagallo, et al., Phys. Rev. Lett. **117**, 152701 (2016).
- [9] S. Pommé, B. Caro Marroyo, App. Rad. Isotopes **96**, 148 (2015).

ANITA (ADVANCED NETWORK FOR ISOTOPE AND TARGET LABORATORIES) – THE URGENT NEED FOR AN EUROPEAN TARGET PREPARATION NETWORK

D. Schumann (PSI)

A wide number of research fields in the nuclear sector requires high-quality and well-characterized samples and targets (Fig.1). In contrast to this, only a handful of laboratories is currently able to deliver the required services. Coordination of activities and sharing of resources is therefore mandatory to meet the increasing needs. This very urgent issue has now been addressed by 6 European target laboratories with an initiative called ANITA (Advanced network for isotope and target laboratories):

- Target chemistry group (Laboratory of Radiochemistry, Nuclear Energy and Safety Research Department) at Paul Scherrer Institute Villigen (PSI), Switzerland
- Target preparation laboratory (Institute for Reference Materials and Measurements) at European Commission, Joint Research Centre Geel (EC-JRC)
- Target laboratory (Heavy Ion Laboratory) at the University of Warsaw, HIL-UW, Poland,
- Target laboratory (Institut für Kernchemie) at the Johannes Gutenberg-Universität in Mainz, (JGU) Germany
- Target laboratory at the Helmholtz Centre for Heavy Ion Research Darmstadt (GSI), Germany
- Target laboratory at Grand Accélérateur National d'Ions Lourds; Caen (GANIL), France

The global aim of ANITA is to establish an overarching research infrastructure service for target production and develop a tight cooperation between the target laboratories in Europe in order to improve the production technique of well-characterized samples/targets.

Moreover, the interaction of the target laboratories with the research teams using these targets shall be triggered and/or intensified to deliver targets best-suited for the envisaged experiments. For the realization of this ambiguous goal, efforts within the European Commission and strong support by the target-using communities will be necessary. In particular, an appropriate funding instrument has to be found and applied, enabling ANITA to develop from an – by interested parties triggered - initiative to a real coordination platform.

The following objectives are envisaged:

- Identification and promotion of synergies with other target producers
- Establishing of a network between the presently leading European infrastructures for isotope and target production
- Development of an open access data base on isotope production facilities and target manufacturers
- Coordination of targets requests, sharing of capacities, distribution of demands
- Transnational visits of scientists and especially students and Postdoc for knowledge exchange and training
- Development of new, innovative equipment for specific applications, accessible for the entire community
- Basic research on target preparation methods and characterization techniques; development of new, improved techniques
- Acquisition of new partners and, also outside Europe, to broaden the network

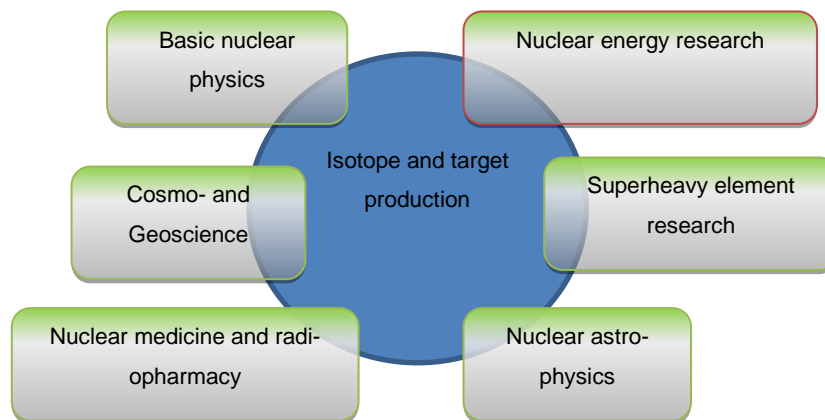


Fig. 1: Sketch of the synergies between different scientific and applied research fields and isotope and target production sites.

EVAPORATION AND ADSORPTION BEHAVIOUR OF RADIOTRACERS RELEASED FROM IRRADIATED TELLURIUM DOPED LBE

E. Karlsson (Univ. Bern & PSI), J. Neuhausen, A. Vögele (PSI), R. Eichler, A. Türler (Univ. Bern & PSI)

INTRODUCTION

To cope with the growing stockpiles of high level nuclear waste around the world, novel reactor designs are required. There is a need for designs which are capable of repurposing used nuclear fuel as well as using new fuel in a more efficient way. An example of such a design is a fast reactor which is capable of making use of ^{238}U in the fuel as well as using ^{232}Th as fuel and also burning off minor actinides in spent fuel. For these types of reactors one can no longer use water as a primary coolant as it would moderate the neutrons to thermal energies which are less suitable for fissioning ^{238}U [1]. Suggested coolants for these reactors are instead gases, molten salts, or heavy liquid metals such as lead or LBE (lead-bismuth eutectic) [2]. This work is focused on LBE as a coolant, studying the evaporation behaviour of fission products as well as activation products from LBE samples and their deposition on SS316L stainless steel surfaces.

EXPERIMENTAL

Preparing samples for these experiments was done by mixing 2 mass% of tellurium into liquid LBE similar to the procedure described in [3]. The sample was then irradiated using the SINQ-neutron source with 10^{13} neutrons/cm²/s for three hours yielding mostly ^{131}I from the (n, γ) reactions with ^{130}Te as well as activation and spallation products from lead and bismuth.

The experiments were conducted using a gas loop to which a gradient tube furnace was connected along with a starting furnace to initially evaporate the sample, a Sicapent® moisture absorber and a dew point meter (Michell PuraOEM) to monitor the moisture content. At the end of the tube furnace, a carbon filter was installed to prevent contamination of the gas loop. Along the tube furnace a temperature gradient was applied from 1000 °C down to room temperature. The gases used in the experiments were helium, oxygen, and hydrogen. These three were selected to represent an inert, oxidizing, and reducing environment. Flow rates varied between 28-45 ml/min (oxygen 28 ml/min, hydrogen 30 ml/min, helium 45 ml/min) due to difficulties calibrating the mass flow controller at such low flow rates. The flow rates were verified using a mini-BUCK Calibrator M-5 from A.P. Buck Inc.

From the irradiated sample smaller pieces of approximately 50-100 mg were cut to be used in the experiments. After cutting the sample it was placed in a stainless steel boat. This boat was subsequently placed inside a stainless steel column in the position where it would sit inside the starting furnace when

the column was inserted into the furnace.

The starting furnace was set to run at 700 °C to ensure complete evaporation of the iodine while not evaporating the LBE-matrix itself [4]. After the initial evaporation period of 90 minutes the starting furnace was turned off and after an additional two hours the tube furnace was switched off as well as the gas flow.

The stainless steel column was measured using an HPGe-detector with a lead collimator in single centimetre steps yielding a distribution of the activity over the column. This distribution was used as a basis for a Monte Carlo simulation of the gas phase transport and adsorption deposition of iodine and other radionuclides in the column. The Monte Carlo simulation was fed with experimental data such as column material data, pressure, gas, experiment time, as well as the temperature gradient. This was combined with a guess of the adsorption enthalpy which was altered until the simulated deposition pattern fitted the experimental results. Thus, an adsorption enthalpy ΔH_{ads} of the species at zero surface coverage with the column material was deduced.

RESULTS AND DISCUSSION

From the plots of the activity distribution in Fig. 1 a) through c) it can be qualitatively concluded that iodine forms compounds with low to very low adsorbance on stainless steel in all three gases.

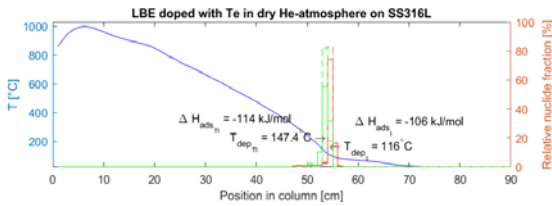
The experiment in dry helium atmosphere (Fig.1 a)) was performed first in the series after the irradiation, which is likely the explanation why ^{200}Tl is visible, as it has a rather short half-life (26.1 h) [5]. Due to the inert conditions thallium would be expected in its elemental form, however, contaminants such as moisture or oxygen can never be completely excluded. In this case, macroscopic amounts of iodine would be expected to be in either monoatomic or dimeric form. However, with the iodine concentrations present in these experiments two iodine atoms are unlikely to interact with each other, therefore generally, simple compounds formed from trace contaminations in the carrier gas containing one single iodine atom or just atomic iodine are expected.

For dry oxygen atmosphere (Fig.1 b)) the situation is more complex as the iodine is now in a reactive environment, where it can form additional compounds. Two depositions are observed here, one at 48 °C and one at 28 °C indicating very weakly adsorbing compounds. Speciation in this case is very difficult as many more variables are introduced compared to the inert helium case. The chemistry of iodine oxides is

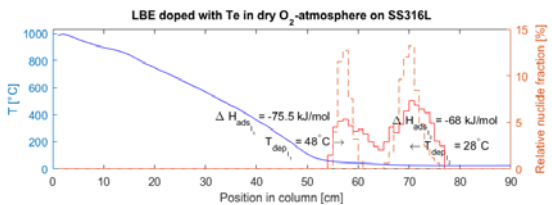
complex and many of these compounds are not well characterized [6]. Beside the rather simple IO_2 and IOH , according to [6, 7] even the endothermic radical IO can exist as gas phase species that could form in the present experiments at high temperatures. However, it remains questionable whether these species are stable enough to be transported over hot steel surfaces to low temperatures in the gradient tube.

The highest-temperature iodine deposition in this experiment series appears under dry hydrogen atmosphere (Fig.1 c)). Given the low deposition temperature, this species still has to be considered weakly adsorbing on stainless steel. Based on chemical reasoning the deposited species could be hydrogen iodide.

a)



b)



c)

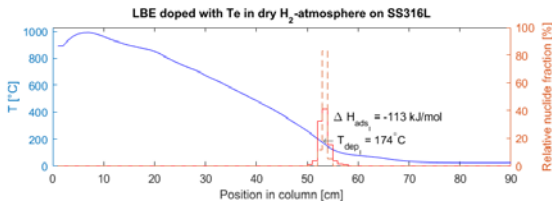


Fig. 1: Histograms of iodine and thallium depositions (red and green curves, respectively) observed in the experiments with steel and dry (a) helium, (b) oxygen, (c) hydrogen as the carrier gas. The blue line is the temperature gradient over the column and the dashed histograms are the output of the Monte Carlo simulation from which ΔH_{ads} is calculated.

After the experiment series was finished, a longer γ -measurement of 2 hours was performed on the charcoal filter, which was attached downstream of the steel column.

The spectrum obtained can be seen in Fig 2. Peaks corresponding to ^{203}Hg and ^{131}I were found in the spectrum. The iodine is likely one or more compounds with yet weaker adsorption formed either by reaction with the gas in the hydrogen/oxygen-experiments or with impurities such as small amounts of H_2O . The mercury deposition in the charcoal filter

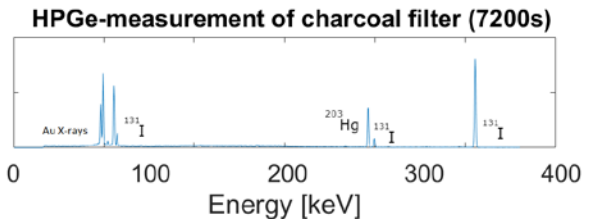


Fig. 2: γ -spectrum of the charcoal filter measured for 2 hours after finishing the LBE series of experiments with dry gases on stainless steel. ^{131}I and ^{203}Hg γ -peaks are visible as well as x-rays of Au originating from Hg decay.

indicates either that a mercury compound with low adsorbance has been formed or that the steel surface is completely oxidized preventing the metallic interaction of elemental mercury with Cr, Ni or Fe. Measuring their adsorption enthalpies will require further cooling by means of either dry ice or liquid nitrogen to bring the temperature of the cold side of the column down. Mercury was observed depositing on oxide surfaces and ice with $\sim 30\text{--}42$ kJ/mol at $(130\text{--}160)$ °C [8]. The results of this experiment series indicate that iodine released from LBE forms several different weakly adsorbing species depending on the gas used. For better speciation, further experiments at varied controlled partial pressures of the involved reactive gases and perhaps additional methods are required.

ACKNOWLEDGEMENT

This work was funded by the project MYRTE under EURATOM HORIZON2020 Grant Agreement No. 662186.

- [1] W. D. Allen et al., Proceedings of the Physical Society. Sec. A **70**, 573 (1957).
- [2] P. Hejzlar et al., Nuc. Eng. & Design **239**, 2672 (2009).
- [3] E. A. Maugeri et al., Ann Rep. Lab. Of Radio-& Environ Chem., Univ. Bern and PSI, p. 50 (2015).
- [4] J. Neuhausen et al., Radiochim. Acta **94**, 239 (2006).
- [5] F. G. Kondev et al., Nuclear Data Sheets **108**, 1471 (1999).
- [6] N. N. Greenwood, A. Earnshaw, Chemistry of the Elements, Pergamon, Oxford, 1990.
- [7] I. V. Nikitin, Russ. Chem. Rev **77**, 739 (2008).
- [8] S. Soverna et al., Radiochim. Acta **93**, 1 (2005).

ADSORPTION BEHAVIOUR OF CAESIUM ON FUSED SILICA AND STAINLESS STEEL SURFACES

E. Karlsson (Univ. Bern & PSI), A. Colldeweih, J. Neuhausen (PSI), R. Eichler, A. Türler (Univ. Bern & PSI)

INTRODUCTION

To license a new reactor design one needs to be able to make accurate simulations of its behaviour during operation as well as during anomalous events. Doing this properly requires knowledge about physical and chemical properties of all materials involved in the design.

This work is concerned with determining adsorption enthalpies of caesium by evaporating it and observing its adsorption behaviour on stainless steel and fused silica surfaces in various gases to which a temperature gradient is applied. The deposition data gathered from these experiments is then fed into a Monte Carlo simulation program from which the characteristic adsorption enthalpies can be extracted that represent crucial data for deposition and transport modelling in real scenarios.

EXPERIMENTAL

To investigate the adsorption behaviour of caesium a technique called thermochromatography is used. This is based on evaporating caesium nitrate marked with ^{137}Cs in a gas stream which is passed over a negative temperature gradient tube furnace reaching from 1000°C down to room temperature in a stainless steel or fused silica column. The various gas compositions used are helium (inert), oxygen (oxidizing) or hydrogen (reducing) with varied moisture contents. When using the dry gases the moisture content is monitored using a dew point meter (Michell PuraOEM) and a Sicapent® absorber is installed to remove residual moisture. From the dew point meter readings a water content of between 2-20 ppm (vol %) in the dry experiment gases could be calculated. The oxygen content is not monitored; however, a tantalum getter is used to reduce it. For the moist gases a bubbler is installed to saturate the gas with water at room temperature prior to entering the column. Preparing the sample is done by allowing a droplet of a CsNO_3 solution (stable caesium with $\sim 5 \text{ kBq } ^{137}\text{Cs}$ tracer, roughly 10^{15} Cs atoms in total) to evaporate on a piece of tantalum foil (or gold foil in the case of oxygen) which is then placed in a stainless steel boat inside the column. The gradient is measured by allowing it to establish along the tube furnace and stabilize over a few hours before inserting a K-type thermocouple in centimetre steps yielding the temperature over the whole column. Starting the experiment is done by turning on a starting furnace enclosing the initial Cs sample upstream of the gradient furnace to evaporate the sample. The only exception to this is the experiment with oxygen atmosphere done in a different setup where the sample is pushed into the hottest part of the gradient at the start of the experiment.

After finishing the experiment the column is scanned in centimetre steps using a lead collimator with a 1-cm-long window in front of an HPGe γ -detector to determine the distribution of activity in the column.

This data along with the experimental parameters such as temperature gradient, time, gas flow speed, pressure, as well as material (minimum oscillation period) and dimensional (inner diameter, length) data for the column is fed into a Monte Carlo simulation program. The program takes this data along with a guess of the adsorption enthalpy and simulates the path and deposition pattern of a large number of particles as they travel down the column. This is repeated while the adsorption enthalpy is adjusted until the simulated deposition pattern agrees best with experiment.

RESULTS AND DISCUSSION

In helium (Fig. 1 a) caesium forms two different species with quite different adsorption behaviour. It is difficult to say with greater precision what they are as the atmosphere is dry and inert. The remaining reaction partners for the caesium are the stainless steel surface, the nitrous gases, nitrogen, and oxygen released from the nitrate and hydrogen released from the tantalum getter.

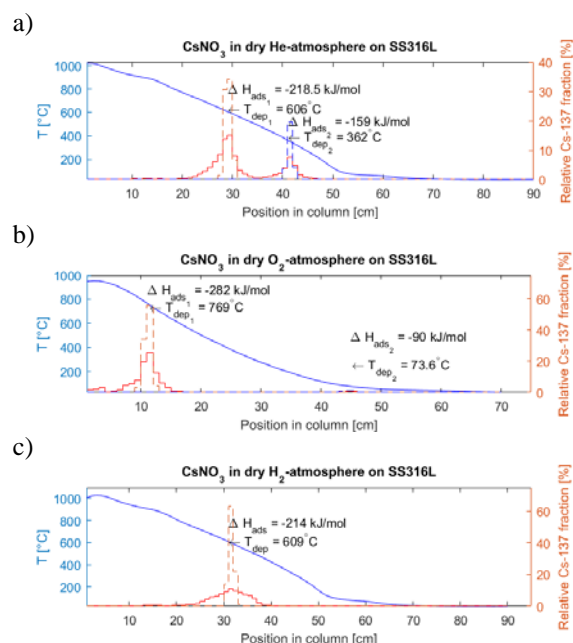


Fig. 1: Histograms of the ^{137}Cs depositions observed in the experiment with steel and dry (a) helium, (b) oxygen, (c) hydrogen as the gas. The blue line is the temperature gradient and the dashed histogram is the output of the Monte Carlo simulation from which the ΔH_{ads} is calculated.

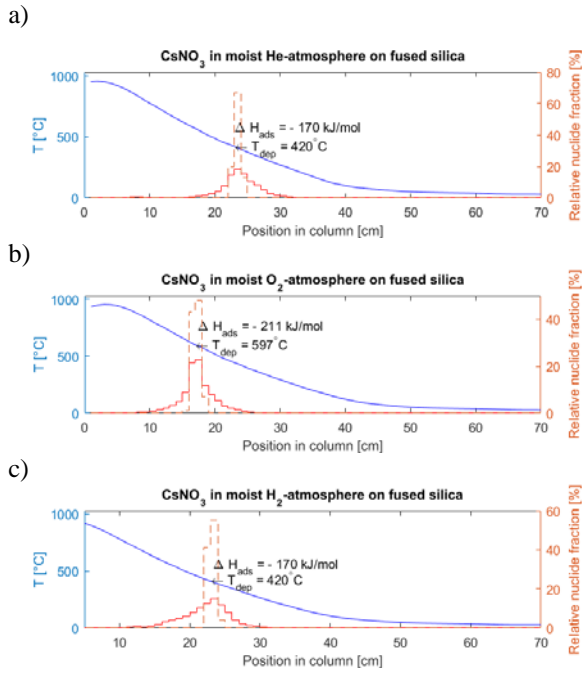


Fig. 2: Histograms of the ^{137}Cs depositions observed in the experiment with fused silica and moist (a) helium, (b) oxygen, (c) hydrogen as the gas. The blue line is the temperature gradient over the column and the dashed histogram is the output of the Monte Carlo simulation from which the ΔH_{ads} is calculated.

The stainless steel surface is made up of a number of elements (Fe, Cr, Ni) in various chemical states which undergo structural changes and reactions depending on the temperature as well as on what atmosphere is applied and how it has been stored, making it difficult to get a clear view of what is happening at the atomic level [1]. Though, it is obvious that caesium does not form compounds in dry helium that adsorb weakly in contact with stainless steel. The same can be said for dry oxygen and hydrogen in Fig. 1 b) & c) while acknowledging a very small amount of caesium transported to low temperature in oxygen.

It is again very difficult to state with confidence what this species is as calculations (Gibbs energy minimization [2]) performed indicate the formation of a single species at the given conditions (CsO_2). What must be considered though is that these calculations may have insufficient thermodynamic data as they disagree with literature, which suggests that CsO_2 decomposes already at temperatures lower than the observed adsorption temperature [3]. There is also a more likely scenario that the small peak at 74 °C is actually a “hot” particle dislodged from the deposition at higher temperature or more likely from the starting position, as the thermal nitrate decomposition is typically quite violent. Otherwise, reactions of CsO_2 with transition metal oxides likely formed on the steel surface in oxygen atmosphere can generally not be excluded. To support the discussion of surface interactions of possible Cs-species with the steel, it is worthwhile to also investigate their interaction with fused silica, since for this material an empirical correlation exists between the sublimation enthalpies of

oxides and hydroxides and their adsorption enthalpies [5] that could allow a speciation of the deposited caesium. In the present study, such experiments have been performed only in moist carrier gases so far.

Despite the presence of moisture as an additional impurity, the situation with the fused silica is still much simpler compared to steel because of its less complex composition and its rather inert character. For example, growth or reduction of surface oxide layers that may play a significant role in adsorption on steel will not occur on fused silica surfaces. Also the capacity for diffusion of the gases into fused silica is low [4]. However, the reaction of the alkali metal species with silica may further complicate the interpretation. In Fig 2. a) - c) the thermochromatograms of caesium on fused silica in the different moist gases are depicted, showing only strongly adsorbing species. Applying the above-mentioned empirical correlation between sublimation and adsorption enthalpies for the most likely candidate in a moist atmosphere (CsOH , calculated by Gibb’s energy minimization [2]) gives large discrepancies, the absolute value of the adsorption enthalpy derived from the sublimation enthalpy [6] being about a factor of 2 smaller than the value determined from experiment. This can be explained by the caesium species having a strong interaction with the fused silica surface, which, as expected earlier, goes beyond normal reversible adsorption making the correlation ineffective in this case. The reaction of silica with an oxidized alkali species is supposed to be stronger than for the metallic species. Our observations of higher deposition temperatures in oxygen support this.

The adsorption behaviour of caesium on the examined surfaces shows favourable features with a good outlook with respect to nuclear safety. Further experiments will include more conditions such as moist stainless steel and dry fused silica as well as noble metals to get a more complete overview of the adsorption behaviour and some prospects for catcher materials.

ACKNOWLEDGEMENT

This work was funded by the project MYRTE under EURATOM HORIZON 2020 Grant Agreement No. 662186.

REFERENCES

- [1] C. E. Milstead et al., *Nuclear Technology* **3**, 495 (1967).
- [2] A. Aerts. Email communication, (September 2016).
- [3] I. I. Volnov. *Peroxides, Superoxides, and Ozonides of Alkali and Alkaline Earth Metals*, Springer, Boston (1966).
- [4] R. W. Lee, *J. Chem. Phys.* **38**, 448 (1963).
- [5] E. A. Maugeri et al. *J. Nuc. Mat.* **450**, 292 (2014).
- [6] I. Barin. *Thermochemical Data of Pure Substances*, VCH, Weinheim (1995).

PREPARATION OF LBE SAMPLES CONTAINING Cs FOR VOLATILIZATION STUDIES

I.I. Danilov, J. Neuhausen, A. Vögele (PSI), E. Müller (PSI/LBR)

INTRODUCTION

Within the HORIZON2020 project MYRTE [1], previous studies on the volatilization of radionuclides from liquid lead-bismuth eutectic (LBE) relevant for the safety of future accelerator driven systems [2-4] will be extended to measuring the volatilization behaviour of fission products such as caesium and iodine from dilute solutions in LBE. It is planned to quantitatively determine the release and deposition of these elements using radiotracers. A prerequisite for this is the production of LBE samples that contain suitable radiotracers of the studied elements. Furthermore, to acquire results that allow extracting physicochemical data for the considered fission product element in dilute solution in the liquid metal, it is important to ensure that the radiotracers present in the sample actually do form a homogeneous dilute solution in the liquid LBE. For this purpose, it is necessary to avoid the formation of oxides containing the radioactive tracers that are insoluble in the liquid metal and therefore tend to separate from the metal phase, as for example observed for electropositive elements in LBE spallation targets [5]. The current strategy for producing samples containing caesium in dilute LBE solution is based on mixing metallic caesium with LBE and subsequent neutron irradiation to obtain ^{134}Cs as tracer isotope that can be quantified by γ -spectrometry. Because of the high affinity of caesium to oxygen, all the work has to be performed under inert gas or vacuum. Furthermore, since LBE as obtained from the manufacturer contains substantial amounts of dissolved oxygen, it is required to reduce oxygen content of the LBE before sample preparation in order to avoid oxidation of the caesium. In this report we describe experiments to prepare LBE samples containing relatively high caesium concentrations that are going to serve as stock samples which will be diluted with inactive LBE after neutron activation to produce the samples for the actual evaporation experiments.

SAMPLE PREPARATION PROCEDURE

Cs was purchased from Aldrich Chemical Co. (99.5% pure ingot). The LBE represents the material to be used within the MYRRHA project and was supplied by Belgian Nuclear Research Centre in Mol (SCK-CEN). Chemical analysis of the LBE was performed at SCK-CEN by neutron activation analysis and ICP-MS (Bi-55.5% / Pb-44.5%; main impurities are: K: 200 $\mu\text{g/g}$, Ca and Fe: 60 $\mu\text{g/g}$ each, Si and Na: 30 $\mu\text{g/g}$ each, Ag: 20 $\mu\text{g/g}$, Se: 9 $\mu\text{g/g}$, Cu: 5 $\mu\text{g/g}$). For the reduction process a Tantalum-foil purchased from Sigma Aldrich was used (purity 99.9% and 0.05 mm thickness).

In order to reduce the oxygen content, the LBE-

material was wrapped in tantalum foil and sealed in a quartz glass ampule under vacuum (5.4×10^{-6} mbar) supplied by a turbomolecular pump. The batch was heated at a rate of 10 K/min up to a holding temperature of 1000°C and processed for 6.5 hours.

Mixtures of LBE with Cs were prepared under high purity argon atmosphere (99.998 Vol%) in a MB 200MOD / 20-G glove box (O_2 and H_2O concentrations < 1ppm) manufactured by MBraun company. The glass ampoule containing the caesium raw material was opened by cutting with a grinding machine equipped with a diamond blade. In order to prevent the oxidation of the Cs, the material was transferred into a gas-tight storage vessel.

For the weighing of the materials we used a balance with a precision of ± 0.0001 mg (Mettler Toledo). About 2 g of the reduced LBE in form of pieces of about 4×3 mm was placed in a boat that was placed on the balance. Then, an appropriate amount of Cs was added directly onto the LBE-pieces. After a short incubation time that depended on the ambient temperature in the glove box, an exothermic reaction took place, accompanied by the release of a green colored fume within one minute. The intensity of the reaction and released fume quantity depends very strongly on the amount of Cs added to the LBE. For Cs amounts of 2 mass% of the LBE, the reaction was relatively mild and a black-grey sintered powder was obtained as reaction product. When larger Cs amounts were used (5-10 mass% with respect to the amount of LBE), the reaction was much more vigorous, causing the metals to melt and form a piece of grey alloy after reaction. The reaction products were then placed into a quartz glass ampule which was sealed under vacuum (10^{-5} to 10^{-6} mbar).

The samples were then homogenized at elevated temperatures. Different homogenization temperatures (300, 450 and 600 °C) were tested to optimize the procedure. The material was heated with 50 °C/h up to the holding temperature and held there for 14 hours. Subsequently, the samples were either quenched or slowly solidified to room temperature. After processing at 600 °C a brown staining of the ampoule walls was observed, while after homogenization at 300 °C and 450 °C the ampoules remained colourless.

PHENOMENOLOGY OF PHASE FORMATION

The samples were ground and polished for the metallographic examination of the surface by SEM and for EDX analysis. Since the alloy is a fairly soft material, we used emery sheets with grit in the range P1200-2500. During the examination of the samples with 2% content of caesium processed at 300 °C a certain tendency to form a bismuth-caesium phase was detected (see Fig. 1).

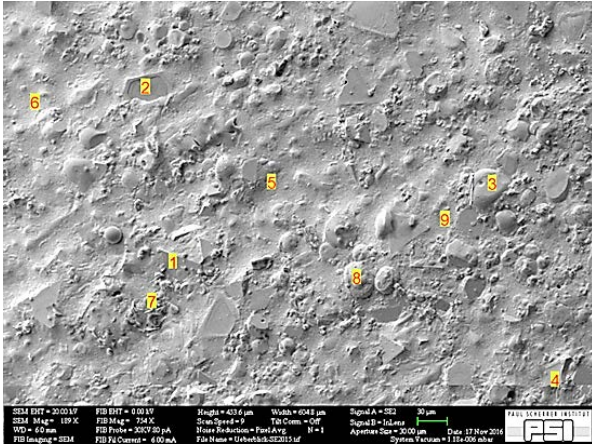


Fig. 1: Polished surface of the sample processed at 300 °C and slowly cooled to room temperature. SEM-Mag.: 189X, Size of green bar: 30 μm .

Tab. 1: Results of EDX-analysis performed at different positions of the sample shown in Fig. 1

Position	Cs, Atom%	Pb, Atom%	Bi, Atom%
1	25.75	0.21	74.04
2	49.14	-2.51	53.37
3	29.27	-0.08	70.81
4	30.04	0.28	69.68
5	0.28	1.47	98.26
6	0.16	59.36	40.47
7	1.34	96.64	2.02
8	29.64	6.06	64.30
9	0.55	62.15	37.31

Apparently, this phase is significantly harder than the surrounding material and hence forms elevated plateaus on the surface after grinding and polishing. The two other samples processed at 450 and 600 °C, respectively, show less pronounced formation of a Cs- and Bi- rich phase and are more homogeneous, especially the quenched samples.



Fig. 2: Plateau observed on the surface of a sample processed at 300 °C after grinding and polishing. In the region of the plateau increased Cs and Bi concentrations were detected.

IRRADIATION OF THE SAMPLES

Various samples were irradiated with neutrons in the SINQ Neutron Source of PSI (typical neutron flux $10^{13} \text{ n}\cdot\text{cm}^{-2}\cdot\text{s}^{-1}$, 1 h irradiation). Apart from ^{134}Cs , typical activation products of LBE such as ^{204}Bi , ^{206}Bi and ^{203}Hg were detected in the sample by γ -spectroscopy. The activated samples contain sufficient ^{134}Cs activity for the planned evaporation studies. As a next step, the homogeneity of the activity distribution will be studied by γ -spectroscopy before evaporation studies are started.

-
- [1] <https://myrte.sckcen.be/>
- [2] Handbook on Lead-bismuth Eutectic Alloy and Lead Properties, Materials Compatibility, Thermalhydraulics and Technologies, OECD-NEA, 2015.
<https://www.oecd-nea.org/science/pubs/2015/7268-lead-bismuth-2015.pdf>.
- [3] B. Gonzalez Prieto, PhD thesis, KU Leuven, Belgium (2015).
- [4] A. Aerts et al., J. Nucl. Mater. **448**, 276 (2014).
- [5] B. Hammer-Rotzler et al., Eur. Phys. J. Plus (2016) 131: 233. doi:10.1140/epjp/i2016-16233-1.

MEASUREMENT OF THE ${}^7\text{Be}(n,\alpha){}^4\text{He}$ REACTION CROSS-SECTION FOR THE COSMOLOGICAL LITHIUM PROBLEM AT THE n_TOF FACILITY AT CERN

M. Barbagallo, A. Musumara (INFN Bari), S. Heintz, E. A. Maugeri (PSI), N. Kivel (PSI/AHL), R. Dressler, D. Schumann (PSI) and the n_TOF collaboration

The theory of Big-Bang Nucleosynthesis (BBN) is one of the most powerful and reliable cosmological models describing the production of elements in the early stage of the Universe. It successfully predicts the abundance of primordial light elements such as H, D, and ${}^4\text{He}$ [1]. For these, as well as for many other isotopes produced in the first minutes of the evolution of the Universe, the predictions of the BBN theory agree very closely with experimental observations of primordial abundances. The only exception is represented by the ${}^7\text{Li}$. In fact, the relative abundance of this isotope predicted by the BBN theory differs from the one inferred from observation of galactic halo dwarf stars, the so-called ‘‘Spite plateau halo stars’’, by as much as a factor of 3. This discrepancy is at present one of the most important unresolved problems in Nuclear Astrophysics, known as the so-called ‘‘Cosmological Lithium problem’’ (CLiP) [2]. Several mechanisms have been put forward to explain this difference: new physics beyond the Standard Model, errors in the inferred primordial ${}^7\text{Li}$ abundance from the Spite plateau stars and, finally, systematic uncertainties in the Nuclear Physics inputs of the BBN calculations. With respect to this last point, since primordial ${}^7\text{Li}$ is produced mostly by electron capture of ${}^7\text{Be}$, a possible explanation for the ${}^7\text{Li}$ -puzzle could be related to an underestimate of ${}^7\text{Be}$ destruction due to the use of incorrect cross sections for neutron-induced reactions on this isotope, in particular for the unknown ${}^7\text{Be}(n,\alpha)$ one. While charged particle induced reactions have been ruled out as possible solution to CLiP in the past, no measurements existed for this reaction cross-section in an extended energy region, namely the range of interest for Nuclear Astrophysics, mainly due to experimental difficulties arising from high specific activity of this isotope (13 GBq/ μg).

The ${}^7\text{Be}(n,\alpha){}^4\text{He}$ reaction-cross section has been measured for the first time in a wide energy range at the newly built second experimental area of the n_TOF facility at CERN [3]. At the neutron energies under investigation, the two α -particles are emitted back-to-back with a maximum energy of 9.5 MeV each. The detection system used in the measurement consisted of two detector sandwiches, each sandwich composed by two single pad silicon detectors 140 μm thick and $3\times 3\text{ cm}^2$ wide [4]. Each sandwich hosted a 1.4 μg ${}^7\text{Be}$ sample, corresponding to about 20 GBq activity. Both samples were prepared at Paul Scherrer Institute (PSI), although two different techniques were used to produce them [5]. The first sample was electroplated on a 5 μm thick Al foil and the second one was prepared by droplet deposition on a 0.6 μm thick polyethylene foil.

Such a system allowed to detect in coincidence the α -particles emitted, providing a peculiar signature of

the occurrence of ${}^7\text{Be}(n,\alpha)$ reactions and a strong rejection of any other source of background. Furthermore, the use of two different sandwich detectors provided redundancy and allowed on the one hand to compare the rate of true events, and on the other hand to estimate the background related to random coincidences evaluated by analysing uncorrelated pairs of detectors. The real and random coincidences can be clearly distinguished in Fig. 1, which shows the amplitude correlation for all silicon pairs: top left and bottom-right panels are related to pairs of silicon hosting the ${}^7\text{Be}$ samples while all the others refer to uncorrelated pairs of detectors.

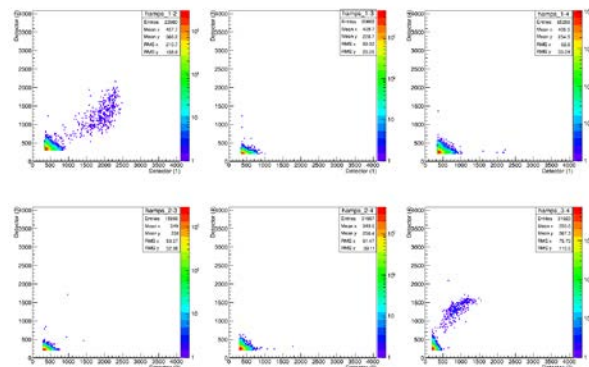


Fig. 1: Scatter plot for signal amplitudes in all possible pairs of detectors of the stack. Top left and bottom right plot refer to pairs hosting the ${}^7\text{Be}$ sample.

The cross-section of the ${}^7\text{Be}(n,\alpha)$ reaction has been determined in the energy range 10 meV-10 keV [6]. The result of this measurement at thermal energy was found to be consistent with the only previous existing measurement [7]. The present data indicate that Wagoner’s compilation [8] overestimates by a factor of 10 the reaction rate. The results of the present measurement leave unresolved the Cosmological Lithium Problem, whose solution should then be searched in other physical scenarios.

-
- [1] T.P. Walker, et al., *Astrophys. J.* **376**, 51 (1991).
 - [2] R.H. Cyburt, et al., *Rev. Mod. Phys.* **88**, 015004 (2016).
 - [3] n_TOF Collab., *Eur. Phys. J. Plus* **131**, 371, (2016).
 - [4] L. Cosentino, et al., *Nucl. Instr. Meth. A* **830**, 197 (2016).
 - [5] E. Maugeri, et al., submitted to JINST, (2016).
 - [6] M. Barbagallo, et al., *Phys. Rev. Lett.* **117**, 152701 (2016).
 - [7] P. Bassi et al. *Il Nuovo Cimento XXVIII* 1049 1963.
 - [8] R.V. Wagoner, *Astrophys J.* **3**, 148 (1967).

PREPARATION AND CHARACTERIZATION OF A ^7Be IMPLANTED TARGET FOR NUCLEAR ASTROPHYSICS RESEARCH

E. A. Maugeri, S. Heinitz, R. Dressler (PSI), N. Kivel (PSI/AHL), D. Schumann (PSI), T. Stora (CERN), R. Reckermann, A. Hagel, H. Orlick, V. Neims (PSI/NUM), O. Morath, N. Frey, T. Schneider (PSI/ASI), K. Geissmann (PSI/NUM)

This report describes the preparation and the characterization of a target obtained implanting ^7Be ions into a thin aluminium disk. The target was used to measure the $^7\text{Be}(n, p)^7\text{Li}$ cross section in the energy range of interest for the Big-Bang nucleosynthesis at the n_TOF-CERN facility.

The standard Big Bang Nucleosynthesis (BBN) is a model that predicts the abundances of light elements produced in the early stage of the Universe [1]. The validity of this model has been largely proven when predicting the abundance of ^2H , ^3He and ^4He , while it fails when predicting the ^7Li abundance. In fact the calculated value of ^7Li abundance is a factor 3-4 higher than the value deduced from observations. This represents one of the most controversial and still pending problems in the nuclear astrophysics, known as the ‘‘Cosmological Lithium problem’’ [2, 3].

^7Li is mainly produced by the electron capture decay of ^7Be , thus its abundance strongly depends on the production/destruction rate of its mother nucleus ^7Be . This isotope is mainly produced via the $^3\text{He}(\alpha, \gamma)^7\text{Be}$ nuclear reaction and mainly destroyed, beside the radioactive decay, via the $^7\text{Be}(n, p)^7\text{Li}$ reaction. The value of the cross section of this nuclear reaction at the energy range of interest for the BBN, ~ 50 keV, is considered well known, with a statistical uncertainty of 0.7% [4]. Nevertheless, the acknowledged value was obtained by extrapolation from cross section values measured only at very low energies, between 25 meV and 13.5 keV [4,5]. In fact, no direct measurements have been performed at ~ 50 keV, and only data for the reverse reaction are available at this high energy [6,7]. This justifies new measurements to obtain a more precise value of this cross section, which could improve the consistency of BBN calculations.

An international project aimed at measuring the cross section of the $^7\text{Be}(n, p)^7\text{Li}$ reaction in a wide range of neutron energies, from thermal to 1 MeV, thus covering the BBN energy range, was started at the new experimental area (EAR2) [8] of the Neutron Time-of-Flight facility (n_TOF) [9] at CERN, Switzerland.

A target with sufficient amount, about 1 GBq, of chemically and isotopically pure ^7Be is the main prerequisite for a successful measurement.

Chemically pure ^7Be was obtained at the Paul Scherrer Institute by extraction from the cooling water of the Spallation Induced Neutron Source facility and separation from other cations, using the method described in [10]. The ^7Be specific activity was measured using a coaxial HPGe-detector as 0.961 ± 0.02 GBq/ mL, while the concentration of ^9Be and the $^9\text{Be}/^{10}\text{Be}$ isotopic ratio were measured by inductively coupled plasma mass spectrometry (ICP-MS) as 0.518 ± 0.022 $\mu\text{g}/\text{mL}$

and 4.86 ± 0.15 $\mu\text{g}/\text{mL}$, respectively. About 80 GBq of ^7Be solubilized in diluted HNO_3 were loaded in a graphite cylindrical crucible, see Fig. 1.

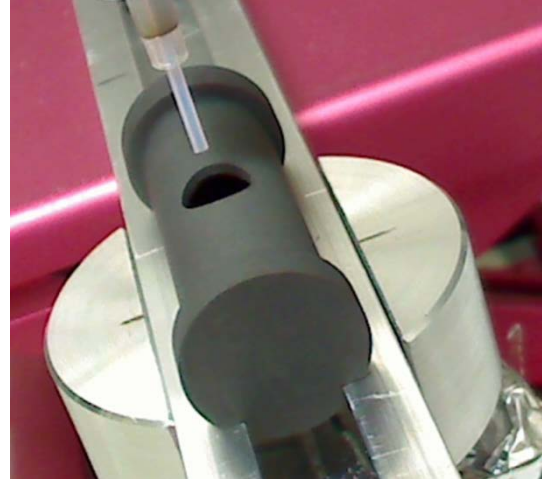


Fig. 1: Graphite crucible used to load the ^7Be activity.

The HNO_3 solution was evaporated at 60°C until dryness. After, the crucible was placed into the ionization chamber. This operation was carried out in the hot cell of the ATEC facility, PSI, see Fig. 2. The ionization chamber was afterwards shipped to the ISOLDE facility at CERN.

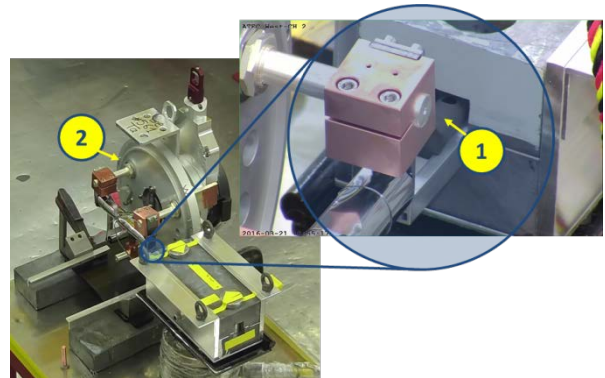


Fig. 2: Loading of the graphite crucible containing the ^7Be activity (1) into the ionization chamber (2).

Here, ^7Be was evaporated, ionized, accelerated to 30 keV, mass-separated (from ^9Be and ^{10}Be) and implanted with a current of 35 nA into a thin aluminium disk. The target was then irradiated with neutrons at n_TOF with different energies and the relative cross sections were evaluated.

After the measurement of the cross sections, the target was sent back to PSI for precise measurements of the activity and the distribution of the implanted ^7Be .

The ^7Be activity in the target was measured with a coaxial HPGe-detector as 1.00 ± 0.05 GBq (referred to the date of its implantation).

The ^7Be distribution was measured using the following method. The target was placed in a 3D positioning system, which allowed precise movement (± 0.01 mm), in front of a coaxial HPGe-detector. The distance between the target and the detector was 32.4 cm. A 10 cm lead collimator with a 2 mm diameter hole was placed in the middle between the detector and the target. The geometrical centre of the target was aligned with the 2 mm hole and with the centre of the detector using a laser pointer. The target was moved along the x -, y -axes by 2 mm steps. A total target area of 4 cm^2 was investigated, including 121 total measured points. 12 additional measurements were done with 1 mm steps from the target centre, to have a better resolution. Fig. 3 shows the result of the investigation.

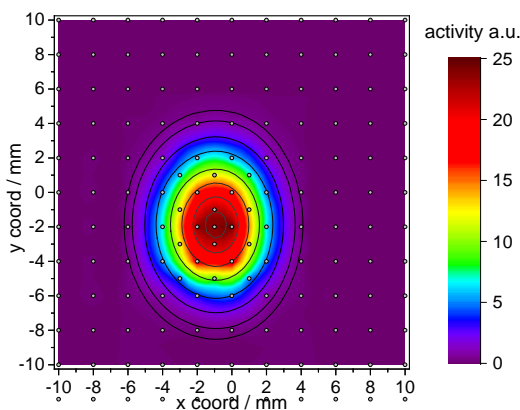


Fig. 3: Distribution map of ^7Be in the implanted target

It is possible to fit the distribution with two Gaussians, relative to the x -axis and y -axis, respectively. The two Gaussian fits are characterized by a value of FWHM of 5.57 mm and 4.40 mm, respectively.

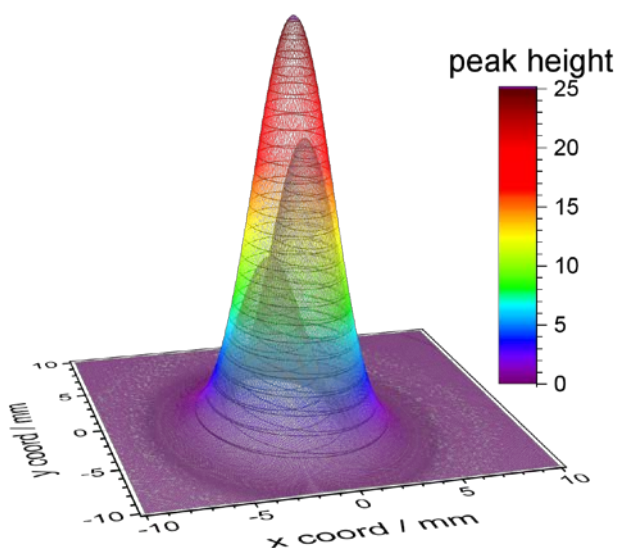


Fig. 4: Fit of the distribution of Fig. 3 using two Gaussians relative to the x -axis and y -axis characterized by values of FWHM of 5.57 mm and 4.40 mm, respectively.

For the first time, thanks to a well-established collaboration between different groups at PSI (ATEC and NES) and at CERN (ISOLDE and n_TOF), high specific activity of ^7Be was successfully implanted in a thin aluminium disk to produce a target for the measurement of the $^7\text{Be}(n, p)^7\text{Li}$ cross section at energy range of interest for the BBN.

ACKNOWLEDGEMENT

The work has partly been funded by CHANDA (grant agreement No FP7 - Fission-2013 – 605203).

- [1] G. Steigman, Annual Review of Nuclear and Particle Science, p. 463 (2007).
- [2] R. H. Cyburt et al., Physical Review D **69**, 123519 (2004).
- [3] B. D. Fields et al., Annual Review of Nuclear and Particle Science, Vol 61, 2011, pp. 47.
- [4] P. D. Serpico et al., J. Cosmol. Astropart. Phys. **12**, 010 (2004).
- [5] P. E. Koehler et al., Phys. Rev. C **37**, 917 (1988).
- [6] R. Taschek et al., Phys. Rev. **74**, 373 (1948).
- [7] K. K. Sekharan et al., Nucl. Instrum. Meth. **133**, 253 (1976).
- [8] S. Barros JINST **10** (2015).
- [9] C. Guerrero EPJ A **49** (2013).
- [10] D. Schumann et al., Radiochim. Acta **101**, 509 (2013).

PREPARATION OF ^{148}Gd AND ^{154}Dy SAMPLES FROM p-IRRADIATED Pb TARGETS

Z. Talip, R. Dressler, A. Vögele, D. Schumann (PSI), R. Michel (IRS Univ. Hannover)

INTRODUCTION

Knowledge about the radionuclide inventory of target materials used in spallation neutron facilities (SNF) and accelerator driven systems (ADS) is essential for the safety assessment of these facilities. In addition, it is important to evaluate and improve computer simulations for many different target-energy combinations, which is possible only with reliable experimental data. This work aims at preparing proper samples to measure the production cross sections of the long-lived α -emitting radionuclides ^{148}Gd and ^{154}Dy , produced in Pb targets irradiated up to 2.6 GeV protons.

EXPERIMENTAL

The Pb targets (typical thickness 125 mg/cm^2 , 15 mm diameter, 99.99% purity) were irradiated with protons in an energy range from 240 to 2600 MeV between 1993 and 1997 with a special stacked foil technique at the SATURNE II synchrotron of the Laboratoire National Saturne (LNS) at Saclay [1]. The irradiations were performed in air and lasted 17-33 h to get sufficient fluences. The details of the irradiation of each target are given in Table 1.

Tab. 1: Description of the p-irradiated Pb targets.

Sample	p-energy (MeV)	Fluence (cm^{-2})	Irradiation time (s)	Target (mg)
PbSh254	240	$3.50 \cdot 10^{13}$	55500	238
PbSk295	272	$1.36 \cdot 10^{15}$	67320	234
PbSg254	321	$9.09 \cdot 10^{13}$	76200	211
PbSf254	553	$1.36 \cdot 10^{14}$	121200	217
PbSc254	759	$1.36 \cdot 10^{14}$	91260	230
PbSn293	996	$1.73 \cdot 10^{15}$	86940	232
PbSd234	1162	$1.55 \cdot 10^{14}$	60480	234
PbSm294	1396	$1.28 \cdot 10^{15}$	74040	236
PbSc234	1567	$2.66 \cdot 10^{14}$	70980	236
PbSb132	1580	$1.82 \cdot 10^{16}$	60180	99
PbSr285	2595	$1.39 \cdot 10^{15}$	63600	232

In previous works, chemical separations of several long-lived β -emitting radionuclides (^{129}I , ^{36}Cl , ^{10}Be , ^{26}Al , ^{53}Mn and ^{60}Fe) [2] and long-lived α -emitting lanthanides (Lns) such as ^{148}Gd and ^{154}Dy [3] from 11 p-irradiated Pb targets were reported.

In the present study, separated Gd and Dy fractions of these samples were taken and molecular plating technique was used to prepare thin ^{148}Gd and ^{154}Dy samples to measure them by α -spectrometry.

Molecular Plating

The used molecular plating cell was similar to the one described in ref [4]. After separation, the Gd and Dy fractions were evaporated to dryness and dissolved in a small volume of diluted HNO_3 (50 μl , 0.1 M HNO_3) to minimize the thickness of the deposited layer. Optimized conditions for the molecular plating were as

follows; solvent: iso-propanol (15 mL), pH: 2.7, anode: platinum spiral shaped (21 mm), cathode (copper) to anode distance: 20 mm, voltage: 300 V, current: 2-4 mA, deposition time: 60 min, diameter of deposited area: 19 mm, backing material: carbon fiber (Good Fellow 99.8%, 75 μm). γ -emitting Lns tracers $^{166\text{m}}\text{Ho}$ and ^{153}Gd were used to monitor deposition yields for ^{154}Dy and ^{148}Gd , respectively.

Vacuum Gold Coating

Contamination of the semi-conductor detectors and the walls of the vacuum chamber by recoil nuclei is one of the common problems for α -spectrometry [5-8]. In this work, in order to avoid the contamination of the detectors due to the small sample detector distance (SDD), the Gd samples surfaces were coated with a thin layer of gold, which is sufficient to stop recoil nuclei but significantly smaller than the stopping range of α -particles. The coating was carried out using the UNIVEX 450 (Leybold vacuum) thermal evaporation system (operational vacuum 10^{-4} to 10^{-6} mbar) (Fig 1).

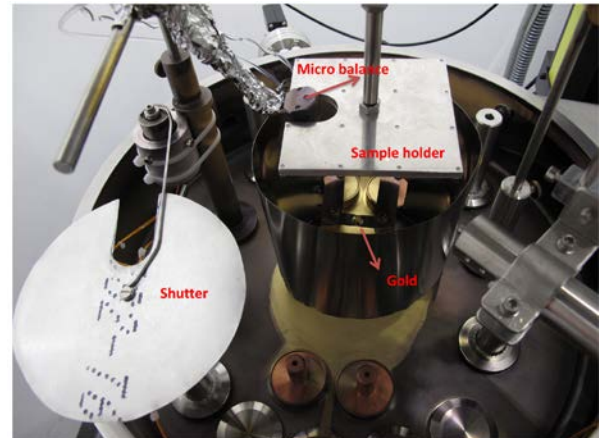


Fig. 1: The image of the thermal evaporation chamber of the UNIVEX 450 used for gold coating.

According to SRIM calculations, the range of an 88 keV Gd recoil nuclei in gold is $\sim 11\text{ nm}$ [9]. Therefore, samples were coated with $\sim 30\text{ nm}$ gold layer. To test the thickness of the coated gold layer, two ^{241}Am sources were prepared and coated with $\sim 30\text{ nm}$ gold. Figure 2 shows an example of comparison of the ^{241}Am source α -spectrum before and after the 30 nm gold coating. An energy shift of 12 keV was observed for the 5.48 MeV peak. The second source was also investigated and coating caused a shift of 14 keV. The mass stopping power, dE/dx [$\text{MeV}/(\text{mg}/\text{cm}^2)$], in gold for 5.5 MeV α -particles is given to be $0.2249\text{ MeV}/(\text{mg}/\text{cm}^2)$ by the SRIM code [9]. Knowing the density of the gold ($19.311\text{ g}/\text{cm}^3$) and the measured energy shifts after gold coating (12 keV and 14 keV), the thicknesses of the gold layers were calcu-

lated as 28 and 32 nm. All the Gd samples were coated with 30 ± 2 nm gold layers. Figure 3 shows the samples before and after gold coating. The sample holder used allowed to coat 8 samples simultaneously.

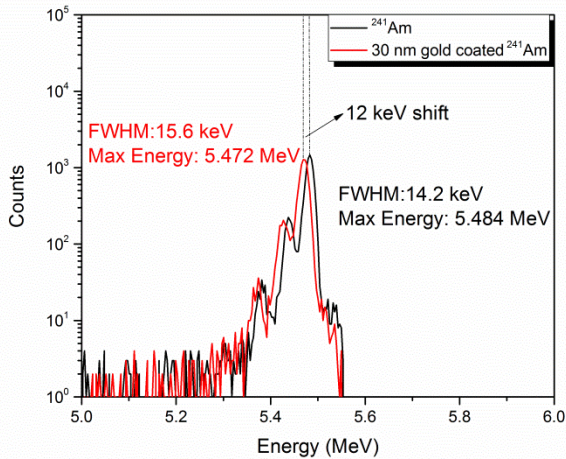


Fig. 2: Comparison of α -spectra: ^{241}Am source before and after 30 nm gold coating (spectra were recorded SDD: 38.64 mm, counting time: 4800 s).

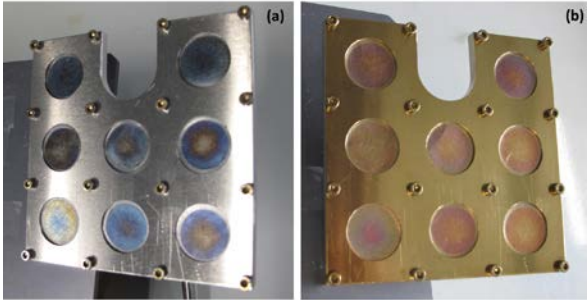


Fig. 3: Gd-deposited samples before (a) and after 30 nm gold coating (b).

RESULTS AND CONCLUSIONS

After all separation steps [2, 3] and molecular plating, between 63-72% total yields were obtained for the 11 samples (Table 2).

Tab. 2: Chemical yields of Gd and Dy from p-irradiated Pb samples after distillation, Dowex 50WX8 resin, Ln resin, molecular plating and total.

Sample	Chemical Yields (%)						
	After distillation	Dowex + Ln column		Molecular plating		Total yield	
	Dy, Gd	Dy	Gd	Dy	Gd	Dy	Gd
PbSh254	72	100	100	95	96	68	69
PbSk295	72	100	99	51	94	37	67
PbSg254	72	100	99	97	100	70	71
PbSf254	72	100	98	96	91	69	64
PbSc254	72	96	97	96	96	66	67
PbSn293	72	100	89	100	99	72	63
PbSd234	72	100	100	100	95	72	68
PbSm294	72	97	98	100	99	70	70
PbSc234	72	94	99	100	98	68	70
PbSb132	72	98	100	100	99	71	71
PbSr285	72	100	100	100	100	72	72

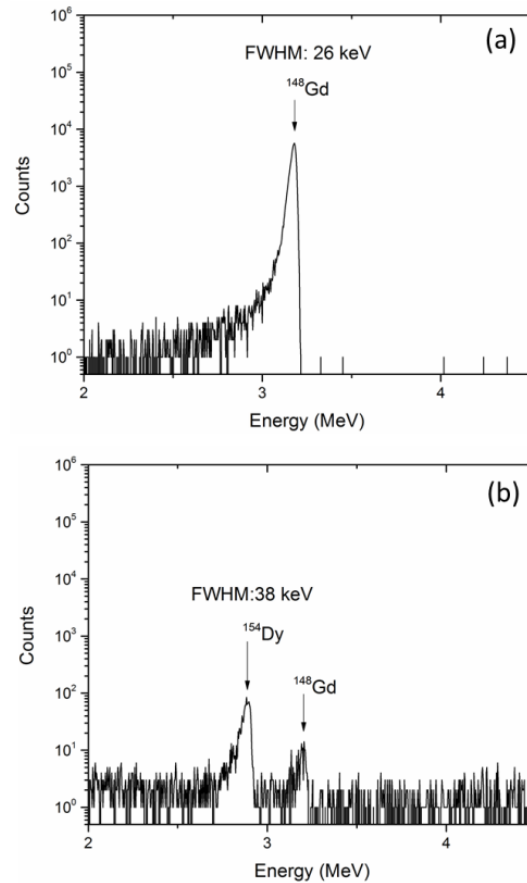


Fig. 4: After molecular plating and gold coating, a spectrum of a Gd sample (a) (SDD: 10.64 mm, counting time: 22 h) and Dy sample (b) (SDD: 2.64 mm, counting time: 80 days), separated from a Pb target irradiated with 1580 MeV protons.

Fig. 4. a and b show an example of the α -spectrum obtained for ^{148}Gd and ^{154}Dy samples, respectively. ^{148}Gd was detected in the Pb targets, irradiated with proton energies higher than 240 MeV, while ^{154}Dy was detected only in the targets irradiated with proton energies higher than 1200 MeV.

In a next step, production cross sections of ^{148}Gd and ^{154}Dy will be calculated and compared with theoretical calculations obtained with the INCL 4.6 and ABLA 0.7 code.

- [1] M. Gloris, PhD thesis, Hannover (1998).
- [2] D. Schumann et al., NIM. A **463**, 593 (2001).
- [3] Z. Talip, Ann Rep. Lab. of Radio- & Environ Chem., Univ. Bern & PSI, p. 46 (2015).
- [4] E. A. Maugeri et al., in print JINST (2017).
- [5] C. Sill et al., Anal. Chem. **42**, 1596 (1970).
- [6] N. Vainblat et al., Appl. Radiat. Isot. **61**, 307 (2004).
- [7] O. Rusu et al., J. Radioanal. Nucl. Chem. **290**, 241 (2011).
- [8] K. Inn et al., J. Radioanal. Nucl. Chem. **276**, 385 (2008).
- [9] <http://www.srim.org/> (17.01.2017).

SEPARATION OF LONG-LIVED RADIONUCLIDES FROM PROTON-IRRADIATED Ta TARGETS

Z. Talip, A. Vögele, D. Schumann (PSI), E. Strub (Univ. Cologne), C. Vockenhuber (ETHZ)

INTRODUCTION

In this study, distillation, precipitation and ion exchange methods were used for separating the long lived β -emitters ^{129}I , ^{36}Cl , and the α -emitters ^{154}Dy , ^{148}Gd , ^{150}Gd , and ^{146}Sm from proton irradiated Ta targets for the purpose of the determination of their production cross sections. After separation, a molecular plating technique was used to prepare thin lanthanide samples to obtain a good quality α -spectrum with high resolution and small low energy tail contribution. $^{129}\text{I}/^{127}\text{I}$ ratios were measured using accelerator mass spectrometry (AMS) and the cross sections of ^{129}I ($T_{1/2}$: 15.7 My) were determined for the Ta targets irradiated up to 2.6 GeV protons.

EXPERIMENTAL

Proton irradiations of 11 Ta targets were performed with a special stacked foil technique between 1993 and 1996 at the SATURNE II synchrotron of the Laboratoire National Saturne (LNS) at Saclay (for details see Table 1 and ref [1, 2]).

Tab. 1: Description of the p-irradiated Ta samples.

Sample	p-energy (MeV)	Fluence (cm ⁻²)	Irradiation time (s)	Target (mg)
TaSP176	220	1.10 ¹⁴	55800	163
TaSK205	256	4.4 10 ¹⁴	67320	276
TaSH205	257	1.110 ¹⁴	76200	270
TaSG205	337	2.610 ¹⁴	121200	268
TaSF206	561	3.3 10 ¹⁴	91260	148
TaSE205	756	3.2 10 ¹⁴	86940	275
TaSN245	986	1.4 10 ¹⁵	60480	273
TaSD182	1180	4.2 10 ¹⁴	74040	277
TaSM245	1386	1.3 10 ¹⁴	70980	273
TaSC182	1574	3 10 ¹⁴	60180	272
TaSR236	2560	1 10 ¹⁵	63600	148

Figure 1 shows the separation procedures for ^{36}Cl , ^{129}I , ^{146}Sm , ^{148}Gd , and ^{154}Dy isolation. Initially, the tantalum targets, together with iodine (10 mg in form of NaI (Woodward Corporation, USA) and chlorine as stable carriers (10 mg in form of NaCl (Riedel-de-Haen), as well as $^{166\text{m}}\text{Ho}$ and ^{182}Ta as radioactive tracers in order to monitor the separation, were dissolved in 10 mL 10 M HNO₃ and 4 mL conc. HF in a PTFE (Polytetrafluoroethylene) two neck-flask in an N₂ atmosphere at 100°C. Iodine and chlorine were distilled into an aqueous hydrazine solution (1:1, total 7 mL). After distillation, separation of I and Cl was performed similar to ref [3].

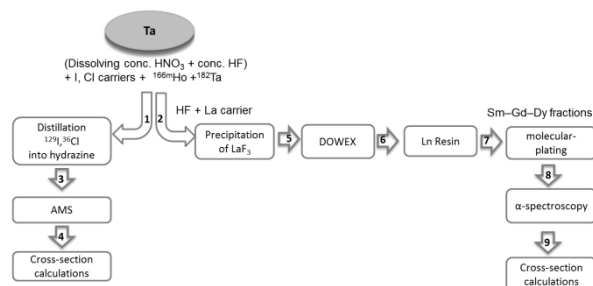


Fig. 1: Schematic diagram of the chemical separation of ^{36}Cl , ^{129}I , ^{146}Sm , ^{148}Gd , ^{150}Gd and ^{154}Dy from p-irradiated tantalum targets.

After the iodine and chlorine distillation, a Ta₂O₅ precipitate was observed in the reaction vessel. The remaining solution and precipitate were transferred in a centrifuge tube and 2 mL conc. HF and 1 mg La carrier (Fluka Analytical, La standard for ICP) were added. The reaction vessel was rinsed with 2 mL 7 M HNO₃ which was transferred to the centrifuge tube. The residual Ta₂O₅ in the solution was dissolved by conc. HF, while LaF₃ was precipitated. The precipitate was washed 4 times with 5 mL of water. Then, it was dissolved in 1 mL 7 M HNO₃ and 1 mL 0.5 M H₃BO₃. The solution was loaded onto a Dowex 50X8 cation exchange column and the lanthanides (Lns) were fractionized by elution with α -HIB at pH 4.6. In a following purification step, a Ln-specific ion exchange column (TRISKEM) was used to get rid of the complexing agent from Lns. γ -emitters $^{166\text{m}}\text{Ho}$, ^{160}Tb , ^{153}Gd , ^{154}Eu , and ^{145}Pm tracers were used to monitor the separation and to calculate the chemical yields.

RESULTS AND CONCLUSIONS

Lanthanides separation

Figure 2 shows an example of γ -spectra before and after Lns separation. After 4 washing steps, the Ta was completely separated from LaF₃. After the Ta separation, the chemical Lns yields were between 94-100% (Table 2).

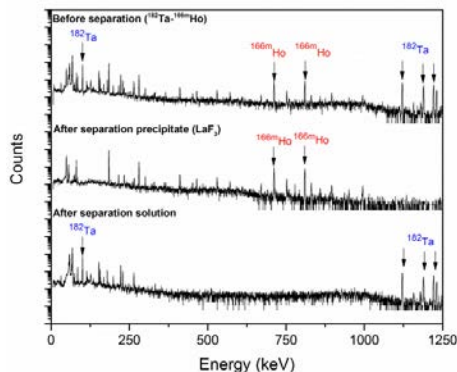


Fig. 2: An example of the γ spectra before and after Lns separation (after 4 washing steps).

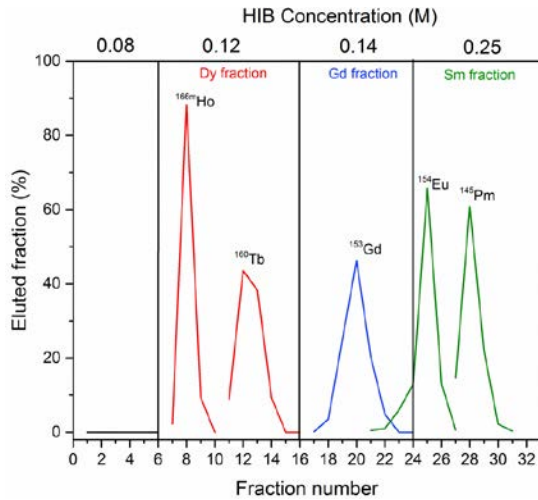


Fig. 3: Separation profile of Lns in the DOWEX 50x8 cation exchanger – α -HIB separation system with gradient elution technique.

An example of the Lns separation profile is presented in Figure 3. Initially, 0.08 M α -HIB was used to separate ^{172}Hf , $^{178\text{m}}\text{Hf}$ and ^{172}Lu , which were present in the p-irradiated Ta targets [4], followed by elution with 0.12 M (Dy fraction), 0.14 M (Gd fraction), and 0.25 M α -HIB (Sm fraction), respectively. After the separation of the Sm fraction, 1 M α -HIB was used to strip the La carrier. Between 96-100% chemical yields were obtained after Dowex 50X8 and Ln Resin separations (Table 2).

Molecular Plating

In a next step, a molecular plating technique was used to prepare thin Ln layers for α -spectrometry to determine the cross sections for the production of ^{154}Dy , ^{146}Sm and $^{148}\text{Gd}/^{150}\text{Gd}$ in Ta (Fig 1). Molecular plating experiments were performed similar to the one reported in the previous report [5].

Tab. 2: Chemical yields of Gd and Dy from p-irradiated Ta samples after distillation, Dowex 50WX8 resin, Ln resin, molecular plating and total.

Sample	Chemical Yields (%)						
	After distillation	Dowex + Ln column		Molecular plating		Total yield	
	Dy, Gd	Dy	Gd	Dy	Gd	Dy Gd	
TaSP176	97	96	100	95	69	88	67
TaSK205	94	100	100	95	90	90	85
TaSH205	98	100	100	94	82	92	80
TaSG205	100	100	100	98	93	98	93
TaSF206	96	100	99	98	94	95	89
TaSE205	97	70	100	82	95	56	92
TaSN245	97	100	100	100	79	96	76
TaSD182	97	100	100	84	98	81	95
TaSM245	99	96	97	99	99	94	95
TaSC182	100	100	100	99	98	99	97
TaSR236	100	100	100	95	95	95	95

After molecular plating, the activity of the Sm samples was measured using α -spectrometry with the smallest sample detector distance (SDD) (2.64 mm). The ^{146}Sm ($E_{\alpha}=2.455$ MeV, $\eta=100\%$) peak was not visible, even after a 45 day measurement. Therefore, chemical yields for ^{146}Sm samples were not presented in Tab. 2. Alpha-spectrometry measurements and cross section calculations for the Gd and Dy samples are currently under way.

Excitation functions of ^{129}I

The $^{129}\text{I}/^{127}\text{I}$ ratios, measured at the Tandy AMS facility (ETH, Zurich) [6], were ranging from 0.2×10^{-12} to 0.54×10^{-12} . From the 11 samples, only 6 showed significant values above the chemistry blank (0.2×10^{-12}) (Fig. 4a). Thus, the final uncertainties of the cross section after the blank correction are relatively large.

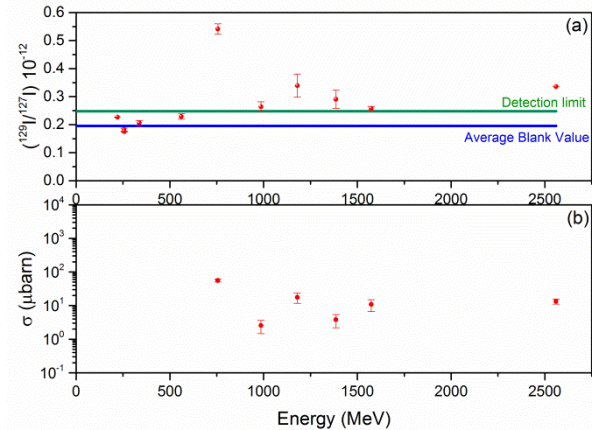


Fig. 4: Results of the AMS measurements without blank correction for $^{129}\text{I}/^{127}\text{I}$ ratios (a), cross section results for ^{129}I in p-irradiated Ta (b).

The main uncertainty components for the cross section calculations are due to the flux density (6%) [1] and AMS measurements (~8-42%). The AMS measurements of the long-lived β -emitting radionuclide ^{36}Cl ($T_{1/2}$: 301 ky) are currently under way.

ACKNOWLEDGEMENT

This project is funded by the Swiss National Science Foundation (SNF grant no 5201.24003.808).

- [1] M. Gloris et al., NIM. A **463**, 593 (2001).
- [2] M. Gloris, PhD thesis, Hannover (1998).
- [3] B. Hammer-Rotzler et al., Radiochim. Acta **103**, 745 (2015).
- [4] Z. Talip, Ann Rep. Lab. of Radio-& Environ Chem., Univ. Bern & PSI, p. 47 (2015).
- [5] Z. Talip, Ann Rep. Lab. of Radio-& Environ Chem., Univ. Bern & PSI, p. 20 (2016).
- [6] M. Christl et al., Nucl. Instrum. Methods Phys. Res. B **294**, 29 (2013).

ON THE PRODUCTION AND SEPARATION OF ^{163}Ho FOR PHYSICS RESEARCH EXPERIMENTS

S. Heinitz (PSI), N. Kivel (PSI/AHL), D. Schumann (PSI), U. Köster (ILL),
A. Nucciotti (Univ. Genova & INFN Genova)

INTRODUCTION

The radioactive isotope ^{163}Ho ($T_{1/2} = 4567$ a) has gained considerable attention within the physics community due to its very low Q-value of only 2.5 keV. This property and recent developments in high precision calorimetric measurements have facilitated several research projects devoted to measure the mass of the neutrino. Among them, the HOLMES collaboration aims towards implanting 3×10^5 Bq of isotopically pure ^{163}Ho into a grid of 10^5 transition edge sensor microcalorimeters to precisely measure the end-point energy of the ^{163}Ho electron capture decay [1]. With an envisaged statistical mass sensitivity of only 0.1 eV, this measurement will provide an alternative technique to spectrometry to answer the long lasting question in physics about the neutrino mass.

In collaboration with the Institut Laue-Langevin, Grenoble, and PSI, the project aims towards producing roughly 100 MBq of ^{163}Ho by irradiation of enriched ^{162}Er material in a nuclear reactor. The production route $^{162}\text{Er}(n,\gamma)^{163}\text{Er}$ followed by decay to ^{163}Ho is depicted in Figure 1 along with other neutron capture reactions.

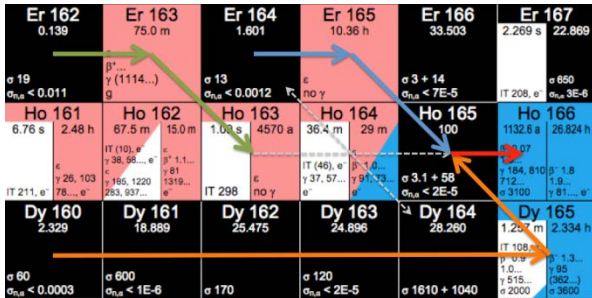


Fig. 1: Excerpt from the nuclide chart showing the main production route of ^{163}Ho (green arrows) together with parasitic formation of ^{166m}Ho (red arrow) from ^{165}Ho . The latter is formed by neutron capture from ^{164}Er (blue arrows) or by Dy impurities (orange arrows) within the irradiated material.

The main problem arising from neutron irradiation of enriched Er is the inevitable formation of ^{166m}Ho (see Figure 1), which drastically deteriorates calorimetric decay measurements. Since this isotope cannot be separated from ^{163}Ho by chemical means, a mass separation of these two isotopes is mandatory. Despite this, all Ho has to be first separated from the irradiated Er seed material. In order to quantify the amount of ^{163}Ho and ^{166m}Ho formed during a reactor irradiation, a careful characterization of the initial Er material including isotope composition and impurity content should be performed as well. This work describes the analysis of a 474 mg batch of ^{162}Er purchased in 2016 and gives some results on the separation of ^{163}Ho from irradiated batches in 2014 and 2015.

EXPERIMENTAL

A total mass of 544.2 mg of 25.1% enriched $^{162}\text{Er}_2\text{O}_3$ was purchased from TraceSciences, Canada, and transferred into two high purity quartz ampoules provided by Wisag AG, Germany. Approx. 4 mg of this material was kept for quantitative analysis of the material using ICP-OES, ICP-MS and neutron activation analysis.

At first, these 4 mg of $^{162}\text{Er}_2\text{O}_3$ were dissolved in 2 ml of 1 M HNO_3 and half of this solution used to prepare dilution series of 1:10, 1:100 and 1:1000 for ICP-OES measurements. Dy, Ho, Er, Tm, and Yb calibration solutions in concentrations ranging from 10 ppb up to 10 ppm were prepared from their respective ICP-MS standard solutions provided by Merck, Germany. A Perkin-Elmer Optima 3000 was used to measure the concentration of these 5 elements in the Er stock solution.

Another 400 μL of the stock solution was evaporated in a PE vessel and irradiated for 10^4 s in the SINQ neutron activation facility at PSI. 3.9 mg of IRMM-527 (Al-0.1%Co) alloy, Sigma Aldrich, USA, was used as flux monitor. Gamma spectra of the ^{162}Er sample were recorded 5 h, 24 h and 4 d after end of irradiation. Then the sample was irradiated with neutrons for another 10^4 s and then immediately underwent chemical separation by ion exchange chromatography using the LN resin, Triskem, France. The separation was monitored by gamma spectrometry. The separated fractions of Dy, Er and Yb were then measured for their isotopic composition using a sector-field based mass spectrometer (Element 2, Thermo Fischer Scientific, Germany). Additionally, 200 μL of the initial Er stock solution, diluted to 1 ml with H_2O , was analysed in the mass range from 85 to 180.

For the separation of ^{163}Ho from irradiated ^{162}Er , the ampoule containing the oxide was cracked, the material dissolved in 7M HNO_3 and the pH adjusted to 4 with NH_4OH . Approx. 0.5 mg of ^{171}Er activated at the PSI SINQ facility was added prior to the separation. The solution was then loaded into a 20 cm long column containing the cation exchange resin Aminex HPX87H from BioRad Laboratories, USA. The elution of the lanthanides was performed at room temperature using increasing concentrations of α -hydroxyisobutyric acid (HIBA) in a similar way described in [2]. The gradual elution of the lanthanides was monitored using gamma spectrometry. All fractions containing chemically pure Ho were then unified, acidified and loaded on a LN resin for final purification from HIBA and residual contaminants. This material is then investigated with ICP-MS and gamma spectrometry to determine the content of ^{163}Ho , ^{165}Ho , and ^{166m}Ho .

RESULTS AND DISCUSSION

The results of the ICP-MS, ISP-OES and neutron activation analysis of the TraceScience material is given in Table 1 together with the original Certificate of Analysis provided by the supplier.

Tab. 1: Isotopic composition and determined impurity content of ^{162}Er as measured by ICP-MS and ICP-OES. The original data provided by TraceScience is also given.

isotope	Analysis PSI	TraceScience CoA
	isotopic composition [%]	
Er-162	26.1 ± 0.4	25.1 ± 1.4
Er-164	6.0 ± 0.2	6.87
Er-166	30.1 ± 0.7	29.75
Er-167	15.5 ± 0.4	15.67
Er-168	15.6 ± 0.6	15.63
Er-170	6.7 ± 0.2	6.98
impurities	concentration relative to Er [atomic ppm]	
Eu	15	/
Gd	29	1000
Tb	7	/
Dy	5160*	5400
Ho	235	/
Tm	357	900
Yb	1530*	/
Lu	265	/
Rb	220	/
Sr	11	/
Y	69	/
Ba	237	/

* - the isotopic composition of Dy and Yb is non-natural, see Table 2; values denoted by “/” were not stated

The isotopic composition of Er was determined to slightly differ from the numbers provided by the supplier. This fact is due to isobaric interferences arising from Dy and Yb impurities, which are present in the material in the ‰ range. It should be noted that the impurity content given by the supplier significantly deviates from what was found by the analysis at PSI.

Tab. 2: The isotopic composition of Dy and Yb present as impurities in the analysed ^{162}Er material

isotope	content	isotope	content
Dy-156	0.02%	Yb-168	0.16%
Dy-158	0.03%	Yb-170	2.17%
Dy-160	0.35%	Yb-171	6.03%
Dy-161	8.40%	Yb-172	8.84%
Dy-162	64.13%	Yb-173	10.42%
Dy-163	15.84%	Yb-174	15.08%
Dy-164	11.23%	Yb-176	57.31%

Apart from much lower Gd content, the provided material contains substantial amounts of Yb. It was also found that Dy and Yb are present in non-natural composition – Dy is enriched in ^{162}Dy and Yb in ^{176}Yb as shown in Table 2. While ^{162}Dy is enriched together with ^{162}Er during isotope enrichment, the origin of ^{176}Yb is supposed to arise from earlier isotope separations of Yb at the enrichment facility.

Table 3 gives an overview on the Ho samples already processed together with the new batch that is planned to be available for reprocessing in 2017. The analysis of the separated Ho fractions from earlier irradiated ^{162}Er provided in 2014 and 2015 revealed that the activity of $^{166\text{m}}\text{Ho}$ linearly scales with the amount of stable ^{165}Ho produced during neutron irradiation. This fact can be explained by the relatively big capture cross-section of $^{166\text{m}}\text{Ho}$, imposing that a fast equilibrium is reached between production and destruction of this isotope in the reactor, as has been shown in [3].

The total amount of ^{163}Ho produced during the last 2 runs in 2014 and 2015 is approx. 1.5 mg, which represents roughly 35 MBq of this isotope.

Tab. 3: Overview on ^{163}Ho samples with their respective mass and composition

sample by year	$m(^{163}\text{Ho})$ [mg]	163/165 ratio	$A(^{166\text{m}}\text{Ho})$ [kBq]
2014	0.255	1.83	6.3
2015	1.22	1.60	38.7
2017	6*	1.5 – 2*	200*

* - estimated numbers

The quartz ampoules with 470 mg of ^{162}Er are currently being irradiated at the high flux reactor at ILL and will be available end of August for chemical separation. Despite for the HOLMES project, the separated material is also planned to be used at the CERN n_TOF facility for cross section measurement of the isotope ^{163}Ho .

ACKNOWLEDGEMENT

Many thanks to S. Tietze and K. Domnanich for the support during ICP-OES measurements. A. Vögele is acknowledged for his help during neutron activation

-
- [1] B. Alpert et al., Eur. Phys. J. C **75**, 1 (2015).
 - [2] S. Heinitz, Ann Rep. Lab. of Radio- & Environ Chem., Univ. Bern & PSI, p. 32 (2015).
 - [3] V. N. Danilenko et al., Appl. Radiat. Isot. **40**, 789 (1989).

PREPARATION OF ^{10}Be SAMPLES FOR NUCLEAR STRUCTURE RESEARCH AT RADIOACTIVE ION BEAM FACILITIES

S. Heinitz, T. Stowasser, D. Schumann (PSI), A. DiPietro (INFN-LNS Catania)

Light exotic nuclei such as ^{11}Be are of major interest in nuclear physics research [1]. The development of radioactive ion beams has facilitated the opportunity to study the properties of such neutron-rich isotopes close to the neutron drip-line. One of their exciting features is the possibility to form neutron halo nuclei with a mass distribution extending far outside the core of the nucleus. The structure of ^{11}Be is such that a neutron is surrounding a ^{10}Be atom, thus only being weakly bound to the core. This and other interesting properties have pushed theoretical and experimental research on light exotic nuclei in the recent years.

The Tandem accelerator facility of the Instituto Nazionale di Fisica Nucleare (INFN), Catania, Italy, is aiming towards physical investigations of Be halo nuclei using the long-lived radionuclide ^{10}Be . The envisaged beam intensities should reach up to 10^7 particles per second. The investigations at this accelerator facility should be complementary to studies already performed on ^7Be at Caserta, Italy [2]. INFN has started a collaboration with PSI capable to provide sufficient amounts of ^{10}Be to achieve the desired radioactive ion beam intensity. This work describes the preparation of suitable samples for the envisaged nuclear structure research on ^{11}Be .

Standard sample holders that are used at the INFN tandem accelerator are Au coated copper cathodes with a 1 mm deep spherical hole in which the actual sample material is loaded. An ICP-MS standard ^9Be solution with 1 g/L of Beryllium serves as source for stable Be test samples. Approx. 40 μL of this solution is placed into a ceramic crucible and mixed with 1.2 mg of Ag powder, provided by Sigma-Aldrich. The crucible is then heated overnight to 500°C to transform $\text{Be}(\text{NO}_3)_2$ into BeO. After cooldown, another 2.4 mg of Ag are added and mixed with the dried residue in the crucible. This mixture is then mechanically tapped into the hole of the Cu cathode in such a way, that the Ag powder is compressed to a uniform body containing BeO. The addition of Ag also assures the conductivity of the matrix during beam extraction at the accelerator facility.

Radioactive ^{10}Be samples have been prepared in a similar way using a stock solution prepared from recovered ^{10}Be originating from the target E92 graphite wheel of the PSI meson facility [3]. The isotopic composition of this material was determined by ICP-MS to have the following atomic ratio $^9\text{Be} : ^{10}\text{Be} = 2 : 1$.

In total, six samples containing ^9Be and two samples containing 100 kBq of ^{10}Be have been produced and shipped to INFN Catania by end of 2016. Table 1 gives an overview on the prepared samples for this batch.

cathode number	mass of ^9BeO [mg]	mass of ^{10}BeO [mg]	mass of Ag added [mg]
1	0.1	/	3.5
2	0.1	/	3.5
3	0.2	/	7
4	0.2	/	7
5	0.3	/	10.5
6	0.3	/	10.5
7	0.2	0.1	10.5
8	0.2	0.1	10.5

Tab. 1: Overview on samples/cathodes prepared for INFN by end of 2016. The addition of Ag was 1/3 before and 2/3 after glowing of BeO. See text for details.

According to results on inactive ^9Be samples provided in 2013 and 2015, cathodes prepared using the described procedure are able to provide a sufficient Be beam intensity over a period of several days. Figure 1 shows a test on the ^9Be beam intensity extracted from a similar cathode provided in 2015. The total charge extracted from this cathode was 5.6 mC with an average ^9Be beam current of 23 nA over a period of 3 days. These tests could successfully show that suitable ^{10}Be beam intensities may be provided for nuclear structure investigations. The experimental work on cathodes containing ^{10}Be is envisaged for early 2017.

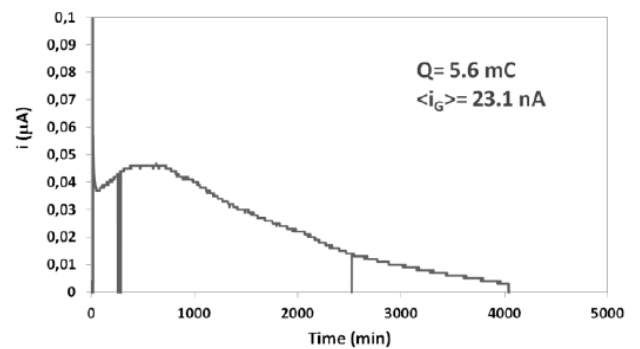


Fig. 1: Extracted ^9Be beam intensity as function of beam time.

-
- [1] B. Jonson, Phys. Rep. **389**, 1 (2004).
 - [2] B.N. Limata et al., Nuc. Inst. Meth. Phys. Res. B **266**, 2117 (2008).
 - [3] S. Heinitz et al., Ann Rep. of Radio- & Environ. Chem., Uni Bern & PSI, p. 44 (2015).

TOWARDS NEUTRON CAPTURE CROSS-SECTION MEASUREMENTS WITH ULTRACOLD NEUTRONS

J. Ulrich, R. Dressler (PSI), B. Lauss (PSI/NUM)

Ultracold neutrons (UCNs) are free neutrons with energies below about 350 neV (corresponds to a velocity of ~ 8 m/s). Their energy is so low that they can be significantly accelerated or slowed down by Earth's gravity. Since most solid and liquid surfaces have positive (i.e. repulsive) nuclear potentials, UCNs can be stored in material "bottles" which makes them interesting for fundamental neutron physics.

The neutron capture cross-section scales with the inverse of the speed of the neutron (or the inverse square root of its energy). Applying the $1/v$ law to the UCNs, a cross-section gain by a factor of about 300 compared to the thermal neutron capture cross-sections can be expected. This effect is further increased for most materials, since the kinetic energy of the UCNs is lowered by the material surface optical potential upon penetration. This process is analogous to slowing down of light by entering a medium with higher refractive index.

Cross-section measurements with UCNs are a challenging topic both from the theoretical and experimental point of view. Despite the large cross-section enhancement, obtainable activities are generally very low because of the low intensity of provided UCNs. Due to their low energy, the behavior of the UCNs is much more accurately described by wave optics than as a particle. This means that effects which are easily negligible in common neutron activation experiments with thermal or cold neutrons like target surface roughness, material granularity, surface contaminants or material impurities may significantly influence the measurement results [1] and make the data evaluation not straightforward.

At PSI, UCNs are produced from spallation neutrons by thermalization in D_2O and subsequent cooling-down and down-scattering in solid deuterium [2-5].



Fig. 1: Overview of the irradiation setup. The collimator with 3 open channels is inside a Plexiglas tube used as UCN guide. The rectangular box mounted on the bottom of the tube is the housing of the neutron detector.

An experimental setup for activation of thin foils by UCNs was built at the West-2 beamline of the PSI UCN source. This setup is depicted in Fig. 1 and consists of an evacuated vertical Plexiglas tube with a

Plexiglas collimator/sample holder mounted at the bottom of the tube and a 100 cm^2 , 8×8 Pixel position sensitive CASCADE-U neutron detector [6]. Plexiglas is a suitable material for restricting UCNs from certain areas. Because of its high hydrogen content, it can up-scatter UCNs to thermal energies very fast, which means effectively removing these neutrons from the setup.

The UCNs are generated and extracted in proton pulses of up to 8 s with a repetition period of 300 s. Due to the source geometry almost all UCN arrive at the West-2 setup in the first minute after the pulse with a mean energy of the neutrons of about 260 neV at the beamport height. This energy is further increased by the fall height of the neutrons inside the Plexiglas tube. UCNs gain 102 neV energy per meter fall in the Earth's gravitational field. Tube lengths of 25 cm and 201 cm were used, the latter nearly doubling the neutrons' kinetic energy.

The collimator is the critical part of the experimental setup. It consists of two Plexiglas cylinders of 0.5 cm and 3 cm height with four drilled collimation channels ($\phi = 1.3$ cm). The sample foils are fixed between the two cylinders (see Fig. 3). The main function of the collimator is to restrict the irradiation exclusively to neutrons perpendicular to the sample foil. The top and bottom of the collimator are shielded by a 0.1 mm aluminum foil covered with a Gd_2O_3 containing epoxy layer. The Gd_2O_3 shielding lowers detector background and inhibits foil activation by diffuse neutrons during the proton beam pulse. Fig. 2 shows one 2D UCN count rate distribution recorded during activation. The different attenuation of UCNs by Au and W foils of the same thickness is clearly visible.

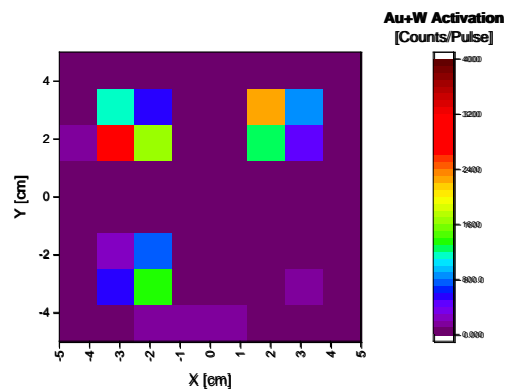


Fig. 2: Measured 2D UCN count rate distribution during activation (top left: empty channel, top right: 3 μm W, bottom left: 3 μm Au, bottom right: channel opening covered with Gd_2O_3 , i.e. showing counts only at the background level).

Autoradiography of an irradiated gold foil showed a very sharp confinement of the activation to a circle of 1.3 cm diameter (i.e. the exact diameter of the irradiation channel) and a good lateral homogeneity of the

activation. The effectiveness of the Gd_2O_3 -shielding was verified by placing a gold foil in an irradiation channel which was covered with a Gd_2O_3 -containing shielding. No ^{198}Au -peak was found in a gamma spectrum recorded over 3 days after irradiation for 2 days.

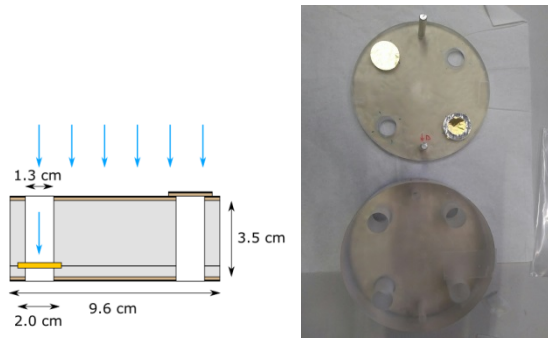


Fig. 3: Drawing of the collimator (left). Open collimator loaded with sample foils (right).

Gold and tungsten were identified as suitable test targets for initial studies, in particular because of their high capture cross-section and their activation product easily measurable by γ -spectrometry. Different gold samples in a thickness range between 0.1 to 3 μm and a tungsten foil of 3 μm thickness were used. Since the Fermi potential of Au and W is comparably low with 120 neV and 80 neV, respectively, only small surface reflection is expected for both materials at given UCN energies, especially for the longer fall height. To investigate the effect of different surface potentials on the ^{197}Au capture cross-section, the intermetallic compound AuAl_2 (Fig. 4) was prepared by heating a 100 nm thin Au layer, created by PVD on 6 μm Al backing, at 500°C in an inert atmosphere. Due to the high aluminum content in AuAl_2 , the surface potential is lowered to 70 neV, i.e. roughly half the one of pure gold.



Fig. 4: AuAl_2 (“purple gold”) created by heating 100 nm Au layer on Al backing.

With a neutron flux of about $10\text{--}15\text{ cm}^{-2}\text{s}^{-1}$ and irradiation periods of about 2-3 days, activities of 0.1-10 Bq of ^{198}Au or ^{187}W were obtained depending on sample material and thickness. Tab. 1 presents a summary of the measured foils together with the irradiation periods and activities at the end of the irradiation.

The samples were γ -spectroscopically measured with an 18 % “broad energy” type HPGGe detector (Canberra BE2825) and the spectra were evaluated by the manufacturer’s GENIE-2000 software. The efficiency calibration was performed numerically with the aid of the commercial LabSOCS-Software (Canberra).

To reach peak area uncertainties of 1 % to 5 % it was necessary to record the γ -spectra in close-up geometry with counting times of 1 to 3 days due to the small total amount of activation products.

The preliminary results suggest significantly larger cross-section values than expected according to the theory by extrapolation of the $1/v$ law from the thermal region down to UCN energies [1]. The reasons for this discrepancy need to be identified and are suspected in the UCN behavior during material transmission and reflection, since the capture cross-section should strictly follow the $1/v$ law. This has been confirmed by both theoretical studies and transmission measurements.

Target	Tube	$t_{\text{irr}} [\text{h}]$	$A_0 [\text{Bq}]$
3 μm Au (99.9%) foil	Short	41.2	4.88
	Long	76.9	6.66
3 μm W (99.95%) foil	Short	41.2	1.50
	Long	76.9	1.32
1 μm Au (99.9%) on Acryl Foil	Long	67.5	1.76
160 nm Au (24K) spanned on Al-Ring	Long	67.5	0.35
100 nm Au by PVD on 6 μm Al foil	Long	64.0	0.29
AuAl_2 (s. text) on 6 μm Al foil	Long	64.0	0.23

Tab. 1: Targets used for activation tests, used tube, the irradiation times at the UCN source and achieved activities A_0 (at the end of the irradiation).

Nevertheless, the relative measurements yielded reasonable values, although with probably big uncertainties which need yet to be quantified. The deduced capture cross section of gold decreases with the long (201 cm) tube in comparison to the short (25 cm) tube as a consequence of the shift of the neutron spectrum to a higher energy. Furthermore, the ratio between the ^{186}W and ^{197}Au capture cross-sections is near the expected value and remains roughly the same between the measurements with the long and short tube.

In the second half of 2017, further activation experiments at the UCN source are planned, focusing on reproducibility of the experimental results and lowering the experimental uncertainties.

- [1] F. Atchison et al., Nucl. Instr. Meth. Phys. Res. A **608**, 144 (2009).
- [2] B. Lauss, Phys. Proc. **51**, 98 (2014).
- [3] B. Lauss, Hyperf. Int. **211**, 21 (2012).
- [4] B. Lauss, AIP Conf. Proc. **1441**, 576 (2012).
- [5] A. Anghel et al., Nucl. Instr. Meth. Phys. Res. A **611**, 272 (2009).
- [6] CDT GmbH, Hans-Bunte-Strasse 8-10, D-69123 Heidelberg, Germany.

PREPARATION OF A ^{60}Fe STANDARD FOR ACCELERATOR MASS SPECTROMETRY (AMS)

D. Schumann (PSI), N. Kivel (PSI/AHL)

AMS is one of the most sensitive analysis techniques to measure long-lived radionuclides, reaching detection limits for isotopic ratios down to 10^{-15} - 10^{-16} in special cases. Its application portfolio covers nearly every field of environmental research, considering processes in the atmosphere, bio-sphere, hydrosphere, cryosphere, lithosphere and the cosmosphere.

The method normally measures the isotope ratio in comparison to a validated standard, the quality of which determines the quality of the result. The need to produce sufficient amounts of high-quality, well-characterized standard material is clearly visible and recognized already for a long time. The difficulty consists in many cases in the availability of the isotope. One example is the extremely rare, long-lived isotope ^{60}Fe . For several decades, most of the results for ^{60}Fe were obtained using standards produced from heavy ion reactions [1], from irradiated copper [2] or extracted in the radioactive beam facility ISOLDE (CERN) from proton-irradiated UC_x [3]. None of these standards have been properly characterized by experimental methods. Their nominal values are based on rough approximations of the production and/or implantation rates. Uncertainties are above 10 % or even not available at all.

Since ^{60}Fe is two mass units heavier than the heaviest stable iron isotope ^{58}Fe , its production possibilities are limited. A very unique opportunity to gain this kind of rare exotic isotopes is the exploitation of radioactive waste from the surrounding of high-power, high-energy accelerators. We used this production route to manufacture several grams of ^{60}Fe standard in form of iron oxide and characterized it using MC-ICP-MS.

Material

The primary source was material drilled out from a copper beam dump irradiated with high-energetic protons at PSI till 1992. Details of the chemical separation can be found in [4]. The obtained Master solution has first been used for the determination of the ^{60}Fe half-life [5]. After this, a part of this solution was used for the standard preparation.

Characterization of the Master solution

The total iron amount and the isotopic composition of the master solution have been determined by isotope dilution mass spectrometry (IDMS), amounting in $N(^{60}\text{Fe}) = 5.873(50) \cdot 10^{15}$ atoms in 4.545(8) g master solution. The results relevant for the standard preparation procedures are shown in Table 1. The radiochemical processes as well as the parameters of the MC-ICP-MS measurements are described in detail in [6].

Tab. 1: Isotopic composition and content of the master solution; data taken from [6]

	Isotopic abundance [%]
^{54}Fe	6.033 (19)
^{55}Fe	87.4990(50)
^{57}Fe	4.2076(68)
^{58}Fe	2.2397(70)
^{60}Fe	0.02048(12)

Dilution series

Three standards were fabricated by successive dilution of the master solution with Fe_2O_3 (Sigma/Aldridge, 99.999%) and HCl (Sigma/Aldridge).

PSI-8

0.09970 g of the master solution were mixed with 1.65277 g Fe_2O_3 and dissolved in concentrated HCl till complete dissolution. The total weight of the final solution amounted to 14.459343 g.

PSI-10

0.16146 g of the PSI-8 solution were mixed with 1.68521 g Fe_2O_3 and dissolved in concentrated HCl till complete dissolution. The total weight of the final solution amounted to 14.58051 g.

PSI-12

1.61563 g of the PSI-10 solution were mixed with 16.85137 g Fe_2O_3 and dissolved in concentrated HCl till complete dissolution.

After finishing the dilution series, iron was precipitated with ammonia solution as $\text{Fe}(\text{OH})_3$. The hydroxide was dried and then calcined at 400°C to obtain Fe_2O_3 .

Uncertainty budget

The total uncertainty is determined by the uncertainty of the ICP-MS measurement (0.3%). Uncertainties coming from the balance are negligible ($< 0.1\%$).

Results

The calculation of the isotope ratios yielded:

$$\text{PSI-8: } I = 1.029(3) \cdot 10^{-8}$$

$$\text{PSI-10: } I = 1.124(3) \cdot 10^{-10}$$

$$\text{PSI-12: } I = 1.242(3) \cdot 10^{-12}$$

The obtained three standards in form of iron oxide powder are shown in Figure 1.

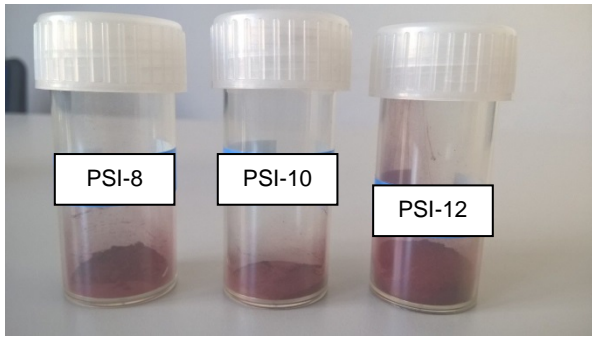


Fig. 1: ^{60}Fe standard material as oxide powder

Studies on ^{60}Fe are currently one of the hottest topics in understanding fundamental processes of star evolution and the development of the Early Solar System. For instance, three independent experimental studies, published in 2016, show high evidence for a nearby super novae explosion occurring around 2.5 Mio years ago [7-9]. Two of these works used AMS [7,8] and applied the new PSI standard material. During these investigations, it turned out, that measurements using former standards showed a deviation of up to a factor two in the absolute values in comparison to the PSI ones [10]. With these findings, it is pretty clear, that a considerable number of former ^{60}Fe data will have to be re-evaluated.

We are going to make the prepared standards, which are now ready for use, available for interested AMS groups world-wide, either on the basis of collaborations or in form of commercially purchasable goods. More batches can be produced soon. The availability of the first ever, well-characterized ^{60}Fe standard material will essentially improve the quality of data and enhance further high-ranking research in nuclear astrophysics.

-
- [1] K. Knie, private comm.; cited in K. Knie et.al., *Meteoritics & Planetary Science* **34**, 729 (1999).
 - [2] W. Kutschera, private comm.; cited in P. Gartenmann, PhD thesis, ETHZ (1999).
 - [3] U. Köster, PhD thesis, TU München 2000.
 - [4] D. Schumann et.al., *J Phys. G: Nucl. Part. Phys.* **35**, 014046 (2008).
 - [5] G. Rugel et. al., *PRL* **103**, 072502 (2009).
 - [6] N. Kivel et. al., *Anal. Bioanal. Chem.* **405**, 2965 (2013).
 - [7] W. R. Binns et. al., *Science*, 10.1126/science.aad6004 (2016).
 - [8] L. Fimiani et. al., *PRL* **116**, 151104 (2016).
 - [9] A. Wallner et. al., *Nature* 10.1038/nature17196 (2016).
 - [10] A. Wallner, private comm.

WASTE TREATMENT AND ISOTOPE RECLAMATION

*M. Lin (Univ. Bern & PSI), I. Kajan (PSI), H.-D. Potthast (PSI/AHL), A. Türler (Univ. Bern & PSI),
D. Schumann (PSI)*

The objective of the project is a chemical treatment of the aqueous solutions containing burned nuclear fuel (ca. 700g) in form of nitric acid solution stored within the HOTLAB facility at PSI. There are several aims within this SWISSNUCLEAR funded project, the primary one is to separate alpha emitters and caesium from the waste bulk in different streams to achieve a suitable composition of the waste for the final deposition. Secondary aim is the extraction of exotic and valuable nuclides (^{244}Cm , ^{79}Se , $^{97-99}\text{Tc}$, several isotopes of lanthanides and others) from the waste solution.

The ongoing experiments are towards the evaluation of suitable ways to extract caesium represented mainly by the isotope ^{137}Cs ($T_{1/2}=30\text{y}$) from the waste solutions. This is due to the high dose rate originating from this radioisotope complicating the practical handling of the waste. A promising way for such separation seems to be use of a novel ion exchanger marketed under the name CLEVASOL [1]. CLEVASOL is a strongly acidic cation exchanger.

CLEVASOL shows excellent properties towards the extraction of caesium ($K_d > 1\text{E}5$ in 0.1M HCl, $K_d > 1.2\text{E}2$ in 10 M HCl), presumably due to the formation of very low-soluble caesium salt.

The ongoing experiments are aimed at examining the selectivity of the ion exchanger towards caesium in the mixture of lanthanides, uranium and fission/activation products in the waste solutions. In this part of experiments different acids (HNO_3 , HClO_4 , HCl) and concentrations (1 mM-8 M) are tested in order to find optimum conditions towards the caesium extraction.

Both batch and column techniques are employed in order to determine the best experimental approach towards caesium separations. Simultaneously with the caesium extraction experiments a suitable approach towards separation of alpha radiation emitting nuclides is examined. These are represented mainly by plutonium and uranium with contribution of so called minor actinides (Am, Cm, Pm). To separate these, a solvent extraction approach using tributyl phosphate (TBP) as an extracting agent was chosen. Currently, the evaluation of the organic phase composition with respect to organic solvent on the extraction properties of plutonium and uranium is ongoing. According to previous uranium and plutonium extraction experiments [2,3] four suitable candidates of the diluents were chosen (dodecane, cyclohexane, kerosene and 1-octanol) for evaluation with respect to flash point, radiation and chemical stability. We focus not only on the extractability and selectivity towards uranium and plutonium but also on avoiding third phase formation, possibly caused by some fission products (e.g. palladium and

molybdenum) that would complicate the extraction process.



Fig. 2: Column setup with use of CLEVASOL for caesium extraction from the radioactive waste solutions.

-
- [1] <https://trademarks.justia.com/791/99/clevasol-79199803.html>.
 - [2] R. G. Geier. Process Engineering Department, US, (1979).
 - [3] L. L. Burger, et al., Ind. Eng. Chem. Res. **50**, 2 (1958).

NEW 6 mm PELLET TARGETS FOR ^{44}Sc PRODUCTION

C. Vermeulen (PSI/CRS), N.P. van der Meulen (PSI)

INTRODUCTION

The Positron Emission Tomography (PET) radionuclide, ^{44}Sc , is primarily produced via the (p,n) nuclear reaction at a cyclotron using $^{44}\text{CaCO}_3$ as target material. ^{44}Ca targets were, in the past, prepared by mixing 10 mg enriched $^{44}\text{CaCO}_3$ with 150 mg graphite powder, pressed and encapsulated in aluminium.[1]

The graphite powder method, however, leads to an uneven target mass which causes large variations in yield. The graphite powder also tends to clog transfer lines and has to be filtered from the mother solution, adding unnecessary complexity to the chemical separation system.



Fig. 1: Commercial die set for 6mm pellet preparation.

Cost vs. yield analysis indicates that 30 mg of enriched material is the ideal amount of powder to use per production. This translates into a target pellet of 0.5 mm thick and 6 mm in diameter. In the interest of worldwide standardization, the use of 6 mm is convenient as die sets can be bought commercially (Fig. 1). The size is also close enough to 1/4 inch (6.35 mm), meaning even imperial die sets will work for this purpose.

An ongoing collaboration between PSI, the University of Bern, the University of Alabama in Birmingham (USA), the University of Iowa (USA), COMECER (Italy), and INMAS (India) aims to create a standardized inner structure for target assemblies using the 6 mm pellet format. Fig. 2 shows a prototype target shuttle that will be compatible with the COMECER target transfer system.



Fig. 2: Prototype target shuttle with pellet in place.

Even though pressed pellet technology is well known at larger cyclotron facilities [2], the need for a simple pellet target that is compatible with small medical cyclotrons is clear. Typically, these systems have enclosed hot cells with rudimentary or no telemanipulators, predicating the need for highly automated encapsulation/decapsulation systems that can be safely introduced into GMP environments.

Part of the design process for the 6 mm target standard is the consideration for these constraints and investigates such novel concepts as magnetic closing, 3D printing and electron-beam welding in the target capsule manufacturing and development processes.

[1] N. P. van der Meulen et al., Nucl. Med. Biol. 42 (2015).

[2] P. van den Winkel, Technical Reports Series No. 432, IAEA, Vienna (2004).

⁴³Sc PRODUCTION DEVELOPMENT BY CYCLOTRON IRRADIATION OF ⁴³Ca & ⁴⁶Ti

K. Domnarich (Univ. Bern & PSI), C. Umbricht, M. Benešová, C. Müller (ETHZ & PSI/CRS), A. Blanc, M. Behe (PSI/CRS), R. Schibli (ETHZ & PSI/CRS), A. Türler (Univ. Bern & PSI), N.P. van der Meulen (PSI)

INTRODUCTION

In the recent years radiometal-based PET (Positron Emission Tomography)-imaging became a widely accepted diagnostic tool in oncology. Currently ⁶⁸Ga-based radiopharmaceuticals are utilised in clinical practice. However, its short half-life of 68 min (Tab. 1) impedes the transportation over long distances and application in longer metabolic processes [1, 2]. The positron emitting radionuclides ⁴³Sc and ⁴⁴Sc are considered as attractive alternatives. Both have nearly 4-times longer half-lives and lower average β^+ -energies (Tab. 1). The decay of ⁴³Sc occurs, unlike to ⁴⁴Sc, without the co-emission of high-energy γ -rays, which is clearly advantageous regarding the dose burden to patients and medical staff [3].

Tab. 1: Comparison of the nuclear properties of ⁴³Sc, ⁴⁴Sc and ⁶⁸Ga.

	⁴³ Sc	⁴⁴ Sc	⁶⁸ Ga
$t_{1/2}$	3.89 h	3.97 h	68 min
$E\beta^+_{av}$ [keV]	476	632	830
$E\gamma$ [keV]	372	1157	1077
$I\gamma$	22.5%	99.9%	3.22%

The production of ⁴³Sc is described by different production routes in the literature: ⁴²Ca(d,n)⁴³Sc, ⁴³Ca(p,n)⁴³Sc and ⁴⁶Ti(p, α)⁴³Sc. However, production of sufficient ⁴³Sc activities of high radionuclidic purity encompasses several challenges, low availability of deuterons, a low cross section and co-production of radionuclidic impurities [3]. Within the scope of the project, both proton induced reactions were investigated and the product quality was proven by radiolabelling experiments.

EXPERIMENTAL

Irradiation: ⁴³Ca and ⁴⁶Ti targets were prepared by placing ~10 mg ⁴³CaCO₃ and ~12 mg reduced ⁴⁶Ti on top of ~150 mg graphite, pressing and encapsulating it in aluminium. The irradiation was performed with ~12 and ~15 MeV protons at varying beam currents (30-50 μ A) for 1-4 hours. Enriched Ti is only available in its hardly soluble oxide form. Therefore, 97% ⁴⁶TiO₂ was reduced to ⁴⁶Ti at GSI (Gesellschaft für Schwerionenforschung), Darmstadt previously [4] and the process further developed at PSI. **Chemical Separation:** After the irradiation, both target materials, ⁴³CaCO₃ and ⁴⁶Ti, were dissolved in hydrochloric acid and ⁴³Sc was chemically separated on the extraction chromatographic resin DGA by subsequent application of HCl at different concentrations. The eluted ⁴³Sc fraction was concentrated on the cation exchange resin SCX and reconcentrated in only 700 μ L 4.8M NaCl/0.13M HCl eluent. **Radiolabelling:** The isolated ⁴³Sc was radiolabelled with DOTANOC and DOTA-conjugated peptides and used for preclinical in vivo PET-imaging.

RESULTS AND DISCUSSION

The Ar-based reduction process for ⁴⁶TiO₂ was changed to vacuum and in combination with a modified sample preparation, the reduction yield was increased to 97.8%. The application of the optimised reduction method will probably allow the preparation of purer ⁴⁶Ti target material.

At the end of bombardment activities of 380–620 MBq were obtained from the ⁴³Ca-targets, while from ⁴⁶Ti-targets only 80-180 MBq ⁴³Sc could be produced.

After the separation from ⁴³Ca, the product contained 66.2% ⁴³Sc and 33.3% ⁴⁴Sc, which was produced from ⁴⁴Ca in the target material via the ⁴⁴Ca(p,n)⁴⁴Sc nuclear reaction. The isolated ⁴³Sc was radiolabelled with DOTA-conjugated minigastrin and several minigastrin-analogues at a specific activity of 7-12 MBq/nmol. As a proof-of-concept, PET/CT imaging was performed 1, 2, 3, and 17 hours after injection into four tumour bearing mice (Fig. 1).

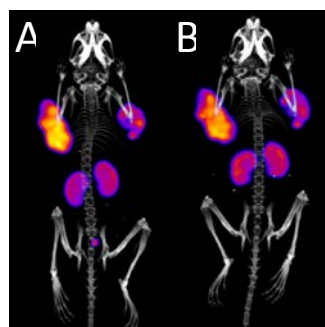


Fig. 1: PET/CT scans of mice bearing s.c. medullary thyroid cancer 3 h (A) and 17 h (B) after injection of ⁴³Sc-DOTA-minigastrin.

The isolated product from the irradiated ⁴⁶Ti-targets was of high radionuclidic purity, containing 98.2% ⁴³Sc, only 1.5% ^{44g}Sc and less than 0.08 % long-lived ^{44m}Sc, ⁴⁶Sc, ⁴⁷Sc and ⁴⁸Sc. The co-produced Y-isotopes (⁸⁶Y, ^{87g/m}Y, ⁸⁸Y), present at 0.29%, probably originate from the introduction of nat. Sr-impurities during the ⁴⁶TiO₂ reduction process. Bench experiments with the extraction chromatographic resin UTEVA allowed successful separation of the Y-impurities, however, the losses of ⁴³Sc activity in the waste fraction were considered too high. The obtained ⁴³Sc was successfully radiolabelled with PSMA and used for in vivo PET/CT imaging of a tumour bearing mouse as a proof of concept (results not shown here).

- [1] G. Kramer-Marek et al., *Curr Pharm Des* **18**, 2657 (2012).
- [2] M. Gabriel et al., *J Nucl Med* **48**, 508 (2012).
- [3] R. Walczak et al., *EJNMMI Physics* **33**, 1 (2015).
- [4] B. Lommel et al., *J Radioanal Nucl Chem* **299**, 977 (2014).

PRODUCTION AND SEPARATION OF ^{47}Sc FOR RADIOPHARMACEUTICAL APPLICATIONS

K. Dommanich (Univ. Bern & PSI), U. Köster (ILL), B. Ponsard (SCK/CEN), M. Benešová, K. Siwowska, C. Müller, R. Schibli (ETHZ & PSI/CRS), A. Türler (Univ. Bern & PSI), N.P. van der Meulen (PSI)

INTRODUCTION

In the past few years an increased demand for novel radionuclides, fulfilling the characteristics of a “matched pair”, emerged in the field of nuclear medicine [1]. The radionuclides of scandium ^{43}Sc , ^{44}Sc and ^{47}Sc satisfy all the requirements due to their identical chemical behaviour but different physical properties. The decay characteristics of ^{43}Sc and ^{44}Sc are well suited for Positron Emission Tomography-imaging, while the low energy β -emitter ^{47}Sc ($t_{1/2}=3.4$ d, $E\beta_{\text{av}}=162$ keV, $E\gamma = 159.4$ keV (68.3%)) could be utilised for targeted tumour therapy. ^{47}Sc is considered as an attractive alternative to the currently clinically applied ^{177}Lu ($t_{1/2}=6.7$ d, $E\beta_{\text{av}}=134$ keV, $E\gamma = 208.4$ keV (11.0%)) [2, 3]. The aim of the following study was the production of sufficient ^{47}Sc activities of high quality, suitable for radiopharmaceutical application. The two neutron induced reactions $^{47}\text{Ti}(n,p)^{47}\text{Sc}$ and $^{46}\text{Ca}(n,\gamma)^{47}\text{Ca}\rightarrow^{47}\text{Sc}$, were investigated and compared.

EXPERIMENTAL

Irradiation: Quartz glass ampoules, containing 0.14–0.35 mg ^{46}Ca were irradiated in the high flux reactors of Institut Laue-Langevin, Grenoble and SCK.CEN, Mol with n_{therm} -fluxes of $\sim 1.2\cdot 10^{15}$ and $3.2\cdot 10^{14}$ n/cm²*s, respectively for 4–11 days. The irradiation of ^{47}Ti containing ampoules (0.6–19.9 mg) was performed at SINQ, PSI (n_{therm} -flux= $3.2\cdot 10^{13}$ n/cm²*s) for 11–19 days or at SCK.CEN for 7 days and both production methods were compared with regard to their yield and radionuclidic purity. **Chemical Separation:** After crushing the irradiated ^{46}Ca ampoule, the target material was dissolved and ^{47}Sc was separated on DGA extraction chromatographic resin using different concentrations of HCl. To up-concentrate the ^{47}Sc in a smaller volume, a second, smaller DGA column was used and the product was eluted in only 700 μL 0.05 M HCl. **Radiolabelling:** Radiolabelling of ^{47}Sc was performed with DOTANOC at a specific activity of 10–25 MBq/nmol immediately and 3 days post separation. The in vitro stability was investigated in PBS (phosphate buffered saline, pH 7.4) at room temperature over 3 days and was compared to ^{177}Lu -DOTANOC.

RESULTS AND DISCUSSION

Neutron irradiation of the ^{46}Ca targets resulted in the formation of 0.2–1.9 GBq ^{47}Sc and considerably less ^{47}Sc (3.9–4.9 MBq ^{47}Sc) could be produced from ^{47}Ti . This is due to a lower nuclear cross section and a lower abundance of fast neutrons, required to induce the nuclear reaction. The separation of $^{46/47}\text{Ca}$ and ^{47}Sc was performed on a custom-made separation panel inside the hot-cell (Fig. 1). A second separa-

tion could be performed after a minimum in-growth time of 3 days, due to the renewed generation of ^{47}Sc from the decay of ^{47}Ca . The obtained product was of high radionuclidic purity (99.995 %), containing max. 0.005 % long-lived ^{46}Sc in the eluate of the first separation. It was directly used for labelling experiments and for in vivo/vitro applications (data not shown here).



Fig. 1: ^{47}Sc separation panel designed for the operation in the hot-cell.

Radiolabelling of ^{47}Sc was reproducibly performed at a specific activity of 10 MBq/nmol DOTANOC. ^{47}Sc -DOTANOC was stable over a period of 3 days in PBS, with less than 2.1% of free ^{47}Sc , which is comparable to the clinically-used analogue ^{177}Lu -DOTANOC (Fig. 2).

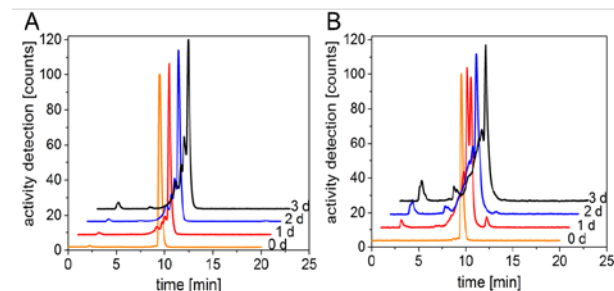


Fig. 2: Stability of ^{47}Sc -DOTANOC (A) in comparison to ^{177}Lu -DOTANOC (B) in PBS.

Regarding the low production yield from the irradiated ^{47}Ti -targets and a higher percentage of long-lived ^{46}Sc (up to 11.5%), the production of sufficiently high ^{47}Sc -activities for radiopharmaceutical purposes was not considered possible, and, thus, chemical isolation of ^{47}Sc from ^{47}Ti was not performed and further investigations of this route were omitted. In view of the promising results from the ^{46}Ca -irradiations, the research focus will be laid on this production pathway.

- [1] F. Kraeber-Bodere et al., *Font Med* 1:16 (2014).
- [2] C. Müller et al., *J Nucl Med* **55**, 1658 (2014).
- [3] B. Bartoś et al., *Radiochim. Acta* **100**, 457 (2012).

THE DCB-UNIBE RADIOPHARMACEUTICAL LABORATORY AT SWAN HOUSE

J. Moreno, O. Leib, M. Bunka, T. Basaco, N. Meneses, A. Türlér (Univ. Bern & PSI)

During 2016, the team at the DCB-UNIBE radiopharmaceutical laboratory (Fig. 1) continued with the routine production of [^{68}Ga]DOTA-TATE, which is used as radiotracer for diagnostic of NETs by PET/CT). The radiotracer was produced to support the clinical study called “GAIN” project, which was coordinated with the Department of Nuclear Medicine at the Inselspital and SWAN Isotopen AG. The number of patients treated with the [^{68}Ga]DOTA-TATE for clinical studies was of approximately 20 as during 2015. In total, within the frame of these studies, 78 patient doses have been released. The [^{68}Ga]DOTA-TATE was also used in patients who received a special authorization from Swissmedic. In this period the number of doses released for these patients increased from 26 in 2015 to 42 in 2016. Indeed, the [^{68}Ga]DOTA-TATE from the DCB-UNIBE radiopharmaceutical laboratory was distributed not only to the local hospital facility in Bern but also to the university hospital in Lausanne.

In addition to the production of [^{68}Ga]DOTA-TATE, special authorizations were received from the regulatory authorities to produce [^{177}Lu]DOTA-TOC for peptide receptor radionuclide therapy (PRRT) treatment of neuroendocrine tumors in selected patients. As a result, the first six doses of 7.4 GBq each were released to the “Kantonsspital St. Gallen” during the year. The overall radiochemical yield of [^{177}Lu]DOTA-TOC was higher than 85 % in these processes as shown in Fig. 3.

In this period, a planned inspection of the RHI “Regionales Heilmittelsinspektorat der Nordwestschweiz” representing the regularity authorities took place and the work of the team was positively evaluated. As a result the Certificate of GMP Compliance was received with the authorization to manufacture investigational medicinal products.



Fig. 1: Team at the DCB-UNIBE Laboratory in SWAN Haus, Bern.

Regarding the research and development work, the validation work for the manufacture of the diagnostic

radiopharmaceutical [^{68}Ga]PSMA-11 at the DCB-UNIBE radiopharmaceutical laboratory was completed. Major concerns affecting the quality were evaluated. The updated assessment was focused on concerns related to the risk of microbiological contamination and radiation protection issues. The synthesis of [^{68}Ga]PSMA-11 was set up based on the acetone free method with optimised parameters for the yield during the pre-purification step. The parameters of the process included in the automatic projects were specifically developed for the ITG and EZAG Ga-Generators. The analytical methods were validated and approved before the production validation.

[^{68}Ga]PSMA-11 is intended to be used as radiotracer for diagnostic of prostate cancer by PET/CT.

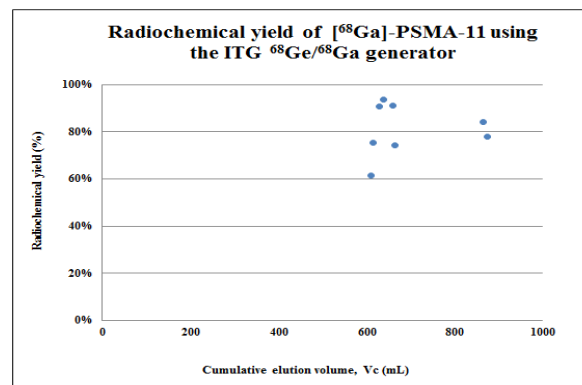


Fig. 2: Radiochemical yield of [^{68}Ga]PSMA-11 in bioburden and validation test batches.

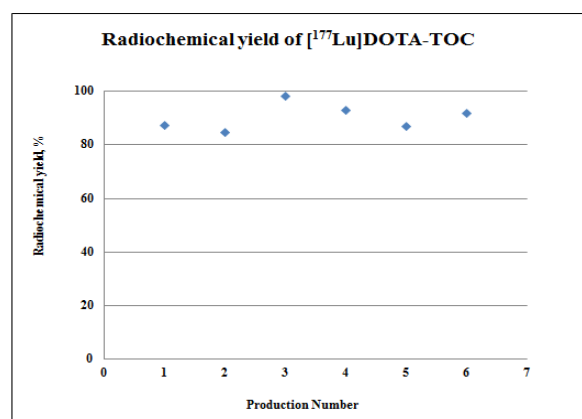


Fig. 3: Radiochemical yield of [^{177}Lu]DOTA-TOC in batches produced during 2016.

After the successful submission of the relevant applications and documents that included the Quality Dossiers, provisional authorizations for the production of therapeutic [^{177}Lu]DOTA-TOC and diagnostic [^{68}Ga]DOTA-TATE and [^{68}Ga]PSMA-11 were approved by Swissmedic.

CHARACTERIZATION OF GIRENTUXIMAB CONJUGATES FOR RADIOIMMUNOTHERAPY

T. Basaco (Univ. Bern & PSI), S. Pektor (Univ. Mainz), J. Moreno (Univ. Bern), M. Miederer (Univ. Mainz), A. Türler (Univ. Bern & PSI)

Radiopharmaceuticals based on conjugated monoclonal antibodies (mAb) have become a potential tool in nuclear medicine, because of their specificity and the large variability and availability of therapeutic radiometals. Girentuximab (G250) is a potential candidate for radioimmunotherapy of renal clear cell carcinomas (RCCs) because it is reactive with CAIX antigen, a transmembrane glycoprotein overexpressed on the cell surface of most of RCCs (>90%) [1-2].

G250 was conjugated with the bifunctional chelating agent DOTA (1,4,7,10-Tetraazacyclododecane-N,N',N'',N'''-tetraacetic acid) via a benzyl-thiocyanato group as a linker (p-SCN-βn-DOTA) using variable incubation times in order to obtain different types of conjugates. DOTA-G250 conjugates were analysed by size exclusion chromatography (SE-HPLC) and by electrophoresis (SDS-PAGE). Different types of DOTA-girentuximab conjugates were obtained and classified depending of the number of molecules of BFC attached to the mAb. The ratio DOTA/mAb decreases in the following order: Type I > Type II > Type III [3].

In order to identify the conjugation sites and number of attached chelator molecules to mAb, the conjugates were characterized by Mass Spectrometry. Potential DOTA modification sites of the chelator were identified in lysine residues (K) by liquid chromatography-mass spectrometry (LC/MS-MS). DOTA modifications were not always allocated to the same lysine residue within a peptide. The occupancy of a lysine residue with the DOTA modification was calculated by MxQuant. Complementary determining regions (CDR) of G250 were not modified by DOTA [3]. The number of linkers per molecule of mAb was calculated using the molecular weight (MW) measured by matrix assisted laser desorption ionization-time of flight mass spectrometry (MALDI-TOF MS) using a saturated solution of α-Cyano-4-hydroxycinnamic acid (CHCA) as a matrix in non-reduced and reduced conditions. The average number of DOTA molecules per molecule of mAb was calculated using the molecular weight mass spectra chromatogram (Fig. 1 and Fig. 3) and 0.552 kDa as molecular weight of p-SCN-βn-DOTA following the formula below:

$$\text{Ratio } \frac{\text{DOTA}}{\text{mAb}} = \frac{\text{MW conjugates (kDa)} - \text{MW native (kDa)}}{\text{MW DOTA (kDa)}}$$

The average number obtained for the conjugates in non-reduced conditions was between 8-10 molecules of DOTA per molecule of mAb. The average number

obtained in the conjugates in reduced conditions was between 1-2 and 3-4 molecules of DOTA per molecule of mAb in the light chain (LC) and heavy chain (HC) respectively.

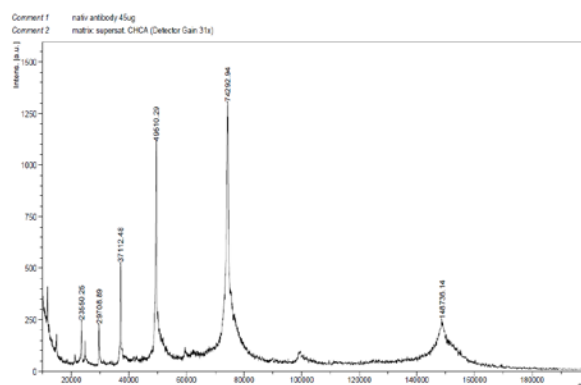


Fig. 1: MALDI-TOF mass spectrum of native G250.

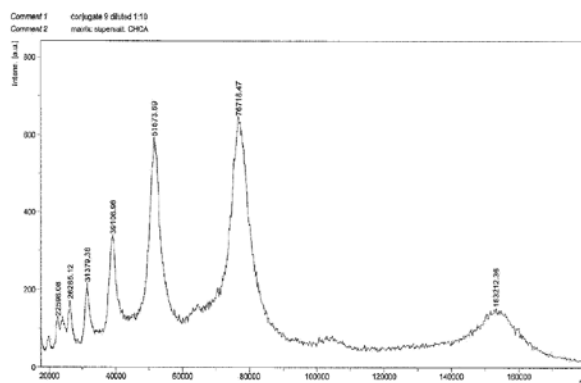


Fig. 2: MALDI-TOF spectrum of p-SCN-βn-DOTA-G250 conjugate (Type II).

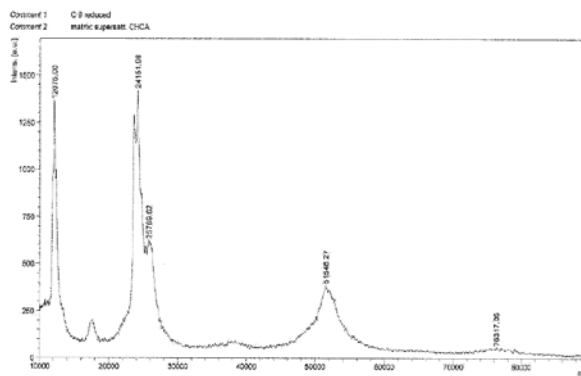


Fig. 3: MALDI-TOF mass spectrum of p-SCN-βn-DOTA-G250 conjugate (Type II) reduced with DTT.

The DOTA-G250 conjugates were labelled with ^{177}Lu with a radiochemical yield > 95% reaching specific activities of 12 MBq/ μg . The radiostability of ^{177}Lu -DOTA-G250 at high specific activity was increased by addition of sodium ascorbate after the labelling.

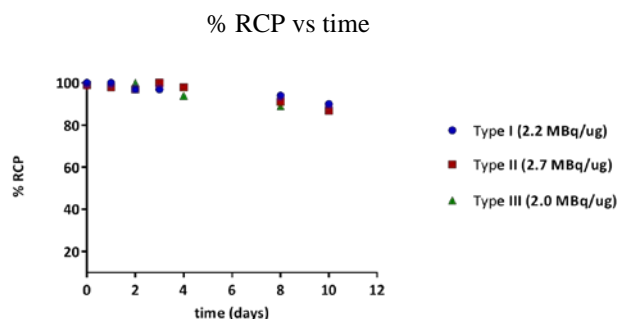


Fig. 4: Radiostability of ^{177}Lu -DOTA-G250 in HSA 1% at 37°C by ITLC.

The in vitro stability of different types of radioconjugates was analyzed in human serum albumin (HSA) and was more than >90% up to 10 days at 2 MBq/ μg specific activity (Fig. 4).

Binding and internalization assays to SK-RC-52 cell were performed using different radioconjugates in HSA 1% at 37°C 48 h after the labeling (Fig. 5). Radioimmunoactivity was higher for conjugates with less DOTA content.

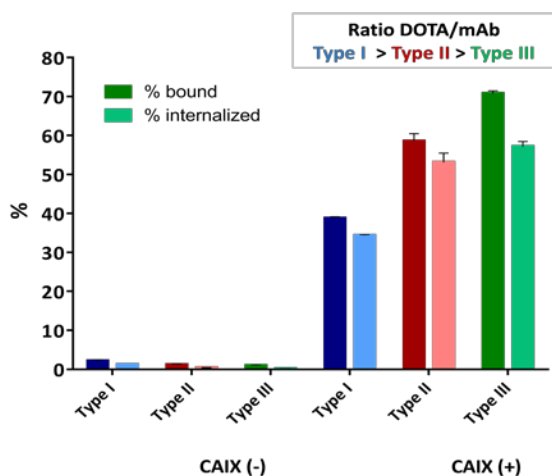


Fig. 5: Radioimmunoactivity in vitro of ^{177}Lu -DOTA-G250.

The animal experiments were performed in male nude BALB/c nu/nu mice (Janvier, le Genest-Saint-Isle, France). Tumor growth was induced by a subcutaneous injection of 0.1 mL of a suspension of 3×10^6 SK-RC-52 cells. Protein dose was optimized in mice with subcutaneously growing SK-RC-52 tumors using different amounts of ^{177}Lu -DOTA-G250. The tumor uptake of ^{177}Lu -DOTA-G250 was higher in the group of animals, who received 30 μg protein doses (Fig. 7).

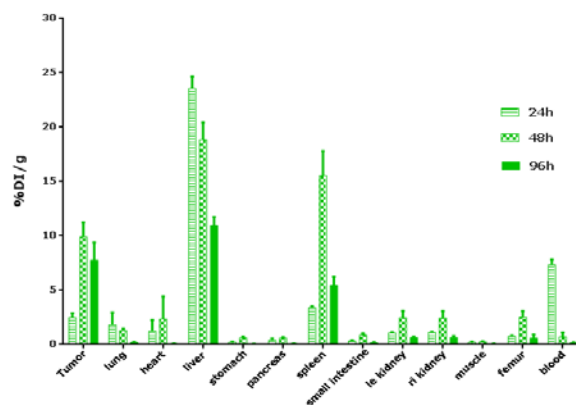


Fig. 6: Biodistribution of ^{177}Lu -DOTA-G250 in mice Balb/c nu/nu with subcutaneous SK-RC-52 tumor 24, 48 and 96 hours after injection.

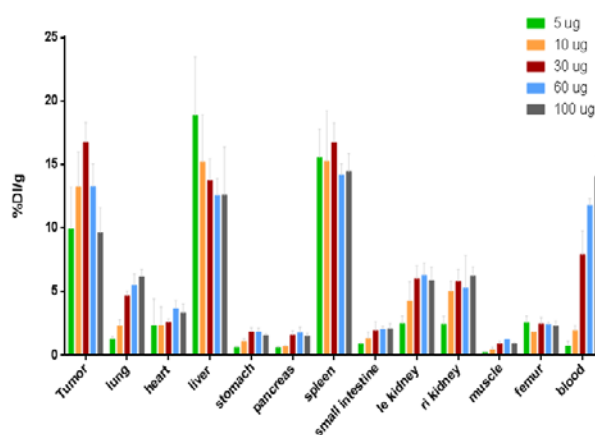


Fig. 7: Biodistribution of ^{177}Lu -DOTA-G250 in mice Balb/c nu/nu with subcutaneous SK-RC-52 tumor 48 hours after injection using different doses of mAb.

Acknowledgements:

Mass spectrometry sequencing data was acquired at the Proteomics and Mass Spectrometry Core Facility, Department of Clinical Research, University of Bern, Switzerland.

MALDI-TOF mass spectra data was obtained at Protein Analysis group, Department of Chemistry and Biochemistry, University of Bern, Switzerland.

All animal experiments were approved by the Animal Experiments Committee of the University Medical Center of Johannes Gutenberg Mainz and performed in accordance with its guidelines.

- [1] E. Oosterwijk et al., *Int. J Cancer* **38**, 489 (1986).
- [2] Oosterwijk-Wakka et al., *Int J Mol Sci* **14**: 11402 (2013).
- [3] T. Basaco et al., *Ann Rep. Lab. of Radio- & Environ. Chem., Univ. Bern & PSI*, p. 59 (2015).
- [4] A. Brouwers, et al., *J Nucl Med* **45**, 327 (2004).

EVALUATION OF CAIX EXPRESSION IN NUDE MOUSE XENOGRAFT MODEL

T. Basaco (Univ. Bern & PSI), J.A. Galván (Univ. Bern), S. Pektor (Univ. Mainz), J. Moreno (Univ. Bern), M. Miederer (Univ. Mainz), A. Türlér (Univ. Bern & PSI)

INTRODUCTION: Girentuximab (G250) is a high-affinity chimeric monoclonal antibody (mAb) reactive against the carbonic anhydrase IX (CAIX) antigen. CAIX is a membrane isoenzyme and hence imparts a membrane-predominant staining pattern by immunohistochemistry [1-2]. Given that CAIX contains an extracellular domain, it has been shown that this will allow for an easier access and direct binding of antibodies. The G250 has shown a remarkable targeting ability and therefore it has become a potential candidate for radioimmunotherapy of clear cell carcinomas (RCC) because CAIX is overexpressed on the cell surface of most (>90%) RCCs [3]. The aim of the experiment is to optimize the in vivo mice model by CAIX immunohistochemistry for further animals studies with conjugated G250 labelled with therapeutic radionuclides such as ^{177}Lu or ^{225}Ac .

MATERIAL & METHODS: Nude Mouse Xenograft Model. The RCC cell line SKRC-52 were cultured in RPMI medium (Life Technologies, CH) supplemented with 10% fetal calf serum (FCS) at 37°C in a humidified atmosphere with 5% CO₂. SKRC-52 cells were injected subcutaneously (Fig. 1) into the right flank of BALB/c nu/nu mice (Janvier, le Genest-Saint-Isle, FR). The procedure was approved by the Animal Experiments Committee of the University Medical Center of Johannes Gutenberg Mainz and performed in accordance with its guidelines.

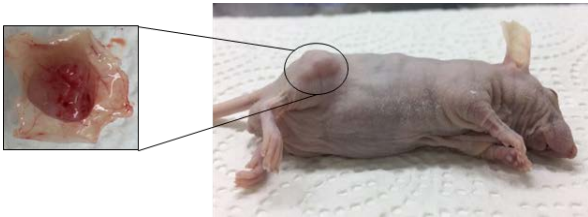


Fig. 1: Picture of the tumor volume on the animal and tumor sample.

The tumor and normal tissue (stomach, liver, gallbladder and spleen) samples were taken after 4, 5 and 6 weeks inoculated the SKRC-52 cells in groups of 3 animals. The samples were briefly washed with PBS, fixed with 4% paraformaldehyde and embedded in paraffin. The paraffin blocks were cut at 3 μm for hematoxylin and eosin (H&E) and immunohistochemistry (IHC).

ICC and IHC. The detection of CAIX expression was performed using anti CAIX rabbit polyclonal antibody (Abcam, UK, Ref ab15086), 1:1500 dilution for 30 min at room temperature. The antigen retrieval was performed in Tris-buffer at 95° for 30 min. During all experiments, human gastric mucosa was used as a positive control.

RESULTS: Tumor volume. After inoculation of the SK-RC-52, tumor size were measured in 2 dimensions (length x width) at least twice a week with a caliper. The tumor volume was calculated using the equation below:

$$V = \frac{\pi}{6} * (\text{higher measure}) * (\text{lower measure})^2$$

The calculated tumor volume growth per animal is shown below (Fig. 2).

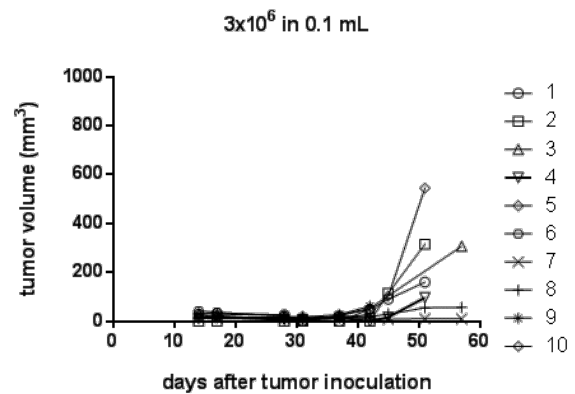


Fig. 3: Tumor volume vs days after inoculation.

CAIX expression. Prior inoculation of the SKRC-52 cells on the animals, conventional immunocytochemistry (ICC) was performed to evaluate the expression of CAIX. As expected, 100% of CAIX was detected in SKRC-52 cells. Strong immunostaining intensity, localized in cell membrane of the SK-RC-52 cell line with a linear pattern and negative on the SK-RC-18 cell line (Fig. 2).

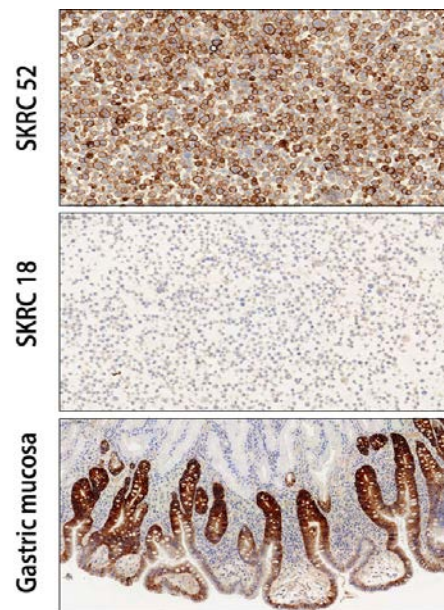


Fig. 2: CAIX immunostaining in SKRC-52 and SK-RC-18 cell lines and gastric mucosa.

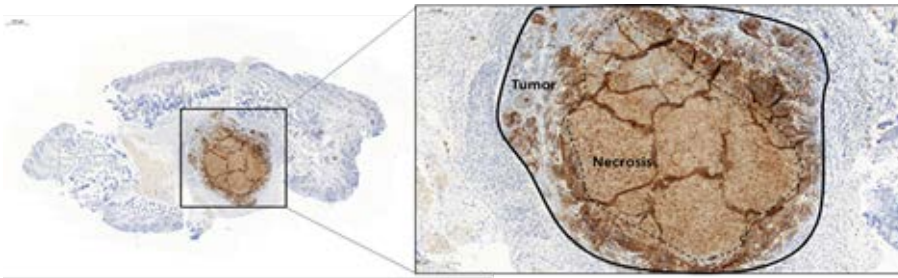


Fig. 4: CAIX immunostaining in tumor, Homogeneous pattern, low vascularity, 80% confluent necrosis, volume 15 mm³. 1x and 20x objective, respectively.

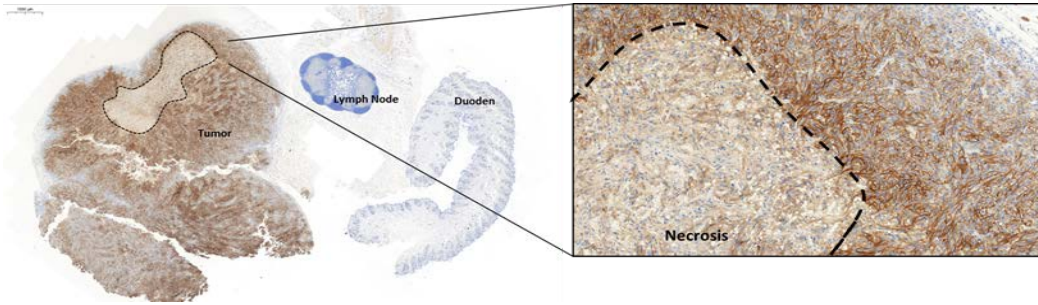


Fig. 5: CAIX immunostaining of tumor, homogeneous pattern, volume 544 mm³. 1x and 20x objective, respectively.

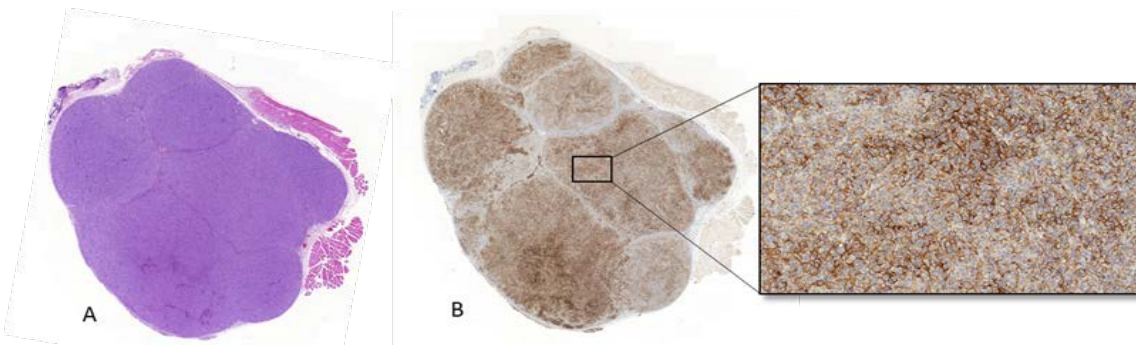


Fig. 6: H&E of the tumor (A), not necrosis. CAIX immunostaining (B), homogeneous pattern, not necrosis, volume 161 mm³. 1x and 20x objective, respectively.

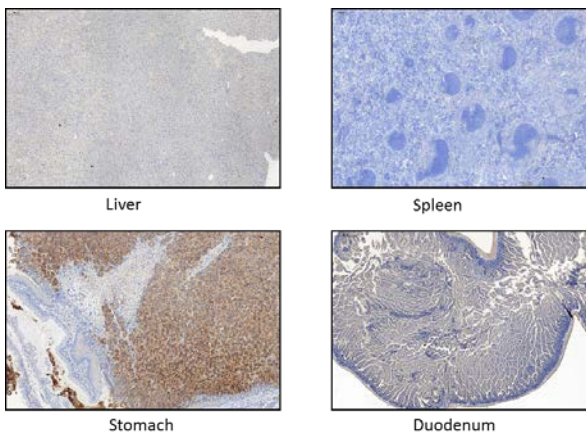


Fig. 7: CAIX immunostaining in healthy tissues. CAIX staining was only positive in gastric mucosa.

IHC analysis of CAIX showed strong intensity, localized in cell membrane of the SK-RC-52 tumor depending of the size and stage of the tumor. Tumors smaller than 20 mm³ and tumors larger than 200 mm³ developed necrosis. In the normal tissue samples, CAIX immunostaining showed strong intensity in the stomach and negative immunostaining in the rest of the organs.

Conclusion: Further experiments with G250 radioconstructs using the nude mouse xenograft model should be carried out between 2 and 4 weeks after inoculation of the SKRC-52 cells. The tumor volume should be in the range of 20 – 200 mm³ to avoid necrosis and to minimize the error associated with the tumor size among the animals.

- [1] A. Luong-Player et al., *Am J Clin Pathol* **141**, 219 (2014).
- [2] P. C. McDonald et al., *Oncotarge* **3**, 84 (2012).
- [3] E. Oosterwijk et al., *Int J Cancer* **38**, 489 (1986).
- [4] A. M. Schläfli et al., *Oncotarget* **7**, 39544 (2016).

SOURCE APPORTIONMENT OF CARBONACEOUS AEROSOLS BY CONTINUOUS-FLOW ^{14}C MEASUREMENTS: STATISTICAL ANALYSIS

G. Salazar (Univ. Bern), K. Agrios (Univ. Bern & PSI), S. Szidat (Univ. Bern)

The carbonaceous aerosol (total carbon, TC) and its sub-fractions organic carbon (OC) and elemental carbon (EC) constitute a significant portion of the atmospheric fine air particulate matter. Fossil vs non-fossil emission sources of OC and EC fractions can be traced back by different radiocarbon (^{14}C) levels. In order to increase the fingerprint information and to separate the interferences, we have developed a method for higher resolution thermal separation to observe sub-fractions within OC [1], taking advantage of slower thermal desorption ramps, online combustion and continuous-flow ^{14}C analysis (See Fig. 1a).

Here, we apply the analysis of variance (ANOVA) method for model selection to the whole sub-fraction $^{14}\text{C}/^{12}\text{C}$ ratios (R values), and t -test at the beginning and end of the linear model to answer the following questions: Are the R values of the thermally desorbed substances constant or do they follow a linear or quadratic trend? Is the total variation ΔR , i.e. the difference of R at the beginning and the end, distinguishable (see Fig. 1b)? How to measure the signal variation strength among samples?

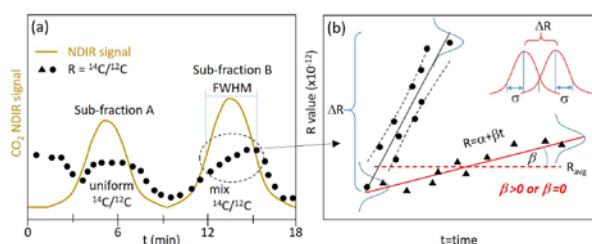


Fig. 1: a) Scheme of the thermal separation of OC sub-fractions. b) Scheme of the statistics applied to the R values ($^{14}\text{C}/^{12}\text{C}$ ratios) showing the constant model (red dashes) and the linear model (red line) with β and α as slope and intercept, respectively.

The OC sub-fractions separation is done with a SUNSET aerosol analyser with an NDIR CO_2 detector [1]. O_2 flow is mixed with a small amount of He and injected into the instrument. The exhaust connects to a hot copper reactor to scrub away the O_2 gas. Then, the system is connected online to a MICADAS AMS with gas ion source through a fused silica capillary [2].

ANOVA was applied with an F -test to the data illustrated in Fig. 1b. The comparison of the linear model [L] versus the constant model [K] is symbolized by [LvsK] and the quadratic [Q] vs linear comparison by [QvsL]. ANOVA indicates if the higher-order model significantly decreases the variance. We also compared if the ΔR between the beginning and the end of the linear model are distinguishable using a t -test and the confidence interval of the model (σ). Table 1 shows the t -score calculated as $t(R)=\Delta R/\sigma$.

15 aerosol samples collected in four Chinese cities [3] containing 58 sub-fractions were statistically analysed. Tab. 1 shows two representative cases, one from an untreated and one from a water-extracted filter, with 3 thermal sub-fractions each. The model is considered linear if the LvsK and the t -test for $t(R)$ show that the R values are distinguishable from a constant value ($p<0.05$). It is regarded as quadratic if QvsL also has a $p<0.05$. The total variation ΔR is reported as a pMC range for the Q and L models. 26% of the sub-fractions showed linearity with OC 200°C as an example. The QvsL of OC 300°C and WINSOC (water-insoluble OC) 200°C indicate that they are even better represented by the quadratic model and this was shared by 19% of the data. For the remaining 55% of the cases, a rejection of the null hypothesis of the statistical test is not justified so that the constant model is the appropriate choice. The $t(R)$ score is also useful to linearly compare the strength of signal variation among different samples. Sub-fractions OC 200°C and WINSOC 200°C have the strongest variations which allows to easily distinguish linear variations of 38-49 and 26-41 pMC, respectively.

Tab. 1: ANOVA results for continuous-flow ^{14}C measurements of different thermal fractions of OC and water-insoluble OC (WINSOC) from an air filter from Beijing [3]. Green and red colours indicate that the higher-order model is statistically significant or not, respectively.

Fraction	ANOVA		$t(R)$	^{14}C (pMC)	σ (pMC)
	QvsL	LvsK			
OC 200°C			4.1	38.4-49.0	3.8
OC 300°C			2.4	51.9-59.7	4.5
OC 375°C			1.0	65.2	1.2
WINSOC 200°C			4.6	26.3-41.0	4.5
WINSOC 300°C			0.2	39.1	1.3
WINSOC 375°C			1.0	50.1	1.1

[1] K. Agrios et al., Radiocarbon, DOI: 10.1017/RDC.2016.88, in press.

[2] S. Szidat et al., Radiocarbon **56**, 561 (2014).

[3] R. J. Huang et al., Nature **514**, 7521 (2014).

RADIOCARBON DATING OF BONES AT THE LARA LABORATORY IN BERN

S. Szidat, E. Vogel (Univ. Bern), R. Gubler (ADB), S. Lösch (Univ. Bern, IRM)

Since the establishment of the Laboratory for the Analysis of Radiocarbon with AMS (LARA) at the University of Bern in 2013, the quality of sample preparation and radiocarbon measurement procedures have been validated for different materials such as plant remains, macrofossils, bulk sediment, charcoals, and wood [1]. For the optimization of the samples pre-treatment of bones, protocols described in the literature ([2] and references therein) were investigated and validated.

The extraction of collagen was performed with an acid-base-acid (ABA) treatment, gelatinization, coarse filtration, lyophilization, and graphitization [3]. In first step, different ABA treatments were applied in order to find out the best suitable procedure for decontamination of the bones from environmental contamination for materials close to the ^{14}C background (Fig. 1). A full ABA treatment with a long initial acid step (60h) was found out to be the most effective. An additional blank contribution for bone treatment was determined by comparison with the preparation of other sample materials. This additional is supposed to mainly originate from the lyophilization step.

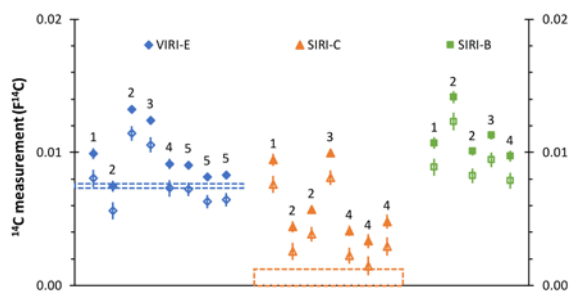


Fig. 1: Comparison of the measured $F^{14}\text{C}$ value and corresponding reference results with 1σ uncertainties for bones >35 kyr using these treatments: (1) acid only, (2) ABA with short (1h) first acid step, (3) ABA with short first acid step and ultrafiltration, (4) ABA with long (60h) first acid step, and (5) ABA with long first acid step after Soxhlet extraction [3]. Filled symbols include a subtraction of the blank for a normal ABA treatment. Open symbols represent an additional blank for bone treatment. Reference $F^{14}\text{C}$ values [4] are indicated as dashed areas.

After the definition of the final preparation method, the second part of the study aimed to validate the bone dating as a whole. For this, 33 samples from the Holocene, predated by other ^{14}C laboratories including materials from VIRI/SIRI Intercomparisons [4] or from well-known archaeological contexts, were analyzed in a blind test (Fig. 2). For these samples, the comparison of the measured and the reference age matched within 2σ confidence for 31 out of the 33 bones. In particular, our measurements agreed well for the samples VIRI-F/H/I [4], whose reference ages are the most reliable of all bones.

The average age offset between expected and measured ^{14}C age of all 33 samples except for the two outliers amounts to -4 yr, i.e. with measured values slightly younger than expected on the average. The standard deviation of the age offsets is ± 44 yr, calculated referring to the single analysis. This scatter reproduces well the average uncertainty of the individual age offsets of ± 48 yr for this subset of data. This outcome suggests that our laboratory is able to date Holocene bones correctly and the outlier cases require closer examination.

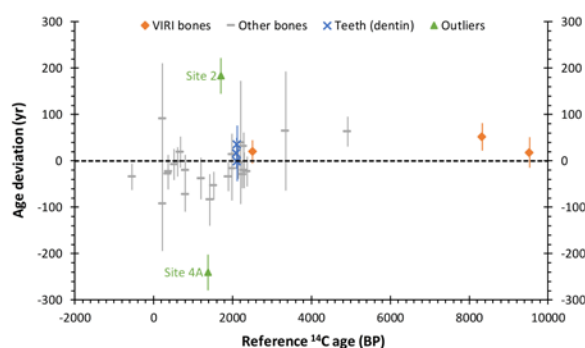


Fig. 2: Deviation of the measured ^{14}C age of bones and teeth from the reference ^{14}C age for Holocene samples with 1σ uncertainties [3]. Reference ^{14}C ages are given in years before present (BP, i.e. referring to the year 1950 AD).

-
- [1] S. Szidat et al., Radiocarbon **56**, 561 (2014).
 - [2] R-H Fülöp et al., Radiocarbon **55**, 491 (2013).
 - [3] S. Szidat et al., Radiocarbon, DOI: 10.1017/RDC.2016.85, in press.
 - [4] E. M. Scott et al., Radiocarbon, **52**, 846 (2010).

ISOLATION OF BLACK CARBON AND ELEMENTAL CARBON FOR SOURCE APPORTIONMENT IN SEDIMENTS BASED ON ^{14}C ANALYSIS

M. Vonwiller (Univ. Bern & PSI), C. Steiner, S. Szidat (Univ. Bern)

Sediments are an important sink for air-borne particulate matter. Lake sediments may therefore serve as environmental archives for atmospheric PM concentrations of the past. However, two major drawbacks limit the potential of lake sediments as such archives. On the one hand, the regional atmospheric input needs to be distinguished from the local input of the catchment of the lake, which has been deposited by surface run-off or resuspended by winds erosion. On the other hand, tracing back atmospheric PM concentrations from sediment records is often hardly possible due to the lack of quantitative information on scavenging and deposition factors.

There is a great inconsistency about the terminology of black carbon (BC) within the literature of sediment and atmospheric sciences. Whereas BC is defined as an ideally light-absorbing substance composed of carbon and discriminated from elemental carbon (EC) as derived from evolved thermal methods in atmospheric sciences [1], it describes a continuum of slightly charred biomass, charcoal and soot in the sediment community [2].

This project aims at the development of an EC isolation procedure from sediment (and soil) samples for subsequent ^{14}C analysis to differentiate between fossil and wood-burning sources. For this, it is crucial to remove the inorganic sediment matrix and organic carbon (OC) to reduce charring of the latter during the thermal removal of the remaining OC. Four different acid digestions were tested based on the methods developed by Han et al. [3, 4]. The procedure shown in Fig. 1 turned out to be the most promising methodology to remove most components interfering with the EC isolation.

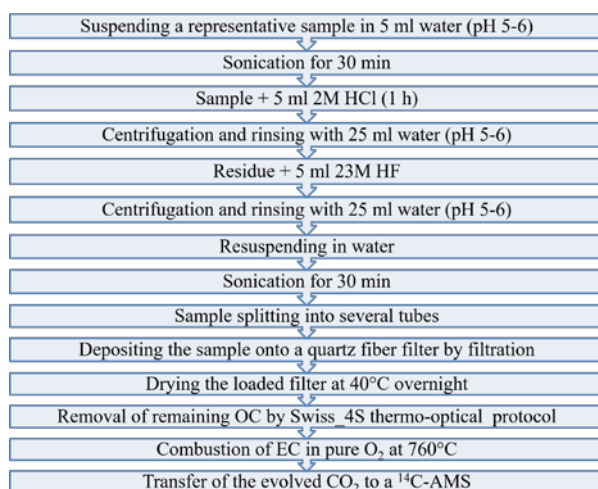


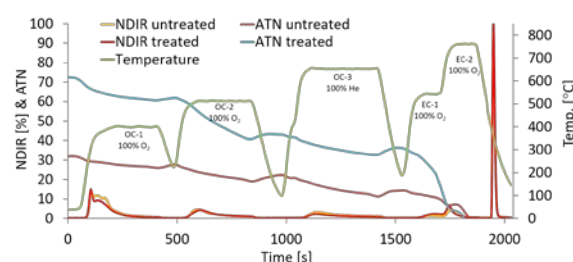
Fig. 1: Complete workflow of the EC isolation procedure and subsequent ^{14}C analysis.

The approach shown in Fig. 1 was motivated by the thorough method development of the acid digestion treatment of sediment samples on the one hand [3, 4] and by our own experiences of EC isolation from atmospheric aerosols collected on quartz fibre filters on the other hand [5].

Two reference materials (NIST SRM-1649a “Urban Dust” and IAEA-SL-1 “Lake Sediment”) and mixtures thereof were used to assess the selectivity of the OC/EC separation.

Energy-dispersive x-ray analysis indicated that Si, Al, Fe and most major earthbound elements are efficiently removed in the acidic pretreatment while minor elements such as Ti and Zr are not affected.

The acid digestion yields an improved EC yield compared to non-treated samples and has furthermore a positive effect on OC charring as well as on the EC recovery (Fig. 2). However, low EC recoveries were observed for the complete procedure ($20\pm 10\%$), whereof $\sim 50\%$ EC loss occurred during the deposition/filtration step. Further tests are necessary including the analysis of ambient sediment samples.



Sample	EC yield after S1	EC yield after S2	EC yield after S3	Total Carbon [$\mu\text{g}/\text{cm}^2$]
SRM-1649a	92%	62%	58-70% (n=3)	21-45
SRM-1649a untreated	90%	66%	20-39% (n=2)	30-65

Fig. 2: Prolonged thermal-optical protocol for OC/EC separation in sediments based on the Swiss_4S protocol [5]. The NDIR shows evolving OC + EC during the thermal steps S1-S4. ATN refers to the decrease of EC due to the change of the optical attenuation.

- [1] A. Petzold et al., *Atmos. Chem. Phys.* **13**, 8365 (2013).
- [2] M. I. Bird and P.L. Ascough, *Org. Geochem.* **42**, 1529 (2012).
- [3] Y. Han et al., *Water Air Soil Pollut.* **17**, 167 (2007).
- [4] Y. Han et al., *Chemosphere* **75**, 92 (2009).
- [5] Y. L. Zhang et al., *Atmos. Chem. Phys.* **12**, 10841 (2012).

RADIOCARBON ANALYSIS OF METHANE 1: OPTIMIZATION OF THE CHROMATOGRAPHIC SEPARATION OF PRECONCENTRATED AIR SAMPLES

C. Espic, M. Liechti, M. Battaglia, S. Szidat (Univ. Bern)

Methane (CH_4) contributes substantially to global warming as the second most important anthropogenic greenhouse gas. Although the global budget of atmospheric CH_4 is quite well constrained, individual sources remain poorly quantified and not well understood [1].

The radiocarbon (^{14}C) content of CH_4 emissions is of growing interest since it can be used as a tool for a CH_4 source apportionment [2]. Indeed, contemporary CH_4 (e.g. from agriculture, biomass burning) contains present-day ^{14}C levels whereas fossil CH_4 (e.g. from fossil fuels, geologic sources) is almost ^{14}C -free [3]. These radiocarbon measurements can be performed by accelerator mass spectrometry (^{14}C -AMS) but this task is challenging given the large amounts of CH_4 required and its very low concentration in the atmosphere. CH_4 is usually cryogenically separated from other trace gases (mainly CO and CO_2), but cross contamination remains an issue difficult to overcome [4].

Our research aims at enabling the extraction of CH_4 from various kinds of environments (atmosphere, fresh waters and wetlands) and performing ^{14}C measurements with the MICADAS AMS in our laboratory [5]. We decided to adapt and develop analytical setups to pre-concentrate CH_4 directly in the field in order to bring small samples to the lab where CH_4 is purified and prepared for ^{14}C measurements. Our strategy is to develop a preparative gas chromatography technique (pGC) [6] to separate CH_4 from other gases, giving the possibility to check the CH_4 purity. Furthermore, this technique also allows the recovery of CO and CO_2 for a more comprehensive environmental study.

The gas samples are injected with a syringe in an Agilent 7890B GC equipped with a purged packed (PP) inlet and a thermal conductivity detector (TCD). We use a Restek Shincarbon ST 80/100 packed column, with an internal diameter of 2 mm and a length of 2 m, as this column contains an ideal medium for the separation of permanent gases and hydrocarbons. Because the gas samples will be pre-concentrated before GC separation on the one hand and the detector is not sensitive enough for the detection of atmospheric trace gases on the other hand, a standard gas mixture "SGM" (79% N_2 , 12% CO_2 , 5% O_2 , 2% CO and 2% CH_4), containing higher concentrations of the trace gases, was used for the GC method optimization.

Figure 1 presents the chromatograms (TCD signals) of the syringe injections of 1 ml and 5 ml standard gas mixture.

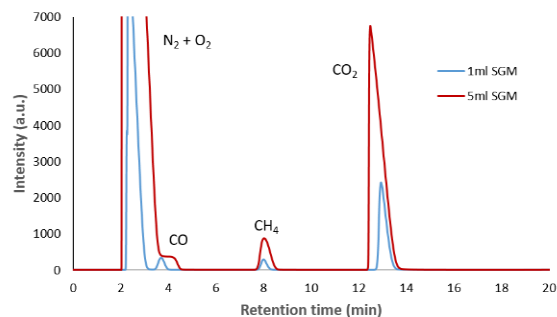


Fig. 1: TCD Chromatograms showing the optimized separation of a 1 ml and 5 ml gas mixture (79% N_2 , 12% CO_2 , 5% O_2 , 2% CO and 2% CH_4)

According to the physical properties of the packing material, the gases are mainly separated depending on their volatility. The oven temperature is kept at 40 °C for the first 4 minutes, to ensure an acceptable separation of CO from bulk air, then a temperature ramp of +10 °C/min is applied to shorten the run. The PP inlet is used in constant pressure mode (20 psi), which causes a gradual decrease of the He carrier gas flow rate from 14 ml/min down to 9 ml/min as the temperature of the oven increases.

Although the separation of CO , CH_4 and CO_2 is successful for a 1 ml injection of the standard gas mixture, the chromatogram of the 5 ml injection shows an incomplete separation of CO from bulk air. This is due to the relatively large amounts injected, causing an overloading of the column. The consequences are a peak broadening, tailing and shift to earlier retention times. However, we are still able to separate CH_4 and CO_2 for the amounts of carbon requested for ^{14}C -AMS measurements. Indeed, 5 ml of the standard gas mixture corresponds to a CH_4 amount of approximately 50 $\mu\text{g C}$, which is a typical amount for ^{14}C -AMS gas measurements.

ACKNOWLEDGEMENT

We are grateful for funding through the Dr. Alfred Bretscher Scholarship.

-
- [1] E. J. Dlugokencky et al., *Philos. Trans. R. Soc. London Ser. A*, **369**, 2058 (2011).
 - [2] K. R. Lassey et al., *Atmos. Chem. Phys.*, **7**, 2141 (2007).
 - [3] V. V. Petrenko et al., *Radiocarbon*, **50**, 53 (2008).
 - [4] M. Pack et al., *Org. Geochem.*, **78**, 89 (2008).
 - [5] S. Szidat et al., *Radiocarbon*, **56**, 561 (2014).
 - [6] T. Özek and F. Demirci, *Methods Mol. Biol.*, **864**, 275 (2012).

RADIOCARBON ANALYSIS OF METHANE 2: DEVELOPING A PREPARATIVE GAS CHROMATOGRAPHY TECHNIQUE FOR METHANE PURIFICATION

M. Liechti, C. Espic, M. Battaglia, S. Szidat (Univ. Bern)

The Methane Purification Setup (MPS) allows the collection of CH_4 -derived CO_2 samples coming from pre-concentrated air samples (see Fig. 1). The general procedure can be described as follows: a gas mixture is injected with a syringe into the GC column where each gas is chromatographically separated (**separation**). The pure gases of interest, mainly CH_4 but also CO and CO_2 are then separately trapped in individual traps (**trapping**). CO , CH_4 and CO_2 are finally successively transferred to a CuO oven where they are oxidized to CO_2 (**combustion**) and sealed in a glass ampoule (**recovery**).

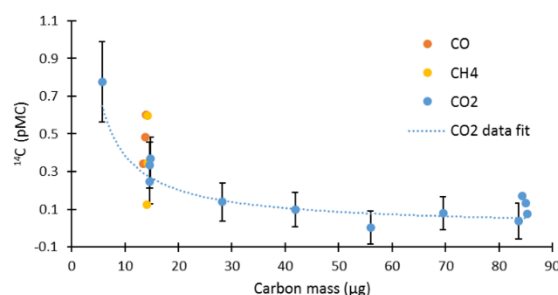
During trapping, the exhaust of the Thermal Conductivity Detector (TCD) is connected to the selector valve (V2) where a trap is chosen as the corresponding gas elutes from the GC column. The traps are filled with activated carbon and cooled at -196°C . The traps are then immersed in a hot water bath (ca. 95°C) to release the adsorbed pure gases, which are successively flushed with an external He flow of 10 ml/min to a CuO oven heated to 950°C . The pure sub-fractions are then sealed in a glass ampoule, using an adaptation of the THEODORE system [1]. The whole procedure lasts 1.5 h, including the separation and recovery of CO , CH_4 and CO_2 from a gas mixture and the cleaning of the system.

No breakthrough during trapping is observed for CH_4 samples containing up to 1 mg C and the combustion of CH_4 is complete for these sample sizes.

A semi-quantitative evaluation of the constant contamination of the system (procedural blank) was performed by injecting, trapping and recovering different amounts of fossil CO_2 (see Fig. 2). Assuming the contamination to be modern, we get a

contamination of $\sim 40\text{ ng C}$. This rather low value is similar to the results obtained for the gas injection system of the MICADAS AMS [2]. We assume the contamination for CO and CH_4 to be in the same order of magnitude. The cross contamination from the previous sample is $\sim 3\%$ for CO_2 samples and is assumed to be lower for CH_4 and CO as they are more volatile.

Fig. 2: ^{14}C measurements of fossil CO , CH_4 and CO_2 .



ACKNOWLEDGEMENT

We are grateful for funding through the Dr. Alfred Bretscher Scholarship.

- [1] S. Szidat et al., Nucl. Instr. Meth. Phys. Res. **223**, 829 (2004).
- [2] M. Ruff et al., Nucl. Instr. Meth. Phys. Res. **268**, 790 (2010).

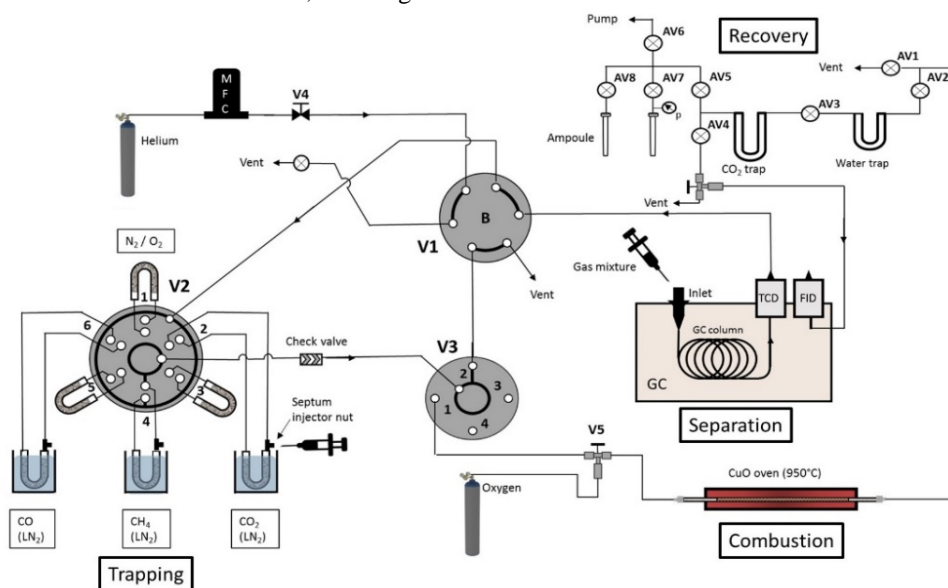


Fig. 1: Flow scheme of the Methane Purification Setup (MPS), showing the system in the trapping mode.

LIST OF PUBLICATIONS

HEAVY ELEMENTS

N.M. Chiera, R. Eichler, D. Piguet, A. Vögele, A. Türler

Microscopic interaction of single atomic elemental Hg with a sulfur surface

J. Radioanal. Nucl. Chem. **310**, 1233 (2016).

DOI: 10.1007/s10967-016-4965-4

R. Eichler, M. Asai, H. Brand, N.M. Chiera, A. Di Nitto, R. Dressler, Ch.E. Düllmann, J. Even, F. Fangli, M. Goetz, H. Haba, W. Hartmann, E. Jäger, D. Kaji, J. Kanaya, Y. Kneyaa, J. Khuyagbaatar, B. Kindler, Y. Komori, B. Kraus, J.V. Kratz, J. Krier, Y. Kudou, N. Kurz, S. Miyashita, K. Morimoto, K. Morita, M. Murakami, Y. Nagame, K. Ooe, D. Piguet, N. Sato, T.K. Sato, J. Steiner, P. Steinegger, T. Sumita, M. Takeyama, K. Tanaka, T. Tomitsuka, A. Toyoshima, K. Tsukada, A. Türler, I. Usoltsev, Y. Wakabayashi, Y. Wang, N. Wiehl, Y. Wittwer, A. Yakushev, S. Yamaki, S. Yano, S. Yamaki, Z. Qin

Complex chemistry with complex compounds

EPJ web conf. **131**, 07005 (2016).

DOI: 10.1051/epjconf/201613107005

P. Steinegger, M. Asai, R. Dressler, R. Eichler, Y. Kaneya, A. Mitsukai, Y. Nagame, D. Piguet, T. K. Sato, M. Schädel, S. Takeda, A. Toyoshima, K. Tsukada, A. Türler, A. Vascon

Vacuum Chromatography of Tl on SiO₂ at the Single-Atom Level

J. Phys. Chem. C **120**, 7122 (2016).

DOI: 10.1021/acs.jpcc.5b12033

A. Türler

Advances in chemical investigations of the heaviest elements

EPJ web conf. **131**, 07001 (2016).

DOI: 10.1051/epjconf/201613107001

I. Usoltsev, R. Eichler, A. Türler

Decomposition studies of group 6 hexacarbonyl complexes. Part 2: Modelling of the decomposition process.

Radiochim. Acta **104**, 531 (2016).

DOI: 10.1515/ract-2015-2447

I. Usoltsev, R. Eichler, Y. Wang, J. Even, A. Yakushev, H. Haba, M. Asai, H. Brand, A. Di Nitto, Ch.E. Düllmann, F. Fangli, W. Hartmann, M. Huang, E. Jäger, D. Kaji, J. Kanaya, Y. Kaneya, J. Khuyagbaatar, B. Kindler, J.V. Kratz, J. Krier, Y. Kudou, N. Kurz, B. Lommel, S. Miyashita, K. Morimoto, K. Morita, M. Murakami, Y. Nagame, H. Nitsche, K. Ooe, T.K. Sato, M. Schädel, J. Steiner, P. Steinegger, T. Sumita, M. Takeyama, K. Tanaka, A. Toyoshima, K. Tsukada, A. Türler, Y. Wakabayashi, N. Wiehl, S. Yamaki, Z. Qin

Decomposition studies of group 6 hexacarbonyl complexes. Part 1: Production and decomposition of Mo(CO)₆ and W(CO)₆

Radiochim. Acta **104**, 141 (2016).

DOI: 10.1515/ract-2015-2445

A. Yakushev, R. Eichler

Gas-phase chemistry of element 114, flerovium

EPJ web conf. **131**, 07003 (2016).

DOI: 10.1051/epjconf/201613107003

RADWASTE ANALYTICS

M. Barbagallo, A. Musumarra, L. Cosentino, E. Maugeri, S. Heinitz, A. Mengoni, R. Dressler, D. Schumann, F. Käppeler, N. Colonna, P. Finocchiaro, M. Ayrarov, L. Damone, N. Kivel, O. Aberle, S. Altstadt, J. Andrzejewski, L. Audouin, M. Bacak, J. Balibrea-Correa, S. Barros, V. Bécáres, F. Bečvář, C. Beinrucker, E. Berthoumieux, J. Billowes, D. Bosnar, M. Brugger, M. Caamaño, M. Calviani, F. Calviño, D. Cano-Ott, R. Cardella, A. Casanovas, D. M. Castelluccio, F. Cerutti, Y. H. Chen, E. Chiaveri, G. Cortés, M. A. Cortés-Giraldo, S. Cristallo, M. Diakaki, C. Domingo-Pardo, E. Dupont, I. Duran, B. Fernandez-Dominguez, A. Ferrari, P. Ferreira, W. Furman, S. Ganesan, A. García-Rios, A. Gawlik, T. Glodariu, K. Göbel, I. F. Gonçalves, E. González-Romero, E. Griesmayer, C. Guerrero, F. Gunsing, H. Harada, T. Heftrich, J. Heyse, D. G. Jenkins, E. Jericha, T. Katabuchi, P. Kavargin, A. Kimura, M. Kokkoris, M. Krčička, E. Leal-Cidoncha, J. Leredegui, C. Lederer, H. Leeb, S. Lo Meo, S. J. Lonsdale, R. Losito, D. Macina, J. Marganec, T. Martínez, C. Massimi, P. Mastinu, M. Mastromarco, A. Mazzone, E. Mendoza, P. M. Milazzo, F. Mingrone, M. Mirea, S. Montesano, R. Nolte, A. Oprea, A. Pappalardo, N. Patronis, A. Pavlik, J. Perkowski, M. Piscopo, A. Plompen, I. Porras, J. Praena, J. Quesada, K. Rajeev, T. Rauscher, R. Reifarth, A. Riego-Perez, P. Rout, C. Rubbia, J. Ryan, M. Sabate-Gilarte, A. Saxena, P. Schillebeeckx, S. Schmidt, P. Sedyshev, A. G. Smith, A. Stamatopoulos, G. Tagliente, J. L. Tain, A. Tarifeño-Saldivia, L. Tassan-Got, A. Tsinganis, S. Valenta, G. Vannini, V. Variale, P. Vaz, A. Ventura, V. Vlachoudis, R. Vlastou, J. Voltaire, A. Wallner, S. Warren, M. Weigand, C. Weiß, C. Wolf, P. J. Woods, T. Wright, P. Žugec

⁷Be(n,α)⁴He Reaction and the Cosmological Lithium Problem: Measurement of the Cross Section in a Wide Energy Range at n_TOF at CERN

Phys. Rev. Letters **117**, 152701 (2016).

DOI: 10.1103/PhysRevLett.117.152701

L. Cosentino, A. Musumarra, M. Barbagallo, A. Pappalardo, N. Colonna, L. Damone, M. Piscopo, P. Finocchiaro, E. Maugeri, S. Heinitz, D. Schumann, R. Dressler, N. Kivel, O. Aberle, J. Andrzejewski, L. Audouin, M. Ayrarov, M. Bacak, S. Barros, J. Balibrea-Correa, V. Bécáres, F. Bečvář, C. Beinrucker, E. Berthoumieux, J. Billowes, D. Bosnar, M. Brugger, M. Caamaño, M. Calviani, F. Calviño, D. Cano-Ott, R. Cardella, A. Casanovas, D.M. Castelluccio, F. Cerutti, Y.H. Chen, E. Chiaveri, G. Cortés, M.A. Cortés-Giraldo, M. Diakaki, C. Domingo-Pardo, E. Dupont, I. Duran, B. Fernandez-Dominguez, A. Ferrari, P. Ferreira, W. Furman, S. Ganesan, A. García-Rios, A. Gawlik, I. Gheorghe, T. Glodariu, K. Göbel, I.F. Gonçalves, E. González-Romero, E. Griesmayer, C. Guerrero, F. Gunsing, H. Haradaz, T. Heftrich, J. Heysez, D.G. Jenkins, E. Jericha, F. Käppeler, T. Katabuchi, P. Kavargin, A. Kimura, M. Kokkoris, M. Krčička, E. Leal-Cidoncha, J. Leredegui, C. Lederer, H. Leeb, S. LoMeo, S. Lonsdale, R. Losito, D. Macina, J. Marganec, T. Martínez, C. Massimi, P. Mastinu, M. Mastromarco, F. Matteucci, A. Mazzone, E. Mendoza, A. Mengoni, P.M. Milazzo, F. Mingrone, M. Mirea, S. Montesano, R. Nolte, A. Oprea, N. Patronis, A. Pavlik, J. Perkowski, J. Praena, J. Quesada, K. Rajeev, T. Rauscher, R. Reifarth, A. Riego-Perez, P. Rout, C. Rubbia, J. Ryan, M. Sabate-Gilarte, A. Saxena, P. Schillebeeckx, S. Schmidt, P. Sedyshev, A.G. Smith, A. Stamatopoulos, G. Tagliente, J.L. Tain, A. Tarifeño-Saldivia, L. Tassan-Got, A. Tsinganis, S. Valenta, G. Vannini, V. Variale, P. Vaz, A. Ventura, V. Vlachoudis, R. Vlastou, J. Voltaire, A. Wallner, S. Warren, M. Weigand, C. Weiß, C. Wolf, P.J. Woods, T. Wright, P. Žugec

Experimental setup and procedure for the measurement of the ⁷Be(n,α)a reaction at n_TOF

Nucl. Instr. Meth. Phys. Res. A **830**, 197 (2016).

DOI: 10.1016/j.nima.2016.05.089

F. Gunsing, O. Aberle, J. Andrzejewski, L. Audouin, V. Bécáres, M. Bacak, J. Balibrea-Correa, M. Barbagallo, S. Barros, F. Bečvář, C. Beinrucker, F. Belloni, E. Berthoumieux, J. Billowes, D. Bosnar, M. Brugger, M. Caamaño, F. Calviño, M. Calviani, D. Cano-Ott, R. Cardella, A. Casanovas, D.M. Castelluccio, F. Cerutti, Y.H. Chen, E. Chiaveri, N. Colonna, M.A. Cortés-Giraldo, G. Cortés, L. Cosentino, L.A. Damone, K. Deo, M. Diakaki, C. Domingo-Pardo, R. Dressler, E. Dupont, I. Durán, B. Fernández-Dominguez, A. Ferrari, P. Ferreira, P. Finocchiaro, R.J.W. Frost, V. Furman, S. Ganesan, A.R. Garcia, A. Gawlik, I. Gheorghe, T. Glodariu, I.F. Gonçalves, E. González, A. Goverdovski, E. Griesmayer, C. Guerrero, K. Göbel, H. Harada, T. Heftrich, S. Heinitz, A. Hernández-Prieto, J. Heyse, D.G. Jenkins, E. Jericha, F. Käppeler, Y. Kadi, T. Katabuchi, P. Kavargin, V. Ketlerov, V. Khryachkov, A. Kimura, N. Kivel, M. Kokkoris, M. Krčička, E. Leal-Cidoncha, C. Lederer, H. Leeb, J. Leredegui, M. Licata, S. Lo Meo, S.J. Lonsdale, R. Losito, D. Macina, J. Marganec, T. Martinez, A. Masi, C. Massimi, P. Mastinu, M. Mastromarco, F. Matteucci, E.A. Maugeri, A. Mazzone, E. Mendoza, A. Mengoni, P.M. Milazzo, F. Mingrone, M. Mirea, S. Montesano, A. Musumarra, R. Nolte, A. Oprea, F.R. Palomo-Pinto, C. Paradela, N. Patronis, A. Pavlik, J. Perkowski, I. Porras, J. Praena, J.M. Quesada, K. Rajeev, T. Rauscher, R. Reifarth, A. Riego-Perez, M. Robles, P. Rout, D. Radeck, C. Rubbi, J.A. Ryan, M. Sabatè-Gilarte, A. Saxena, P. Schillebeeckx, S. Schmidt, D. Schumann, P. Sedyshev, A.G. Smith, A. Stamatopoulos, S.V. Suryanarayana, G. Tagliente, J.L. Tain, A. Tarifeño-Saldivia, D. Tarrío, L. Tassan-Got, A. Tsinganis, S. Valenta, G. Vannini, V. Variale, P. Vaz, A. Ventura, V. Vlachoudis, R. Vlastou, J. Voltaire, A. Wallner, S. Warren, M. Weigand, C. Weiß, C. Wolf, P.J. Woods, T. Wright, P. Žugec

Nuclear data activities at the n_TOF facility at CERN

Eur. Phys. J. Plus **131**, 371 (2016).

DOI: 10.1140/EPJP/I2016-16371-4

- B. Hammer-Rotzler, J. Neuhausen, V. Boutellier, M. Wohlmuther, L. Zanini, J.-C. David, A. Türler, D. Schumann
Distribution and Surface Enrichment of Radionuclides in Lead-Bismuth Eutectic from Spallation Targets
Eur. Phys. J. Plus **131**, 233 (2016).
DOI: 10.1140/epjp/i2016-16233-1
- D. Hougbo, A.P. Bernardes, J.C. David, M. Delonca, K. Kravalis, S. Lahiri, R. Losito, C. Maglioni, A. Marchix, T.M. Mendonca, L. Popescu, D. Schumann, P. Schuurmans, T. Stora, J. Vollaire, J. Vierendeels
Development of a liquid Pb-Bi target for high-power ISOL facilities,
NIM **376**, 57 (2016).
DOI: 10.1016/j.nimb.2016.01.021
- I. Leya, A. Grimberg, J-C. David, D. Schumann, J. Neuhausen, L. Zanini, E.N. Messomo
Post-irradiation analysis of an ISOLDE lead-bismuth target: Stable and long-lived noble gas nuclides
JNM **475**, 19 (2016).
DOI:10.1016/j.jnucmat.2016.03.013
- S. Lo Meo, M.A. Cortes-Giraldo, C. Massimi, J. Lerendegui-Marco, M. Barbagallo, N. Colonna, C. Guerrero, D. Mancusi, F. Mingrone, J.M. Quesada, M. Sabate-Gilarte, G. Vannini, V. Vlachoudis, n_TOF Collaboration
GEANT4 spallation simulations of the n_TOF source and their validation
Eur. Phys. J. A **52**, 100 (2016).
DOI: 10.1140/epja/i2016-16100-8
- E. A. Maugeri, J. Neuhausen, R. Eichler, R. Dressler, K. Rijpstra, S. Cottenier, D. Schumann
Adsorption of volatile polonium and bismuth species on metals in various gas atmospheres: Part I – Adsorption of volatile polonium and bismuth on gold
Radiochim. Acta **104**, 757 (2016).
DOI: 10.1515/ract-2016-2573
- E. A. Maugeri, J. Neuhausen, R. Misiak, R. Eichler, R. Dressler, D. Schumann
Adsorption of volatile polonium species on metals in various gas atmospheres: Part II – Adsorption of volatile polonium and bismuth on platinum, silver and palladium
Radiochimica Acta **104**, 769 (2016).
DOI: 10.1515/ract-2016-2575
- A. Nucciotti, B. Alpert, D. Becker, D. Bennett, M. Biasotti, C. Brofferio, V. Ceriale, G. Ceruti, D. Corsini, P. Day, M. De Gerone, R. Dressler, M. Faverzani, E. Ferri, J. Fowler, E. Fumagalli, J. Gard, F. Gatti, A. Giachero, J. Hays-Wehle, S. Heinitz, G. Hilton, U. Koester, M. Lusignoli, M. Maino, J. Mates, S. Nisi, R. Nizzolo, A. Orlando, L. Parodi, G. Pessina, G. Pizzigoni, A. Puiu, S. Ragazzi, C. Reintsema, M. Ribeiro-Gomes, D. Schmidt, D. Schumann, F. Siccardi, M. Sisti, D. Swetz, F. Terranova, J. Ullom, L. Vale
Status of the HOLMES detector development
NIM A **824**, 182 (2016).
DOI: 10.1016/j.nima.2015.09.066
- G. Pizzigoni, B. Alpert, M. Balata, D. Bennett, M. Biasotti, C. Boragno, C. Brofferio, M. Gerone, R. Dressler, M. Faverzani, E. Ferri, J. Folwer, F. Gatti, A. Giachero, S. Heinitz, G. Hilton, U. Koster, M. Lusignoli, M. Maino, J. Mates, S. Nisi, R. Nizzolo, A. Nucciotti, G. Pessina, A. Puiu, S. Ragazzi, C. Reintsema, MR Gomes, D. Shmidt, D. Schumann, M. Sisti, D. Swetz, F. Terranova, J. Ullom, PK. Day
Inside HOLMES experiment: Ho-163 metallic target production for the micro-calorimeter absorber
NIM A **824**, 223 (2016).
DOI: 10.1016/j.nima.2015.11.020
- D. Schumann, M. Barbagallo, T. Stora, U. Köster, M. Gai
How Radioactive Samples and Targets Can Help to Better Understand the Big Bang Theory
Nuclear Physics News **26**, 20 (2016).
DOI: 10.1140/EPJP/I2016-16371-4
- D. Schumann, R. Dressler
Development of an extraction system for the separation of dubnium from rutherfordium using MIBK and HCl/HF solutions
Radiochim. Acta **104**, 41 (2016).
DOI: 10.1515/ract-2015-2398

P. Žugec, D. Bosnar, N. Colonna, F. Gunsing, n_TOF collaboration

An improved method for estimating the neutron background in measurements of neutron capture reactions
NIM A **826**, 80 (2016).

DOI: 10.1016/j.nima.2016.04.086

P. Žugec, N. Colonna, D. Bosnar, A. Ventura, A. Mengoni, S. Altstadt, J. Andrzejewski, L. Audouin, M. Barbagallo, V. Bečáres, F. Bečvář, F. Belloni, E. Berthoumieux, J. Billowes, V. Boccone, M. Brugger, M. Calviani, F. Calvino, D. Cano-Ott, C. Carrapico, F. Cerutti, E. Chiaveri, M. Chin, G. Cortes, M.A. Cortes-Giraldo, L. Cosentino, M. Diakaki, C. Domingo-Pardo, R. Dressler, I. Duran, C. Eleftheriadis, A. Ferrari, P. Finocchiaro, K. Fraval, S. Ganesan, A.R. Garica, G. Giubrone, M.B. Gomez-Hornillos, I.F. Goncalves, E. Gonzalez-Romero, E. Griesmayer, C. Guerrero, F. Gunsing, P. Gurusamy, S. Heintz, D.G. Jenkins, E. Jericha, F. Käppeler, D. Karadimos, N. Kivel, M. Kokkoris, M. Krčička, J. Kroll, C. Langer, C. Lederer, H. Leeb, L.S. Leong, S. Lo Meo, R. Losito, A. Manousos, J. Marganiec, T. Martinez, C. Massimi, P. Mastinu, M. Mastroianni, E. Mendoza, P.M. Milazzo, F. Mingrone, M. Mirea, W. Mondalaers, A. Musumarra, C. Paradela, A. Pavlik, J. Perkowski, A. Plompen, J. Praena, J. Quesada, T. Rauscher, R. Reifarth, A. Riego, F. Roman, C. Rubbia, R. Sarmiento, A. Saxena, P. Schillebeeckx, S. Schmidt, D. Schumann, G. Tagliente, J.L. Tain, D. Tarrio, L. Tassan-Got, A. Tsinganis, S. Valenta, G. Vannini, V. Variale, P. Vaz, R. Versaci, M.J. Vermeulen, Vlachoudis, R. Vlastou, A. Wallner, T. Ware, M. Weigand, C. Weiss, T. Wright

Measurement of the $^{12}\text{C}(n,p)^{12}\text{B}$ integral cross section up to 10 GeV

Eur. Phys. J. A **52**, 101 (2016).

DOI: 10.1140/epja/i2016-16101-7

P. Žugec, C. Weiß, C. Guerrero, F. Gunsing, V. Vlachoudis, M. Sabate-Gilarte, A. Stamatopoulos, T. Wright, J. Lerendegui-Marco, F. Mingrone, J.A. Ryan, S.G. Warren, A. Tsinganis, M. Barbagallo, n_TOF collaboration

Pulse processing routines for neutron time-of-flight data

Nucl. Instr. Meth. Phys. Res. A **812**, 134 (2016).

DOI: 10.1016/j.nima.2015.12.054

RADIONUCLIDE DEVELOPMENT - CHEMISTRY

M. Bunka, C. Müller, C. Vermeulen, S. Haller, A. Türlér, R. Schibli, N. P. van der Meulen
Imaging quality of ^{44}Sc in comparison with five other PET radionuclides using Derenzo phantoms and preclinical PET
Appl. Rad. Isot. **10**, 129 (2016).
DOI: 10.1016/j.apradiso.2016.01.006

K. Domnanich, C. Müller, R. Farkas, R. Schmid, B. Ponsard, R. Schibli, A. Türlér, N. P. van der Meulen
 ^{44}Sc for labeling of DOTA- and NODAGA-functionalized peptides: preclinical in vitro and in vivo investigations
EJNMMI Radiopharmacy and Chemistry **1**, 8 (2016).
DOI: 10.1186/s41181-016-0013-5

R. Farkas, K. Siwowska, S. Ametamey, R. Schibli, N. P. van der Meulen, C. Müller
 ^{64}Cu - and ^{68}Ga -Based PET Imaging of Folate Receptor-Positive Tumors: Development and Evaluation of an Albumin-Binding NODAGA-Folate
Mol. Pharm. **13**, 1979 (2016).
DOI: 10.1021/acs.molpharmaceut.6b00143

S. Haller, G. Pellegrini, C. Vermeulen, N. P. van der Meulen, U. Köster, P. Bernhardt, R. Schibli, C. Müller
Contribution of Auger/conversion electrons to renal side effects after radionuclide therapy: Preclinical comparison of ^{161}Tb -folate and ^{177}Lu -folate
EJNMMI Res. **6**, 13 (2016).
DOI: 10.1186/s13550-016-0171-1

H. Honarvar, C. Müller, S. Cohrs, S. Haller, K. Westerlund, A. Eriksson Karlström, N. P. van der Meulen, R. Schibli, V. Tolmachev
Evaluation of the First ^{44}Sc -Labeled Affibody Molecule for Imaging of HER2-Expressing Tumors
Nucl. Med. Biol. **45**, 15 (2016).
DOI: 10.1016/j.nucmedbio.2016.10.004

C. Müller, C. Vermeulen, U. Köster, K. Johnston, A. Türlér, R. Schibli, N. P. van der Meulen
Alpha-PET with Terbium-149: Evidence and Perspectives for RadioTheragnostics
EJNMMI Radiopharmacy and Chemistry **1**, 5 (2016).
DOI: 10.1186/s41181-016-0008-2

C. Müller, C. Vermeulen, K. Johnston, U. Köster, R. Schmid, A. Türlér, N. P. van der Meulen
Preclinical in vivo application of ^{152}Tb -DOTANOC: a radiolanthanide for PET imaging
EJNMMI Research **6**, 35 (2016).
DOI: 10.1186/s13550-016-0189-4

N.P. van der Meulen, G.F. Steyn, C. Vermeulen, T.J. van Rooyen.
Production of ^{28}Mg by bombardment of ^{nat}Cl with 200 MeV protons: Proof-of-concept study for a stacked LiCl target
Appl. Radiat. Isot. **115**, 125 (2016).
DOI: 10.1016/j.apradiso.2016.04.026

ENVIRONMENTAL RADIONUCLIDES UNIVERSITÄT BERN

K.R. Daellenbach, C. Bozzetti, A. Krepelová, F. Canonaco, R. Wolf, P. Zotter, P. Fermo, M. Crippa, J.G. Slowik, Y. Sosedova, Y. Zhang, R.-J. Huang, L. Poulain, S. Szidat, U. Baltensperger, I. El Haddad, A.S.H. Prévôt
Characterization and source apportionment of organic aerosol using offline aerosol mass spectrometry
Atmos. Meas. Tech. **9**, 23 (2016).
 DOI: 10.5194/amt-9-23-2016

J. Liu, J. Li, D. Liu, P. Ding, C. Shen, Y. Mo, X. Wang, C. Luo, Z. Cheng, S. Szidat, Y.L. Zhang, Y. Chen, G. Zhang
Source apportionment and dynamic changes of carbonaceous aerosols during the haze bloom-decay process in China based on radiocarbon and organic molecular tracers
Atmos. Chem. Phys. **16**, 2985 (2016).
 DOI: 10.5194/acp-16-2985-2016

J. Liu, J. Li, M. Vonwiller, D. Liu, H. Cheng, K. Shen, G. Salazar, K. Agrios, Y. Zhang, Q. Hea, X. Ding, G. Zhong, X. Wang, S. Szidat, G. Zhang
The importance of non-fossil sources in carbonaceous aerosols in a megacity of central China during the 2013 winter haze episode: A source apportionment constrained by radiocarbon and organic tracers
Atmos. Environ. **144**, 60 (2016).
 DOI:10.1016/j.atmosenv.2016.08.068

A. Matter, A. Mahjoub, E. Neubert, F. Preusser, A. Schwalb, S. Szidat, G. Wulf
Reactivation of the Pleistocene trans-Arabian Wadi ad Dawasir fluvial system (Saudi Arabia) during the Holocene humid phase
Geomorphology **270**, 88 (2016).
 DOI: 10.1016/j.geomorph.2016.07.013

M.C. Minguillón, N. Pérez, N. Marchand, A. Bertrand, B. Temime-Roussel, K. Agrios, S. Szidat, B. L. van Drooge, J.P. Krüger, C. Alewell, K. Minkinen, S. Szidat, J. Leifeld
Calculating carbon changes in peat soils drained for forestry with four different profile-based methods
For. Ecol. Manage. **381**, 29 (2016).
 DOI: 10.1016/j.foreco.2016.09.006

P. Rinta, M. van Hardenbroek, R.I. Jones, P. Kankaala, F. Rey, S. Szidat, M.J. Wooller, O. Heiri
Land use affects carbon sources to the pelagic food web in a small boreal lake
PLOS ONE **11**, e0159900 (2016).
 DOI: 10.1371/journal.pone.0159900

G. Salazar, K. Agrios, R. Eichler, S. Szidat
Characterization of the axial jet separator with a CO₂/helium mixture: Towards GC-AMS hyphenation
Anal. Chem. **88**, 1647 (2016).
 DOI: 10.1021/acs.analchem.5b03586

A. Sylvestre, A. Alastuey, C. Reche, A. Ripoll, E. Marco, J.O. Grimalt, X. Querol
Secondary organic aerosol origin in an urban environment. Influence of biogenic and fuel combustion precursors
Faraday Discuss. **189**, 337 (2016).
 DOI: 10.1039/C5FD00182J

Ch. Uglietti, A. Zapf, T.M. Jenk, M. Sigl, S. Szidat, G. Salazar, M. Schwikowski
Radiocarbon dating of glacier ice: overview, optimisation, validation and potential
The Cryosphere **10**, 3091 (2016).
 DOI: 10.5194/tc-10-3091-2016

V. Ulevicius, S. Byčenkienė, C. Bozzetti, A. Vlachou, K. Plauškaitė, G. Mordas, V. Dudoitis, G. Abbaszade, V. Remeikis, A. Garbaras, A. Masalaite, J. Blees, R. Fröhlich, K. R. Dällenbach, F. Canonaco, J.G. Slowik, J. Dommen, R. Zimmermann, J. Schnelle-Kreis, G.A. Salazar, K. Agrios, S. Szidat, I. El Haddad, A.S.H. Prévôt
Fossil and non-fossil source contributions to atmospheric carbonaceous aerosols during extreme spring grassland fires in Eastern Europe
Atmos. Chem. Phys. **16**, 5513 (2016).
 DOI: 10.5194/acp-16-5513-2016

H. Veit, J.-H. May, A. Madella, R. Delunel, F. Schlunegger, S. Szidat, J.M. Capriles
Palaeo-geoecological significance of Pleistocene trees in the Lluta Valley, Atacama Desert
J. Quaternary Sci. **31**, 203 (2016).
DOI: 10.1002/jqs.2857

J. Xu, J. Shi, Q. Zhang, X. Ge, F. Canonaco, A.S.H. Prévôt, M. Vonwiller, S. Szidat, J. Ge, J. Ma, Y. An, S. Kang, D. Qin
Wintertime organic and inorganic aerosols in Lanzhou, China: sources, processes and comparison with the results during summer
Atmos. Chem. Phys. **16**, 14937 (2016).
DOI: 10.5194/acp-16-14937-2016

Y.-L. Zhang, K. Kawamura, K. Agrios, M. Lee, G. Salazar, S. Szidat
Fossil and nonfossil sources of organic and elemental carbon aerosols in the outflow from Northeast China
Environ. Sci. Technol. **50**, 6284 (2016).
DOI: 10.1021/acs.est.6b00351

BOOKCHAPTERS

H. Gäggeler, S. Szidat

Nuclear dating

Nuclear- and Radiochemistry, Volume 2: Modern Applications, F. Rösch (ed.), S. 133-168, August 2016.

REPORTS AND TECHNICAL NOTES

T. Stocker, P. Düring, R. Purtschert, T. Wagner, S. Szidat, C. Schlosser, M. Konrad, S. Schmid, J. Eikenberg,

R. Siegwolf

Kohlenstoff-14, Krypton-85, Argon-37

Bundesamt für Gesundheit (BAG), Report „Umweltradioaktivität und Strahlendosen in der Schweiz 2015“, S. 96-105, Juli 2016.

INTERNAL REPORTS

Pharmaceutical Quality Dossier on [⁶⁸Ga]-PSMA-11

Pharmaceutical Quality Dossier on [⁶⁸Ga]-DOTA-TATE

Pharmaceutical Quality Dossier on [¹⁷⁷Lu]-DOTA-TOC

CONTRIBUTIONS TO CONFERENCES, WORKSHOPS AND SEMINARS

HEAVY ELEMENTS

N. Chiera

Superheavy Elements copernicium and flerovium selenides: first Cn-Se bond observation

NES PhD Day, Villigen, Switzerland, 9 May, 2016.

N. Chiera

Towards Cn and Fl selenides: unexpected Cn-Se bond formation

9th International Conference on Nuclear and Radiochemistry - NRC9, Helsinki, Finland, 29 August - 2 September, 2016.

N. Chiera

Towards the Selenides of the Superheavy Elements Copernicium and Flerovium

PhD-defense University of Bern, Bern, Switzerland, 28 October, 2016.

R. Eichler

Experimentally assessing the metal-carbon bond stability in Sg(CO)₆

9th International Conference on Nuclear and Radiochemistry - NRC9, Helsinki, Finland, 29 August - 2 September, 2016.

R. Eichler

Complex Chemistry with Metal complexes

Nobel Symposium NS160 - Chemistry and Physics of Heavy and Superheavy Element, Scania, Sweden,

29 May - 3 June, 2016.

P. Steinegger

Towards Vacuum Adsorption Chromatography of Superheavy Elements

PhD-defense University of Bern, Bern, Switzerland, 19 February, 2016.

P. Steinegger

First on-line vacuum chromatography experiments with single atoms of Tl on SiO₂

9th International Conference on Nuclear and Radiochemistry - NRC9, Helsinki, Finland, 29 August - 2 September, 2016.

P. Steinegger

Fast Gas-Phase Experiments with Transactinide Elements

Seminar at the Department of Nuclear Chemistry at the Czech Technical University in Prague, Prague, Czech Republic,

21 October, 2016.

P. Steinegger

High-Temperature α -Spectroscopy with Diamond Sensors,

5th ADAMAS Workshop, GSI Darmstadt, Germany, 15-16 December, 2016.

A. Türler

Progress in Superheavy Element Research (invited)

RANC-2016, Budapest, Hungary, 10-15 April, 2016.

A. Türler

Advances in Chemical Investigations of Heaviest Elements

Nobel Symposium NS160 - Chemistry and Physics of Heavy and Superheavy Element, Scania, Sweden,

29 May - 3 June, 2016.

A. Türler

Recent Highlights from SHE Chemistry Experiments (invited)

XXIII Nuclear Physics Workshop „Marie & Pierre Curie”, Kazimierz Dolny, Poland, 27-29 Sept. 2016.

RADWASTE ANALYTICS

R. Dressler, S. Heinitz, E. A. Maugeri, Z. Talip, D. Schumann

Towards A New Quality Of High-precision Half-life Measurements: ^{60}Fe , ^{53}Mn , ^{146}Sm , ^{32}Si

International Nuclear Physics Conference (INPC2016), Adelaide, Australia, 11-16 September, 2016.

B. Gonzalez Prieto, K. Rijpstra, A. Aerts, J. Neuhausen, R. Eichler, E. Maugeri, M. Mertens, A. Van Yperen-De Deyne, S. Cottenier

Polonium evaporation from liquid lead bismuth eutectic coolant for accelerator driven systems

RANC International Conference on Radioanalytical and Nuclear Chemistry, Budapest, Hungary, 10-15 April, 2016.

B. Gonzalez Prieto, A. Aerts, J. Neuhausen, E. A. Maugeri, R. Eichler

Polonium evaporation from liquid lead-bismuth eutectic coolant and its capture for accelerator driven systems

9th International Conference on Nuclear and Radiochemistry – NRC9, Helsinki, Finland, 29 August – 2 September, 2016.

S. Heinitz, E. Maugeri, M. Ayranov, D. Schumann

Production and separation of radioactive beryllium isotopes at PSI

RANC - International Conference on Radioanalytical and Nuclear Chemistry, Budapest, Hungary, 10-15 April, 2016.

S. Heinitz, E. Maugeri, R. Dressler, D. Schumann

Sample preparation at PSI

n_TOF Collaboration meeting, Catania, Italy, 18-19 May, 2016.

S. Heinitz

Pyrochemical extraction of radionuclides from liquid Pb, Bi and LBE

ESNII+ Workshop on Coolant Quality Control, Physico-Chemistry & Dosimetry, ÚJV, Řež, Czech Republic, 5-7 October, 2016.

S. Heinitz

Radioactive lanthanides – from isotope production to nuclear physics experiments

28th International Conference of the International Nuclear Target Development Society (INTDS2016), Cape Town, South Africa, 13-18 November, 2016.

C. Jégou, S. Peugeot, S. Miro, Z. Talip, L. Desgranges, R. Mohun, G. Guimbretière, A. Canizares, P. Simon

Characterization of actinides oxides by Raman spectroscopy: from model systems to real spent fuel

Plutonium Futures - The Science 2016, Baden Baden, Germany, 18-22 September, 2016.

I. Kajan, C. Ekberg

Radiolysis of air-water systems

RANC International Conference on Radioanalytical and Nuclear Chemistry, Budapest, Hungary, 10-15 April, 2016.

I. Kajan, T. Kärkelä, A. Auvinen, C. Ekberg

Effect of air radiolysis products on the chemistry of ruthenium during a severe nuclear accident

9th International Conference on Nuclear and Radiochemistry – NRC9, Helsinki, Finland, 29 August – 2 September, 2016.

E. Karlsson, F. Espegren, T. Retegan

Initial studies of LBE, UO₂ fuel and 15-15Ti cladding material interactions

9th Annual International Conference on Sustainable Development through Nuclear Research and Education, RATEN ICN, Pitești, Romania, 18-20 May, 2016.

E.A. Maugeri, R. Dressler, S. Heinitz, D. Schumann

Production and separation of exotic radionuclides in the framework of the ERAWAST project

SESTEC-2016: Emerging Trends in Separation Science and Technology, Guwahati, India, 17-20 May, 2016.

E.A. Maugeri, S. Heinitz, R. Dressler, D. Schumann

Production and characterization of ^7Be targets

International Nuclear Target Development Society (INTDS-2016), Cape Town, South Africa, 13-8 November, 2016.

J. Neuhausen

MYRTE WP4 Chemistry of volatile radionuclides, Task4.3 Status and Outlook

1st MYRTE work package 4 Technical Meeting, Paul Scherrer Institut, Villigen, Switzerland, 4 March, 2016.

J. Neuhausen on behalf of the MYRTE WP4 collaboration

Chemistry of volatile radionuclides

2nd MYRTE TEC & GOV Meetings, SCK·CEN Headquarters, Brussels, Belgium, 17 June, 2016.

J. Neuhausen, E. A. Maugeri, M. Rizzi, R. Eichler, D. Schumann, B. Gonzalez Prieto, A. Aerts, K. Rijpstra, A. Van Yperen-De Deyne, M. Mertens, S. Cottenier

Release of volatile radionuclides from ADS and their capture

3rd International Workshop on Technology and Components of Accelerator-Driven Systems TCADS-3, Mito, Japan, 6-9 September, 2016.

J. Neuhausen

Radionuclide Behaviour in MEGAPIE

ESNII+ Workshop Coolant Quality Control, Physico-Chemistry & Dosimetry, ÚJV, Řež, Czech Republic, 5-7 October, 2016.

J. Neuhausen on behalf of the MYRTE WP4 collaboration

Chemistry of volatile radionuclides

3rd MYRTE TEC & GOV Meetings, Von Karman Institute, St. Genesius Rode, Belgium, 26 October, 2016.

D. Schumann

Status report

CHANDA meeting WP3, Mainz, Germany, 2-3 February, 2016.

D. Schumann, R. Dressler, M. Wohlmuther, D. Kiselev, J-C., David

Integral measurements of the residue nuclide production induced by protons in heavy metal targets

Nuclear Data Conference 2016, Brugge, Belgium, 11-16 September, 2016.

D. Schumann, R. Dressler, E. Maugeri, S. Heinitz

Isotope production and target preparation for nuclear astrophysics data

Nuclear Data Conference 2016, Brugge, Belgium, 11-16 September, 2016.

D. Schumann

Exotic Radionuclides – what are they good for?

NES colloquium, PSI, Villigen, Switzerland, 12 October, 2016.

D. Schumann

Contribution of PSI to WP11

CHANDA meeting, Madrid, Spain, 17-18 October, 2016.

D. Schumann

Isotope production and target fabrication at PSI

International Nuclear Target Development Society (INTDS-2016), Cape Town, South Africa, 13-8 November, 2016.

Z. Talip, S. Pfister, R. Dressler, D. Schumann

Separation of the long lived lanthanides from proton-irradiated metal targets

SESTEC-2016: Emerging Trends in Separation Science and Technology, Guwahati, India, 17-20 May, 2016.

Z. Talip, S. Pfister, R. Dressler, A. Vögele, E. Strub, R. Michel, D. Schumann

Cross Sections for the proton-induced production of long-lived radionuclides in heavy metal targets

Nuclear Data Conference 2016, Brugge, Belgium, 11-16 September, 2016.

RADIONUCLIDE DEVELOPMENT

K. Domnanich

⁴³Sc production development by cyclotron irradiation of ⁴³Ca and ⁴⁶Ti
ICTR-PHE 2016, Geneva, Switzerland, 16 February, 2016.

K. Domnanich

⁴³Sc production development by cyclotron irradiation of ⁴³Ca and ⁴⁶Ti
9th International Conference on Nuclear and Radiochemistry - NRC9, Helsinki, Finland, 29 August - 2 September, 2016.

N. van der Meulen

New radionuclides for theragnosis: nice to have or need to have?
Lecture at University of Padova, Italy, 22 January, 2016.

N. van der Meulen

Novel Diagnostic and Therapeutic Radionuclides for the Development of Innovative Radiopharmaceuticals
Meeting of ISOLDE Committee, CERN, Geneva, Switzerland, 3 February, 2016.

N. van der Meulen

The use of ¹⁴⁹Tb and ¹⁵²Tb in preclinical investigations: an update on its mass separation and subsequent application for imaging and therapy
ICTR-PHE 2016, Geneva, Switzerland, 19 February, 2016.

N. van der Meulen

Preclinical imaging study using ¹⁴⁹Tb-DOTANOC – Promising features of ¹⁴⁹Tb for theragnostics combining α -therapy and PET
EMIM 2016, Utrecht, Netherlands, 10 March, 2016.

N. van der Meulen

The production of radionuclides for diagnostic and therapeutic application in nuclear medicine
RANC International Conference on Radioanalytical and Nuclear Chemistry, Budapest, Hungary, 10-15 April, 2016.

N. van der Meulen

The use of ¹⁴⁹Tb and ¹⁵²Tb in preclinical investigations: an update on its mass separation and subsequent application for imaging and therapy
SGNM 2016, Davos, Switzerland, 20 May, 2016.

N. van der Meulen

Scandium radionuclides for radiotheragnostics: preclinical investigations
IRIST 2016, Lausanne, Switzerland, 27 May, 2016.

N. van der Meulen

The production of exotic radionuclides towards theragnostics
UAB Radiology, Seminar in Molecular Imaging, Birmingham, Alabama, USA, 26 August, 2016.

A. Türler

Theranostics and tracer development (invited)
Norwegian Association of Medical Physics, Kvitfiell, Norway, 8-10 February, 2016.

A. Türler

Possibilities for Production of Uncommon Radionuclides with Commercial Cyclotrons (invited)
First Kuopio Symposium on PET Imaging and Radiotracer Production, Kuopio, Finland, 16-17 May, 2016.

C. Vermeulen

Radionuclide developments at PSI
CYCLEUR 2016, Bern, Switzerland, 27 June, 2016.

C. Vermeulen

Report from the lab: Paul Scherrer Institut
WTTC16, Santa Fe, USA, 31 August, 2016.

DCB-UNIBE RADIPHARMACEUTICAL LABORATORY AT SWAN HAUS-2016

M. Bunka

Postgraduate certificate course in radiopharmaceutical chemistry/radiopharmacy, module III “radiopharmacology and clinical radiopharmacy”

Leipzig, Germany, 5-16 September, 2016.

T. Basaco Bernabeu

Characterization of Girentuximab-Dota conjugates for labelling with therapeutic radionuclides

RANC-2016, Budapest, Hungary, 10-15 April, 2016.

T. Basaco Bernabeu

Characterization of Girentuximab-Dota conjugates for labelling with therapeutic radionuclides

NRC9-2016, Helsinki, Finland, 29 August - 2 September, 2016.

O. Leib

Postgraduate Certificate Course in Radiopharmaceutical Chemistry/Radiopharmacy, Module II “Radiopharmaceutical Chemistry”

Zurich, Switzerland, 8-19 February, 2016.

ENVIRONMENTAL RADIONUCLIDES UNIVERSITÄT BERN

C. Alewell, J.P. Krüger, P. von Sengbusch, S. Szidat, J. Leifeld

Carbon isotopes as indicators of peatland growth?

European Geosciences Union, General Assembly 2016, Vienna, Austria, 17-22 April, 2016.

B. Amann, S. Szidat, M. Grosjean

Varved sediments of Lake Oeschinen, NW Alps: filling the gap in the flood frequency-precipitation relationship for the last millennium

European Geosciences Union, General Assembly 2016, Vienna, Austria, 17-22 April, 2016.

T. Berhanu, S. Szidat, M. Leuenberger

First results of the ^{14}C in CO_2 at Beromünster

CarboCount-CH project meeting, EMPA, Dübendorf, Switzerland, 13 May, 2016.

T.A. Berhanu, E. Satar, S. Szidat, D. Brunner, M. Steinbacher, R. Schanda, P. Nyfeler, M. Leuenberger

Quantification of fossil fuel associated CO_2 emissions based on radiocarbon measurements at the Beromünster tall tower, Switzerland

2nd ICOS Science Conference, Helsinki, Finland, 27-29 September, 2016

L.R. Crilley, W.J. Bloss, J. Yin, D.C.S. Beddows, R.M. Harrison, P. Zotter, A. Prevot, J.D. Allan, S. Szidat,

F. Lucarelli, G. Calzolari, S. Nava, G. Valli, V. Bernardoni, R. Vecchi

Are regional sources of airborne particles significant in London? Results from Clearflo winter and summer measurements

Faraday Discussion "Chemistry in the urban atmosphere", London, UK, 6-8 April, 2016.

B.Z. Cvetković, E. Wieland, D. Kunz, G. Salazar, S. Szidat

Analytical strategy for the identification of carbon-14 containing organics released during anoxic corrosion of activated steel in alkaline conditions

2016 Materials Research Society (MRS) Fall Meeting, Boston, USA, 27 November - 2 December, 2016.

A. Madella, R. Delunel, S. Szidat, F. Schlunegger

High Holocene coastal uplift gives insight into the seismic behavior at the Arica Bend (Peru-Chile subduction zone)

European Geosciences Union, General Assembly 2016, Vienna, Austria, 17-22 April, 2016.

M.C. Minguillon, N. Pérez, N. Marchand, A. Bertrand, B. Temime-Roussel, K. Agrios, S. Szidat, B. van Drooge,

A. Sylvestre, A. Alastuey, C. Reche, A. Ripoll, E. Marco, J.O. Grimalt, X. Querol

Secondary organic aerosol origin in an urban environment. Influence of biogenic and fuel combustion precursors

Faraday Discussion "Chemistry in the urban atmosphere", London, UK, 6-8 April, 2016.

A.S.H. Prévôt, P. Zotter, H. Herich, M. Gysel, I. El-Haddad, Y.L. Zhang, G. Močnik, C. Hüglin, U. Baltensperger, S. Szidat

Evaluation of the absorption Ångström exponents for traffic and wood burning in the Aethalometer based source apportionment using radiocarbon measurements of ambient aerosol

22nd European Aerosol Conference, Tours, France, 4-9 September, 2016.

A.S.H. Prévôt, P. Zotter, H. Herich, M. Gysel, I. El-Haddad, Y.L. Zhang, G. Močnik, C. Hüglin, U. Baltensperger, S. Szidat

Evaluation of the absorption Ångström exponents for traffic and wood burning in the Aethalometer based source apportionment using radiocarbon measurements of ambient aerosol

AAAR 35th Annual Conference, Portland, USA, 17-21 October, 2016.

C.J. Sapart, N. Shakhova, I. Semiletov, J. Jansen, S. Szidat, D. Kosmach, O. Dudarev, C. van der Veen, V. Sergienko,

A. Salyuk, V. Tumskey, J.-L. Tison, M. Egger, T. Röckmann

The origin of methane in the East Siberian Arctic Shelf unraveled with triple isotope analysis

2nd ICOS Science Conference, Helsinki, Finland, 27-29 September, 2016

T. Sprafke, R. Zech, P. Schulte, S. Meyer-Heintze, S. Knoll, J. Zech, G. Salazar, S. Szidat, T. Einwögerer, F. Lehmkuhl, B. Terhorst

High-resolution, multi-proxy analyses of the MIS3/2 loess-paleosol sequence Krems-Wachtberg, Austria

European Geosciences Union, General Assembly 2016, Vienna, Austria, 17-22 April, 2016.

C. Steiner, M. Vonwiller, G.A. Salazar, S. Szidat

Identification and ^{14}C analysis of black carbon and elemental carbon in sediments

22nd European Aerosol Conference, Tours, France, 4-9 September, 2016.

S. Szidat

Source apportionment of carbonaceous aerosols using radiocarbon

Institute seminar, MTA Atomki, Debrecen, Hungary, 9 February, 2016.

S. Szidat, K. Agrios, G.A. Salazar

Online coupling of thermal-optical and ^{14}C AMS analysis in atmospheric aerosols source apportionment

German Physical Society (DPG), Spring Meeting, Hannover, Germany, 29 February - 4 March, 2016.

S. Szidat

Resultate der ^{14}C -Vergleichsmessungen an der Universität Bern (LARA-KUP)

Federal Office of Public Health (BAG), Meeting at the Section of Environmental Radioactivity, Bern, Switzerland,

3 June, 2016.

S. Szidat, G. Salazar, K. Agrios, C. Espic, C. Uglietti, B.Z. Cvetcović, E. Wieland

Advanced approaches of compound-specific radiocarbon analysis (CSRA) of environmental and radiolabeled materials

9th International Conference on Nuclear and Radiochemistry, Helsinki, Finland, 29 August - 2 September, 2016.

S. Szidat, K. Agrios, G.A. Salazar

Insights into fossil vs. non-fossil SOA from online TOT- ^{14}C analysis

22nd European Aerosol Conference, Tours, France, 4-9 September, 2016.

C. Uglietti, A. Zapf, T. Jenk, S. Szidat, G. Salazar, D.R. Hardy, M. Schwikowski

The debate on the basal age of Kilimanjaro's plateau glaciers

2nd IPICS (International Partnership in Ice Core sciences) Conference, Hobart, Australia, 7-11 March, 2016.

A. Vlachou, K.R. Daellenbach, C. Bozzetti, F. Canonaco, G.A. Salazar, K. Agrios, S. Szidat, U. Baltensperger,

I. El Haddad, A.S.H. Prévot

Coupled AMS and radiocarbon analysis of organic aerosols for a yearly cycle in Magadino

AAAR 35th Annual Conference, Portland, USA, 17-21 October, 2016.

K. Zenker, M. Vonwiller, S. Szidat, G. Calzolari, M. Giannoni, V. Bernardoni, A.D. Jedynska, J.S. Henzing,

H.A.J. Meijer, U. Dusek

Evaluation of self-developed separation methods for OC-EC analysis in aerosol particles against a standard method

in dependence of sampling frequency and with regard to ^{14}C analysis

22nd European Aerosol Conference, Tours, France, 4-9 September, 2016.

PUBLIC RELATIONS AND OUTREACH ACTIVITIES

Environmental Radionuclides Universität Bern

Open Day Department of Chemistry and Biochemistry, Uni Bern

Wie datiert man ein Mammut?

http://www.dcb.unibe.ch/ueber_uns/aktuelles/veranstaltungen/tag_der_offenen_tuer/index_ger.html

5 November 2016.

LECTURES AND COURSES

Prof. Dr. A. Türler

Universität Bern, FS2016

Bachelor

- Instrumentalanalytik II (with Dr. K. Krämer and Prof. M. Schwikowski) (3 ECTS)
- Allgemeine Chemie (Einführung Radioaktivität) (with Prof. R. Hähner and Prof. J. Hulliger) (4 ECTS)

Master

- Introduction to Radiopharmaceutical Chemistry (with Dr. M. Behe) (1.5 ECTS)

Universität Bern, HS2016

Bachelor

- Physikalische Chemie IV (with PD P. Broekmann) (3,75 ECTS)
- Praktikum Phys. Chemie II (with others) (4 ECTS)
- Biochemische Methoden I (with others) (3 ECTS)

Master

- Nuclear and Radiochemistry (with Dr. R. Eichler) (3 ECTS)
- Seminar Radio- und Umweltchemie in collaboration with Paul Scherrer Institut (organized by Dr. N. van der Meulen FS2016 / HS2016)

Dr. R. Eichler

Universität Bern, HS2016

Master

- Nuclear and Radiochemistry (with Prof. A. Türler) (3 ECTS)

Universität Bern, HS2016

Bachelor

- Praktikum Phys. Chemie II (with Prof. A. Türler) (4 ECTS)

PD Dr. S. Szidat

Universität Bern, FS2016

Bachelor

- Ergänzungen zur analytischen Chemie für Pharmaziestudierende (2 ECTS)

Universität Bern, HS2016

Bachelor

- Chemie für Studierende der Veterinärmedizin (with P. Küpfer) (4.5 ECTS)
- Praktikum Physikalische Chemie II (with others) (4 ECTS)

Y. Wittwer

- Practice Course Physical Chemistry II “ γ -Spectroscopy”, DCB University of Bern 2016

J. Ulrich

- Practice Course Physical Chemistry II “Liquid Scintillation”, DCB University of Bern 2016

MEMBERS OF SCIENTIFIC COMMITTEES EXTERNAL ACTIVITIES

Dr. Robert Eichler

- Associate Editor of the International Journal of Modern Physics E (IJMPE) World Scientific Publishing

Dr. Dorothea Schumann

- PSI internal Neutron Source Development Group, member
- LIEBE, steering committee member

PD Dr. Sönke Szidat

- Bernese Chemical Society (Berner Chemische Gesellschaft, BCG), president
- Naturforschende Gesellschaft in Bern (NGB), board member
- Oeschger Centre for Climate Change Research (OCCR), member
- Swiss Accreditation Service (SAS), technical expert
- Department of Chemistry and Biochemistry of the University of Bern, head of the non-professorial lecturers (Oberer Mittelbau)

Prof. Dr. Andreas Türler

- Eidgenössische Kommission für Strahlenschutz und Überwachung der Radioaktivität (KSR), Vizepräsident
- Gesellschaft Deutscher Chemiker (GDCh), Fachgruppe Nuklearchemie, Vorstands-Beirat
- Radiochimica Acta, member of the advisory board
- Oeschger Centre for Climate Change Research (OCCR), Mitglied des Wissenschaftlichen Ausschusses
- Nuklearforum Schweiz, Mitglied des Vorstandes
- Member of the Albert Einstein Center for Fundamental Physics (AEC) Bern

Dr. Nicholas van der Meulen

- United States Department of Energy (DOE Isotope R&D FOA), Panel Reviewer
- Accelerator for Research in Radiochemistry and Oncology at Nantes Atlantique (ARRONAX) International Scientific Committee, member
- PSI internal research commission (FoKo), member

Dr. Christiaan Vermeulen

- International Workshop on Targetry and Target Chemistry (WTTC) Scientific Committee, member

MASTER THESIS

Christian Steiner

Identification and ^{14}C analysis of black carbon in sediments

PD Dr. S. Szidat / Uni Bern

January 2016

Prisca Lehmann

Separation of radioisotopes ^{231}Pa und ^{230}Th from natural sample material

PD Dr. S. Szidat / Uni Bern

Dr. J. Lippold / Uni Bern

February 2016

Jan Strähl

Development of a new wet extraction technique for the determination of CH_4 , N_2O and CO_2 mixing ratios in ice core samples

PD Dr. S. Szidat / Uni Bern

Prof. Dr. H. Fischer / Uni Bern

Prof. Dr. Th. Stocker / Uni Bern

July 2016

DOCTORAL THESIS



Patrick Steinegger

Towards Vacuum Adsorption Chromatography of Superheavy Elements

Dr. Robert Eichler / PSI
Prof. Dr. A. Türler / PSI & Uni Bern
February 2016



Nadine Chiera

Toward the Selenides of the Superheavy Elements Copernicium and Flerovium Towards the Selenides

Dr. Robert Eichler / PSI
Prof. Dr. A. Türler / PSI & Uni Bern
October 2016

AWARDS**Nadine Chiera***Superheavy Elements copernicium and flerovium selenides: First Cn-Se bond observation*

Best presentation award
NES PhD Day, Villigen, Switzerland
May 2016

Katharina Domnanich*⁴³Sc production development by cyclotron irradiation of ⁴³Ca and ⁴⁶Ti*

Best PhD student presentation
NRC9, Helsinki, Finland,
August 2016

SUMMER STUDENTS

Janosch Gartmeier

Optimization of beryllium molecular plating procedure

9 June - 29 August 2016

Severin Martz

Selenium vapor deposition onto fused silica columns and pin diodes

11 July - 19 August 2016

Denis Vollmer

Basics in radionuclide development

11 July - 12 August 2016

SEMESTERWORK Nuclear Engineering Master

Aaron Colldeweih

Thermochromatography of Cesium in moist carrier gases

10 October 2016 – 9 January 2017

VISITING GUESTS AT PSI 2016

3 - 9 April / 9 - 11 August / 5 - 9 September 2016

Björn Dittmann, Uni Köln, Germany

⁵³Mn standard

16 August 2016

Paul Papka, Stellenbosch University, Themba LABS, South Africa

Target applications developed within the Nuclear Physics group of Stellenbosch in collaboration with iThemba LABS

16 August 2016

Yuri Amelin, Australian National University Canberra,

Geochronology, SPIDE2R style: mass spectrometers, half-lives, zircons and meteorites

7 - November 2016

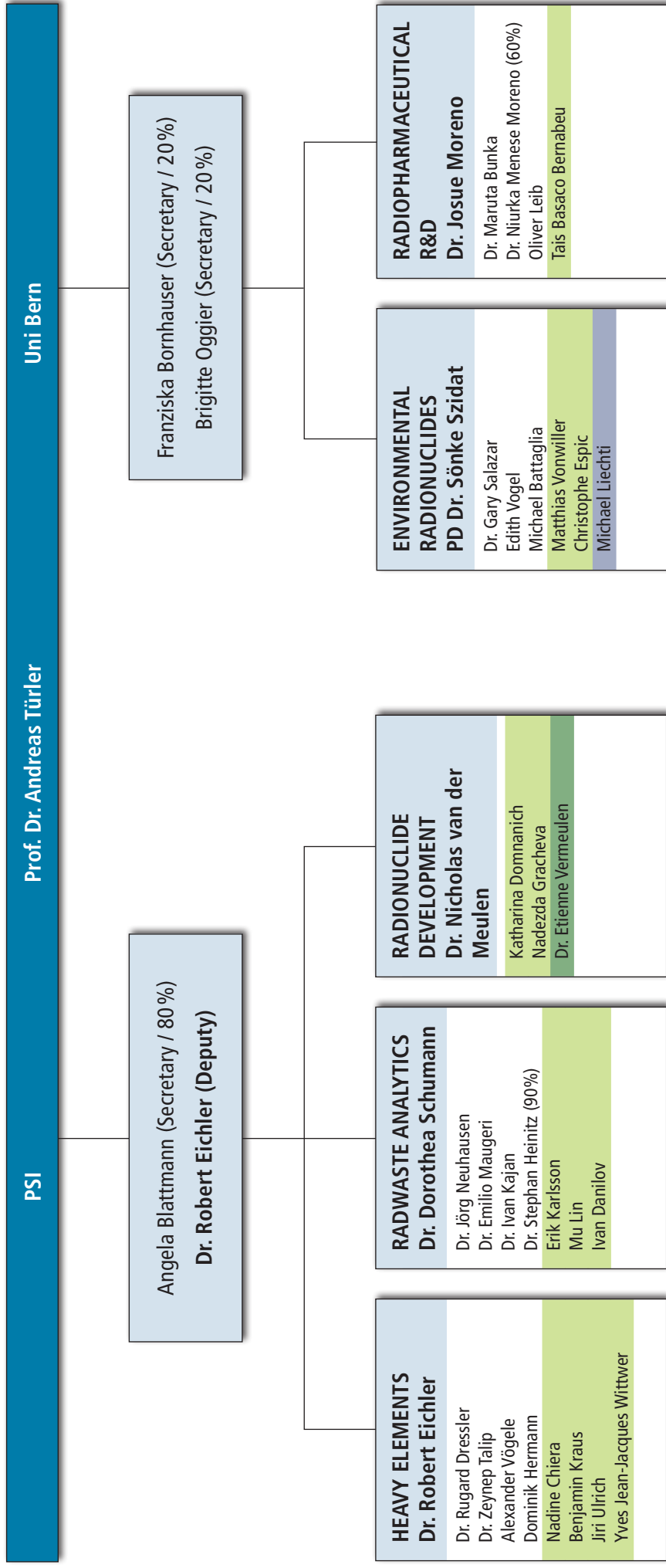
Enrico Chiaveri, Genf, CERN, Switzerland

n_TOF at CERN: a bright future for neutrons

28 November 2016

Hongyan Zhang and Shaoming Pan, School of Geography and Ocean Science, Nanjing University, China

Radiocarbon analysis with MICADAS



■ Graduate student
■ Master student
■ Position of CRS

AUTHOR INDEX

- Agrios, K., 40
 Aksenov, N.V., 3
 Barbagallo, M., 17
 Basaco, T., 35, 37, 39
 Battaglia, M., 43, 44
 Behe, M., 33
 Benešová, M., 33, 34
 Blanc, A., 33
 Bozhikov, G.A., 3
 Bunka, M., 39
 Chepigin, V.I., 3
 Chiera, N.M., 3
 Colldeweih, A., 13
 Danilov, I.I., 15
 DiPietro, A., 26
 Dmitriev, S.N., 3
 Domnanich, K., 33, 34
 Dressler, R., 3, 8, 17, 18, 20, 27
 Eichler, R., 3, 4, 5, 8, 11, 13
 Espic, C., 43, 44
 Frey, N., 18
 Galván, J.A., 37
 Geissmann, K., 18
 Gruber, R., 41
 Hagel, A., 18
 Heinitz, S., 17, 18, 24, 26
 Herrmann, D.P., 5
 Kajan, I., 31
 Karlsson, E., 11, 13
 Kivel, N., 17, 18, 24, 29
 Kraus, B., 3, 7
 Köster, U., 24, 34
 Lauss, B., 27
 Leib, O., 39
 Liechti, M., 43, 44
 Lin, M., 31
 Löch, S., 41
 Madumarov, S., 3
 Malyshev, O.N., 3
 Martz, S., 3
 Maugeri, E.A., 17, 18
 Meneses, N., 39
 Michel, R., 20
 Miederer, M., 35, 37
 Morath, O., 18
 Moreno, J., 35, 37, 39
 Müller, C., 33, 34
 Müller, E., 15
 Mussumara, A., 17
 Neims, V., 18
 Neuhausen, J., 11, 13, 15
 Nucciotti, A., 24
 Orlick, H., 18
 Pektor, S., 35, 37
 Piguet, D., 3
 Ponsard, B., 34
 Popov, Y.A., 3
 Potthast, H.D., 31
 Reckermann, R., 18
 Sabel'nikov, A.V., 3
 Salazar, G., 40
 Schibli, R., 33, 34
 Schneider, T., 18
 Schumann, D., 10, 17, 18, 20, 22, 24, 26, 29, 31
 Siwowska, K., 34
 Steinegger, P., 3, 7
 Steiner, C., 42
 Stora, T., 18
 Stowasser, T., 26
 Strub, E., 22
 Svirikhin, A.I., 3
 Szidat, S., 40, 41, 42, 43, 44
 Talip, Z., 20, 22
 Türler, A., 3, 5, 7, 11, 13, 31, 33, 34, 35, 37, 39
 Ulrich, J., 27
 Umbricht, C., 33
 Van der Meulen, N.P., 32, 33, 34
 Vermeulen, C., 32
 Vockenhuber, C., 22
 Vögele, A., 3, 11, 15, 20, 22
 Vogel, E., 41
 Vonwiller, M., 42
 Vostokin, G.K., 3
 Wittwer, Y., 3, 5
 Yeremin, A.V., 3

AFFILIATION INDEX

ADB	Archaeological Service of the Canton. of Bern, Brünnenstrasse 66, 3001 Bern, Switzerland
AHL	Hot Laboratory Division of the Nuclear Energy and Safety Department (NES), Paul Scherrer Institut, 5232 Villigen, Switzerland
CERN	European Organization for Nuclear Research, CERN CH-1211, Genève 23, Switzerland
CRS	Center for Radiopharmaceutical Sciences, Paul Scherrer Institut, 5232 Villigen, Switzerland
DCB	Departement für Chemie und Biochemie, Universität Bern, Freiestrasse 3, 3012 Bern, Switzerland
ETHZ	Eidgen. Technische Hochschule Zürich, 8092 Zürich, Switzerland
EU	European Union
FLNR	Flerov Laboratory of Nuclear Reactions, Joliot-Curie, 6, Dubna, Moscow region 141980, Russia
ILL	Institut Laue-Langevin, 71 avenue des Martyrs 38000 Grenoble, France
INFN LNS Catania	INFN - Laboratori Nazionali del Sud, Via S. Sofia 62, 95123 Catania, Italy
INFN Genova	Istituto Nazionale di Fisica Nucleare Sezione di Genova, Via Dodecaneso, 33, 16146 Genova, Italy
INFN Bari	Istituto Nazionale di Fisica Nucleare Sezione di Bari, Via Orabona, 4, 70125 Bari, Italy
IRM	Department of Physical Anthropology, Institute of Forensic Medicine, University of Bern, Bühlstrasse 20, 3012 Bern, Switzerland.
IRS	Institut für Radioökologie und Strahlenschutz, Leibniz Universität Hannover, Herrenhäuser Str. 2, 30419 Hannover, Germany
JAEA	Japan Atomic Energy Agency, Tokai, Ibaraki 319-1195, Japan
JINR	International Intergovernmental Organization, Joint Institute for Nuclear Research Joliot-Curie, 6, Dubna, Moscow region 141980, Russia
LBR	Laboratory for Biomolecular Research, Paul Scherrer Institut, 5232 Villigen, Switzerland
NUM	Forschung mit Neutronen und Myonen, Paul Scherrer Institut, 5232 Villigen, Switzerland
PSI	Paul Scherrer Institut, 5232 Villigen, Switzerland
SCK CEN	Belgian Nuclear Research Centre, Boeretang 200, 2400 Mol, Belgium
Univ. Bern	Departement für Chemie und Biochemie, Universität Bern, Freiestr. 3, 3012 Bern, Switzerland
Univ. Cologne	Universität zu Köln, Albertus-Magnus-Plat, 50923 Köln, Germany
Univ. Genova	Università degli studi di Genova, Via Balbi, 5, 16126 Genova, Italien
Univ. Hannover	Gottfried Wilhelm Leibniz Universität Hannover, Welfengarten 1, 30167 Hannover, Germany
Univ. Mainz	Johannes Gutenberg-Universität Mainz, Saarstr. 21, 55122 Mainz, Germany

